bioRxiv preprint doi: https://doi.org/10.1101/735811; this version posted January 21, 2020. The copyright holder for this preprint (which was not certified by peer review) is the author/funder. All rights reserved. No reuse allowed without permission.

KAT2-mediated acetylation switches the mode of PALB2 chromatin association to safeguard genome integrity

Marjorie Fournier[1,*], Jean-Yves Bleuyard[1], Anthony M. Couturier[1], Jessica Ellins[2], Svenja Hester[1,3], Stephen J. Smerdon[4,#], László Tora[5,6,7,8] and Fumiko Esashi[1,*]

[1] Sir William Dunn School of Pathology, University of Oxford, Oxford, OX1 3RE, UK

[2] Department of Biochemistry, University of Oxford, Oxford, OX1 3QU, UK

[3] Advanced Proteomics Facility, University of Oxford, Oxford, OX1 3RE, UK

[4] The Francis Crick Institute, 1 Midland Rd, London, NW1 1AT, UK

[5]Institut de Génétique et de Biologie Moléculaire et Cellulaire, 67404 Illkirch, France

[6]Centre National de la Recherche Scientifique, UMR7104, 67404, Illkirch, France

[7]Institut National de la Santé et de la Recherche Médicale, U1258, 67404, Illkirch, France

[8]Université de Strasbourg, 67404, Illkirch, France

[#] Current address: Institute of Cancer and Genomic Sciences, University of Birmingham, Vincent Drive, Edgbaston, Birmingham, B15 2TT, UK

* Co-correspondence to:

marjorie.fournier@path.ox.ac.uk and fumiko.esashi@path.ox.ac.uk

bioRxiv preprint doi: https://doi.org/10.1101/735811; this version posted January 21, 2020. The copyright holder for this preprint (which was not certified by peer review) is the author/funder. All rights reserved. No reuse allowed without permission.

Summary

The tumour suppressor PALB2 stimulates error-free repair of DNA breaks, whilst its steady-state chromatin association protects active genes from genotoxic stress. Here, we report that the lysine acetyltransferases 2A and 2B (KAT2A/B), commonly known to promote transcriptional activation, acetylate the PALB2 chromatin association motif (ChAM), providing a dynamic regulatory mechanism for PALB2. ChAM acetylation within a cluster of seven lysine residues (7K), detected in the chromatin-enriched fraction in undamaged cells, enhanced its association with nucleosomes while decreasing its non-specific binding to naked DNA. DNA damage triggered a rapid deacetylation of ChAM and a concomitant increase in PALB2 mobility. Significantly, a 7K-null mutation, which hindered ChAM binding to both nucleosomes and DNA, conferred deficiency in DNA repair and hypersensitivity to the anti-cancer drug olaparib. Thus, our study reveals a unique mechanism mediated by KAT2A/B-dependent acetylation of a non-histone protein, which fine-tunes the DNA damage response and hence promotes genome stability.

bioRxiv preprint doi: https://doi.org/10.1101/735811; this version posted January 21, 2020. The copyright holder for this preprint (which was not certified by peer review) is the author/funder. All rights reserved. No reuse allowed without permission.

Introduction

PALB2, the partner and localizer of the breast cancer susceptibility 2 protein (BRCA2) (Xia et al, 2006), plays essential roles in the maintenance of cellular homeostasis and disease prevention in humans. Biallelic mutations in *PALB2* cause Fanconi anaemia (FA), a rare genetic disorder characterised by bone marrow failure, developmental abnormalities and increased incidence of childhood cancers (Reid et al, 2007; Xia et al, 2007). Hereditary monoallelic *PALB2* mutations also increase the risk of breast and pancreatic cancer (Jones et al, 2009; Rahman et al, 2007), similarly to inherited *BRCA1* and *BRCA2* mutations (O'Donovan & Livingston, 2010). PALB2 works together with BRCA1 and BRCA2 to promote the error-free repair of highly genotoxic double-strand DNA breaks (DSBs) by homologous recombination (HR). Current models propose that BRCA1 acts as a DNA damage sensor, which in turn recruits PALB2 and BRCA2 to sites of DNA damage. The essential RAD51 recombinase is subsequently recruited and catalyses the strand invasion and homology search phases of HR repair (Sy et al, 2009b; Xia et al, 2006).

We have recently revealed a repair-independent role of PALB2 in protecting transcriptionally active chromatin from DNA damage arising from replicative stress (Bleuyard et al, 2017b). This role of PALB2 is mediated through its high-affinity binding partner the MORF-related gene 15 protein (MRG15), which recognises an epigenetic marker of active genes, histone H3 trimethylated at lysine 36 (H3K36me^3), *via* its N-terminal chromodomain (Bleuyard et al, 2017b; Hayakawa et al, 2010; Sy et al, 2009a). Moreover, PALB2 intrinsic chromatin association is reinforced by the chromatin-association motif (ChAM), an

bioRxiv preprint doi: https://doi.org/10.1101/735811; this version posted January 21, 2020. The copyright holder for this preprint (which was not certified by peer review) is the author/funder. All rights reserved. No reuse allowed without permission.

evolutionarily conserved domain uniquely found in PALB2 orthologues, which directly binds to nucleosomes (Bleuyard et al, 2012). Notably, our locus-specific chromatin immunoprecipitation (ChIP) analyses revealed a decrease in PALB2 association with active genes following an exposure to a topoisomerase inhibitor camptothecin (CPT), suggesting that the mode of PALB2 chromatin association is actively regulated (Bleuyard et al, 2017b). Despite these observations, the regulatory mechanism by which PALB2 is switched between different modes of chromatin association (i.e. association with damaged DNA to promote HR repair and with actively transcribed genes to assist in their protection) remains elusive.

Numerous studies in recent decades have provided evidence that reversible post-translational modifications (PTMs), such as phosphorylation, ubiquitylation, SUMOylation, poly(ADP-ribosyl)ation, methylation and acetylation, are orchestrated to promote genome stability, including the DNA damage response (DDR) (Dantuma & van Attikum, 2016). For example, the damage-responsive ATM and ATR kinases mediate phosphorylation of PALB2 at residues S59, S177 and S376, which in turn facilitate PALB2 interaction with BRCA1, RAD51 foci formation, and hence HR repair of DSBs (Ahlskog et al, 2016; Buisson et al, 2017; Guo et al, 2015). Conversely, in G1 phase, the E3 ligase KEAP1-CUL3-RBX1 ubiquitylates PALB2 at K25, a key residue involved in BRCA1 interaction, and in this way, suppresses PALB2-BRCA1 interaction and HR activation (Orthwein et al, 2015). Furthermore, our recent work identified PALB2 as a key substrate of the lysine acetyltransferases 2A (GCN5/KAT2A) and 2B (PCAF/KAT2B) (Fournier et al, 2016), two well-known transcriptional regulators (reviewed in Nagy et al, 2010), in undamaged cells. However, the physiological role of these modifications is as yet unknown. Notably, KAT2A/B use the

bioRxiv preprint doi: https://doi.org/10.1101/735811; this version posted January 21, 2020. The copyright holder for this preprint (which was not certified by peer review) is the author/funder. All rights reserved. No reuse allowed without permission.

metabolite acetyl coenzyme A (acetyl-CoA) as a cofactor (Tanner et al, 2000), and hence are proposed to fine-tune cellular processes in accordance with the metabolic status of the cell (Wellen et al, 2009). The study of acetylation would have important implications in the context of tumorigenesis, as cancer cells are characterised by reprogrammed metabolism and elevated genome instability.

In this study, we investigated the role of KAT2A/B-mediated lysine acetylation in regulating PALB2. We found that KAT2A/B acetylate a cluster of seven lysine residues (the 7K-patch) within the PALB2 ChAM. ChAM acetylation enhanced its association with nucleosomes, while restricting its non-specific binding to naked DNA. Notably, DNA damage triggered rapid ChAM deacetylation and a concomitant increase in PALB2 mobility. Importantly, lysine to glutamine substitutions in the 7K-patch impeded PALB2 association with chromatin and its function in the DDR. On the basis of these observations, we propose that PALB2 chromatin association is actively regulated by KAT2A/B, which hence play a significant role in the maintenance of genome stability.

Materials and Methods

Cell culture and cell lines

All cells were grown at 37°C in an incubator with a humidified atmosphere with 5% CO_2. HEK293T cells were grown in Dulbecco's Modified Eagle's Medium (DMEM, Sigma) supplemented with 10% fetal bovine serum (FBS), 100 U/mL penicillin, and 0.1 mg/mL streptomycin. U2OS Flp-In T-REx P2shRNA cell line (Bleuyard et al, 2017b), carrying a doxycycline-inducible shRNA targeting the endogenous *PALB2* 3' UTR, referred to as U2OS-shPALB2, were used to generate stable isogenic cell lines with constitutive expression of N3xFLAG-PALB2 variants.

bioRxiv preprint doi: https://doi.org/10.1101/735811; this version posted January 21, 2020. The copyright holder for this preprint (which was not certified by peer review) is the author/funder. All rights reserved. No reuse allowed without permission.

U2OS-shPALB2 were co-transfected with pOG44 and pcDNA5/FRT GW/N3×FLAG-PALB2 (7Q or 7R), and resultant stable cell lines were selected in DMEM supplemented with 10% FBS, 100 U/mL penicillin, 0.1 mg/mL streptomycin, 10 μg/mL blasticidin, 200 μg/mL hygromycin B (100 μg/mL to maintain the cell lines), and 1 μg/mL puromycin. Stable U2OS-shPALB2 lines carrying the empty pcDNA5/FRT GW/N3×FLAG vector or the pcDNA5/FRT GW/N3×FLAG-PALB2 WT vector have been previously described (Bleuyard et al, 2017b).

Antibodies

The primary antibodies used (with their respective working dilutions) were: anti-FLAG (Sigma F1804, mouse, WB: 1/1000), anti-pan-acetyl lysine (AcK) (Cell Signaling Technology 9441S, rabbit, WB: 1/1000), anti-PALB2 (Bethyl A301-246A, rabbit, WB: 1/500), anti-BRCA2 (Millipore OP95, mouse, WB: 1/1000), anti-RAD51 (Yata et al, 2014) (rabbit, 7946 IF: 1/1000), anti-lamin A (Sigma L1293, rabbit, WB: 1/2000), anti-γ-H2AX (Millipore 05-636, mouse, WB: 1/1000), anti-GFP (Sigma G1544, mouse, WB: 1/1000), anti-histone H3 (Bethyl A300-823A, rabbit, WB: 1/1000), anti-GST (Santa Cruz Biotechnology sc-138, mouse, WB:1/1000), biotin-HRP conjugated (Sigma A0185, mouse, WB:1/1000), anti-KAT2A/GCN5 (Cell Signaling Technology 3305, rabbit, WB:1/1000), anti-α-tubulin (Cell Signaling Technology 3873, mouse, WB: 1/2000). Secondary antibodies coupled with horseradish peroxidase (HRP): goat anti-mouse (Dako P0447, WB: 1/1000), goat anti-rabbit (Dako P0448, WB: 1/1000).

DNA damage and cell treatment

bioRxiv preprint doi: https://doi.org/10.1101/735811; this version posted January 21, 2020. The copyright holder for this preprint (which was not certified by peer review) is the author/funder. All rights reserved. No reuse allowed without permission.

For ionising radiation-induced DNA damage, cells were exposed to 4 Gy γ-rays using a ^{137}Cs source, delivering a dose rate of 1.68 Gy/min (Gravatom). For genotoxic drug treatments, cells were incubated for 2 h at 37°C with either 1 mM MMC (Sigma M0503) or 2.5 μM olaparib (Enzo Life Sciences LKT-O4402). DMSO was used as negative vehicle control. KDAC inhibition was performed by treating cells with a cocktail of 5 mM sodium butyrate (NaB, Sigma 303410), 5 μM trichostatin (TSA, Sigma T8552) and 0.5 mM nicotinamide (NaM) for 2 h at 37°C.

siRNA treatment

For KAT2A/GCN5 and KAT2B/PCAF knockdowns, U2OS cells at 30% confluence were transfected using DharmaFECT (Dharmacon) according to the manufacturer's instructions, with 50 pmol each of ON-Targetplus SMARTpools siRNAs targeting KAT2A (Dharmacon L-009722-02-0005) and KAT2B (Dharmacon L-005055-00-0005) in serum-free DMEM. As a negative control, 100 pmol of ON-TARGETplus non-targeting pool siRNAs (Dharmacon D001810-10-05) were used. The serum-free medium was replaced with DMEM supplemented with 10% FBS at 24 h after transfection, and after further 48 h incubation, the cells were collected by trypsinisation (total of 72 h siRNA exposure).

Fluorescence recovery after photobleaching (FRAP)

For FRAP experiments, cells were plated into CELLview cell culture dishes (Greiner Bio-One) and analysed in phenol red-free Leibovitz's L15 medium (Gibco). FRAP experiments were performed on a spinning-disk confocal microscope (Ultra-View Vox, Perkin Elmer) mounted on an IX81 Olympus microscope with an Olympus 60x 1.4 oil PlanApo objective, in a controlled

bioRxiv preprint doi: https://doi.org/10.1101/735811; this version posted January 21, 2020. The copyright holder for this preprint (which was not certified by peer review) is the author/funder. All rights reserved. No reuse allowed without permission.

chamber at 37°C and 5% CO_2 (TOKAI HIT stage top incubator). The fluorescence signal was detected using an EMCCD camera (ImagEM, Hamamatsu C9100-13). Cells were bleached in the GFP channel at maximum laser power with a single pulse for 20 ms, within a square region of interest of 5 μm^2. After bleaching, GFP fluorescence recovery was monitored within the bleached area every second for 40 s. FRAP parameters were controlled using Volocity software 6.0 (QuorumTechnologies). FRAP data were fitted and normalised using the FRAP plugins in ImageJ/Fiji (Cardona et al, 2012). From the FRAP curve fitting, half-time recovery time values after photobleaching ($t_{1/2}$) were extracted and plotted in Prism 7.02, in which statistical analyses were performed. Normalised fluorescence intensity after photobleaching was calculated by dividing the fluorescence intensity at the bleached area by the whole cellular fluorescence intensity.

Protein purification

FLAG-KAT2A, FLAG-KAT2A catalytic mutant, and FLAG-KAT2B proteins were purified as described previously (Fournier et al, 2016). GST-PALB2 full-length and fragments were purified from 1 L of ArcticExpress cells (Agilent Technologies), grown at 37°C in LB broth medium containing 50 µg/mL ampicillin and 25 µg/mL gentamycin. Protein expression was induced by 0.1 mM IPTG exposure for 24 h at 13°C. Cells were collected by centrifugation for 15 min at 1,400 × *g* at 4°C and washed with ice-cold phosphate-buffered saline (PBS). Cells lysis was performed by 30 min incubation on ice in 15 mL of ice-cold extraction buffer (50 mM Tris-HCl pH 8.0, 150 mM KCl, 1 mM EDTA, 2 mM DTT, 10% glycerol, and protease inhibitor cocktail (PIC, Sigma P2714) supplemented with 2 mg/mL Lysozyme (Sigma) and 0.2% Triton X-100), followed by sonication. Cell lysates were collected after 45

bioRxiv preprint doi: https://doi.org/10.1101/735811; this version posted January 21, 2020. The copyright holder for this preprint (which was not certified by peer review) is the author/funder. All rights reserved. No reuse allowed without permission.

min centrifugation at 35,000 × *g*, 4°C. GST-fusion proteins were pull-down with glutathione Sepharose 4B beads (GE Healthcare), pre-washed with ice-cold PBS. After overnight incubation at 4°C on a rotating wheel, beads were washed three times with ice-cold extraction buffer, three times with 5 mL of ice-cold ATP-Mg buffer (50 mM Tris-HCl pH 7.5, 500 mM KCl, 2 mM DTT, 20 mM $MgCl_2$, 5 mM ATP, and 10% glycerol) and three times with ice-cold equilibration buffer (50 mM Tris-HCl pH 8.8, 150 mM KCl, 2 mM DTT, and 10% glycerol). Proteins were eluted from beads in ice-cold elution buffer (50 mM Tris-HCl pH 8.8, 150 mM KCl, 2 mM DTT, 0.1% Triton X-100, 25 mM L-glutathione, and 10% glycerol).

For GFP-ChAM purification for mass spectrometry analysis, HEK293T cells (3×10^7 cells) transiently expressing GFP-ChAM were collected by centrifugation for 5 min at 500 × *g*, 4°C and washed once with ice-cold PBS. Cells were further resuspended in 5 mL ice-cold sucrose buffer (10 mM Tris-HCl pH 8.0, 20 mM KCl, 250 mM sucrose, 2.5 mM $MgCl_2$, 10 mM Benz-HCl and PIC). After addition of 10% Triton X-100 (Sigma) to a final concentration of 0.3%, the cell suspension was vortexed four times for 10 s with 1 min intervals. The intact nuclei were collected by centrifugation for 5 min at 500 × *g*, 4°C, and the supernatant was discarded. The nuclear pellet was washed once with ice-cold sucrose buffer and resuspended in ice-cold NETN250 buffer (50 mM Tris-HCl pH 8.0, 250 mM NaCl, 2 mM EDTA, 0.5% NP-40, 10 mM Benz-HCl and PIC). After 30 min incubation on ice, the chromatin fraction was collected by centrifugation for 5 min at 500 × *g*, 4°C, washed once with 5 mL ice-cold NETN250 buffer and lysed for 15 min at room temperature (RT) in ice-cold NETN250 buffer supplemented 5 mM $MgCl_2$ and 125 U/mL benzonase (Novagen 71206-3). After addition of EDTA and EGTA to respective final concentrations of 5 mM and 2 mM to inactivate the benzonase and

bioRxiv preprint doi: https://doi.org/10.1101/735811; this version posted January 21, 2020. The copyright holder for this preprint (which was not certified by peer review) is the author/funder. All rights reserved. No reuse allowed without permission.

centrifugation for 30 min at 16,100 × *g*, 4°C, the supernatant was collected as the chromatin-enriched fraction. GFP-ChAM were pull-down using 15 µL GFP-Trap Agarose (Chromotek), pre-washed three times with ice-cold NETN250 buffer and blocked for 3 h at 4°C on a rotating wheel with 500 µL ice-cold NETN250 buffer supplemented with 2 mg/mL bovine serum albumin (BSA, Sigma). After 3 h protein binding at 4 °C on a rotating wheel, the GFP-Trap beads were collected by centrifugation for 5 min at 1,000 × *g*, 4°C and washed four times with ice-cold NETN250 buffer.

For the analysis of ChAM acetylation upon DNA damage, a GFP-ChAM fusion was transiently expressed from pDEST53-GFP-ChAM for 24 h in HEK293T cells. Whole-cell extracts (WCE) were prepared from ~1.5 × 10^7 cells resuspended in NETN150 buffer (50 mM Tris-HCl pH 8.0, 150 mM NaCl, 2 mM EDTA and 0.5% NP-40 alternative (NP-40 hereafter) (Millipore 492018)) supplemented with 1 mM DTT, PIC, lysine deacetylase inhibitor (5 mM NaB), 1 mM $MgCl_2$ and 125 U/mL benzonase. After 30 min incubation on ice, cell debris was removed by 30 min centrifugation at 4°C, and the supernatant was collected as WCE. WCE was then incubated with 15 µl of GFP-Trap Agarose for GFP-pull down. After 1 h protein binding at 4°C on a rotating wheel, GFP-Trap beads were collected by 5 min centrifugation at 500 × *g* at 4°C and washed three times with NET150 buffer (50 mM Tris-HCl pH 8.0, 150 mM NaCl and 2 mM EDTA) supplemented with 0.1% NP-40, 1 mM DTT, PIC, 5 mM NaB and 1 mM $MgCl_2$. Proteins were eluted from beads by heating at 85°C for 10 min in Laemmli buffer supplemented with 10 mM DTT. The proteins were separated by SDS-PAGE and analysed by western blot.

For the nucleosome pull-down assays, GFP-ChAM variants were affinity-purified from HEK293T cells (3 × 10^7 cells) following transient expression. After

bioRxiv preprint doi: https://doi.org/10.1101/735811; this version posted January 21, 2020. The copyright holder for this preprint (which was not certified by peer review) is the author/funder. All rights reserved. No reuse allowed without permission.

collecting cells by centrifugation for 5 min at 500 × *g*, 4°C, the cell pellet was washed twice with ice-cold PBS and resuspended in ice-cold NETN150 buffer supplemented with 10 mM benzamidine hydrochloride (Benz-HCl) and PIC. After 30 min incubation on ice, the chromatin was pelleted by centrifugation for 5 min at 500 × *g*, 4°C, and the supernatant was collected as NETN150 soluble fraction and centrifuged for 30 min at 16,100 × *g*, 4°C to remove cell debris and insoluble material. For each sample, 10 µL of GFP-Trap Agarose were washed three times with 500 µL ice-cold NETN150 buffer. NETN150 soluble proteins (2.5 mg) in a total volume of 1 mL ice-cold NETN150 buffer were incubated with the GFP-Trap beads to perform a GFP pull-down. After 2 h incubation at 4°C on a rotating wheel, the GFP-Trap beads were collected by centrifugation for 5 min at 500 × *g*, 4°C and washed four times with ice-cold NETN150 buffer. Human nucleosomes were partially purified from HEK293T cells (4×10^7 cells), collected by centrifugation for 5 min at 500 × *g*, 4°C, washed twice with ice-cold PBS and lysed in ice-cold NETN150 buffer supplemented with 10 mM Benz-HCl and PIC. After 30 min of incubation on ice, the chromatin was pelleted by centrifugation for 5 min at 500 × *g*, 4°C, washed once with ice-cold NETN150 buffer and digested for 12 min at 37 °C with 50 gel units of micrococcal nuclease (NEB) per milligram of DNA in NETN150 buffer containing 5 mM $CaCl_2$, using 200 µL buffer per mg of DNA. The reaction was stopped with 5 mM EGTA and the nucleosomes suspension cleared by centrifugation for 30 min at 16,100 × *g*, 4°C.

Acetyltransferase assays

Radioactive ^{14}C-acetyltransferase assays on recombinant proteins were performed by incubating purified GST-PALB2 (full length and fragments) or purified RAD51

bioRxiv preprint doi: https://doi.org/10.1101/735811; this version posted January 21, 2020. The copyright holder for this preprint (which was not certified by peer review) is the author/funder. All rights reserved. No reuse allowed without permission.

with purified FLAG-KAT2B in the presence of ^{14}C-labeled acetyl-CoA in the reaction buffer (50 mM Tris-HCl pH 8.0, 10% glycerol, 100 mM EDTA, 50 mM KCl, 0.1 M NaB, PIC, and 5 mM DTT) for 1 h at 30°C. The reactions were stopped by addition of Laemmli buffer containing 10% beta-mercaptoethanol, boiled for 5 min, resolved by SDS-PAGE and stained using Coomassie blue to reveal overall protein distribution. The acrylamide gel was then dried and exposed to phosphorimager to reveal ^{14}C-labeled proteins. Non-radioactive acetyltransferase assays were performed as described above using cold acetyl-CoA instead. After 1 h incubation at 30°C, the reactions were stopped by addition of Laemmli buffer containing 10 mM DTT, boiled for 5 min, resolved by SDS-PAGE, and after Ponceau S staining of the membrane to reveal overall protein distribution, analysed by western blot using anti-acetyl lysine antibody. Acetyltransferase assays performed for mass spectrometry analyses were performed as previously described (Fournier et al, 2016)

Nucleosome pull-down assay

Nucleosome pull-down assays were performed by mixing 250 µg of partially purified nucleosomes and GFP-ChAM variants immobilised on GFP Trap beads in NETN150 buffer supplemented with 2 mg/mL BSA, followed by 30 min incubation at RT, then 1.5 h incubation at 4 °C, on a rotating wheel. GFP-Trap beads were further washed four times with NETN150 buffer, and samples were analysed by SDS-PAGE and western blot.

DNA binding assays

bioRxiv preprint doi: https://doi.org/10.1101/735811; this version posted January 21, 2020. The copyright holder for this preprint (which was not certified by peer review) is the author/funder. All rights reserved. No reuse allowed without permission.

For ChAM peptides binding to DNA, proteins or peptides were incubated in NDTN150 buffer (50 mM Tris HCl pH 7.5, 150 mM NaCl, 0.5% NP-40 and 2 mM DTT) with 300 ng pBluescript plasmid DNA for 1 h at room temperature (RT). Reactions were loaded onto a 1% agarose Tris-Acetate-EDTA (TAE) gel and run at 100 V for 60 min. The gel was stained for 1 h at RT with 0.5 µg/mL ethidium bromide in Tris-Borate-EDTA (TBE) buffer. Binding of ChAM peptide to histone H3 was performed by incubating for 1 h at 4°C biotinylated ChAM peptides and histone H3 protein in NDTN250 buffer (50 mM Tris HCl pH 7.5, 250 mM NaCl, 0.5% NP-40, and 2 mM DTT) supplemented with 5 mg/mL BSA. Dynabeads MyOne T1 blocked with BSA in NDTN250 buffer were added to the peptide-Histone H3 mixture and incubated for 1 h at 4°C. Immobilised complexes were washed three times with NDTN250 buffer and proteins were visualised by western blotting using the indicated antibodies.

Immunofluorescence microscopy

For γ-H2AX foci analysis, cells were grown on coverslips and washed with PBS before pre-extraction with 0.1% Triton in PBS for 30 s at RT. Cells were then fixed twice with 4% PFA in PBS, first for 10 min on ice and then for 10 min at RT. After permeabilisation in 0.5% Triton X-100 in PBS for 10 min at RT, cells were blocked with 5% BSA in PBS supplemented with 0.1% Tween 20 solution (PBS-T-0.1) and incubated with anti-γ-H2AX antibody for 3 h at RT. After washing with PBS-T-0.1 for 5 min at RT, cells were incubated with secondary antibodies coupled with a fluorophore, washed with PBS-T-0.1 for 5 min at RT, and mounted on slides using a DAPI-containing solution. For RAD51 foci analysis, cells were grown on coverslips and washed twice with PBS before fixation with 4% PFA in PBS for 15

bioRxiv preprint doi: https://doi.org/10.1101/735811; this version posted January 21, 2020. The copyright holder for this preprint (which was not certified by peer review) is the author/funder. All rights reserved. No reuse allowed without permission.

min at RT. After washing twice with PBS, cells were permeabilised with 0.5% Triton X-100 in PBS for 5 min at RT and blocked with 3% BSA in PBS supplemented with 0.1% Triton X-100 before incubation with anti-RAD51 antibody for 2 h at RT. After washing three times with PBS supplemented with 0.5% Tween 20 (PBS-T-0.5), cells were incubated with secondary antibody coupled with a fluorophore, washed three times with PBS-T-0.5 and mounted on slides using a DAPI-containing solution. Cells were analysed on a spinning-disk confocal microscope (Ultra-View Vox, Perkin Elmer) mounted on an IX81 Olympus microscope, with a 40x 1.3 oil UPlan FL objective. The fluorescence signal was detected using an EMCCD camera (ImagEM, Hamamatsu C9100-13). Images were processed in Image J (https://imagej.nih.gov/ij/) (Schneider et al, 2012) .

Sequence alignment analysis

Sequences of PALB2 orthologues from 12 species were retrieved from the Ensembl (http://www.ensembl.org) and NCBI (https://www.ncbi.nlm.nih.gov) and aligned using MUSCLE (http://www.ebi.ac.uk/Tools/msa/muscle/).

Results

PALB2 is acetylated within a 7K-patch in its ChAM domain

Our previous shotgun mass spectrometry (MS) study of the endogenous KAT2A/B-acetylome in HeLa cells identified a number of lysine residues within the central region of PALB2 as acetylation acceptors (Fournier et al, 2016) (**Fig. 1*A*,** highlighted in blue). To confirm the direct acetylation of PALB2 by KAT2A/B, we performed *in vitro* acetylation assays using either recombinant full-length PALB2 or a series of PALB2 fragments (**Fig, 1*A***) with purified KAT2A or KAT2B.

bioRxiv preprint doi: https://doi.org/10.1101/735811; this version posted January 21, 2020. The copyright holder for this preprint (which was not certified by peer review) is the author/funder. All rights reserved. No reuse allowed without permission.

Lysine acetylation of full-length PALB2 and fragment 2, which encompasses the DNA/chromatin binding region of PALB2 (residues 295-610), was clearly visible by ^{14}C-autoradiography (**Fig. 1*B***) or western blot (WB) against acetylated lysine (pan-AcK) following *in vitro* acetylation with KAT2A or KAT2B, but not with a catalytically inactive mutant of KAT2A (KAT2A-ED) (**Fig. S1*A* and *B***). Our MS analyses of these products identified acetylated lysine residues in the PALB2 chromatin association motif (ChAM) within the C-terminal cluster of seven lysine residues composed of K436, K437, K438, K441, K443, K445, and K449 (**Fig. 1*C***, highlighted in orange), denoted the 7K-patch, which is common to PALB2 orthologs (Bleuyard et al, 2012) (**Fig. 1*D***). A cluster of lysine residues is often found in KAT2A/B substrates (Fournier et al, 2016), corroborating our finding that the ChAM is favorably targeted for KAT2A/B-mediated acetylation.

The 7K-patch promotes ChAM nucleosome association

To evaluate the impact of the 7K-patch on ChAM chromatin association property, we generated a series of GFP-tagged ChAM truncations (**Fig. 2*A***). Consistent with our previous observations, the full-length ChAM fragment (PALB2 residues 395-450) was highly enriched in the chromatin fraction in HEK293T cells (**Figs. 2*A*, *B* and S2*A***). Further analysis of ChAM truncations revealed that the region containing the 7K-patch was essential for its chromatin association (**Fig. 2*A* and *B***). Considering the possibility that the deletion of 7K-patch might lead to aberrant subcellular localisation and have contributed to the reduced chromatin enrichment, we also affinity purified the corresponding fragments from the soluble fraction of HEK293T, and assessed their interaction with separately prepared nucleosomes (**Fig. S2*A***). Again, the pull-down assay showed that

bioRxiv preprint doi: https://doi.org/10.1101/735811; this version posted January 21, 2020. The copyright holder for this preprint (which was not certified by peer review) is the author/funder. All rights reserved. No reuse allowed without permission.

deletion of the 7K-patch impaired ChAM interaction with nucleosomes (**Fig. 2*A* and *C***).

To further assess the direct role of the 7K-patch acetylation on nucleosome binding, we purified recombinant GST-fusions of ChAM WT and mutants harboring glutamine substitutions at all seven lysine residues (7Q), three conserved lysine residues, K436, K437 and K438 (3Q4K), or the four remaining lysine residues, K441, K443, K445, and K449 (3K4Q) within the 7K-patch (**Fig. 2*A* and *D***). K to Q substitutions nullify the positive charge of lysine and are therefore commonly considered to mimic acetyl-lysine. Significantly, *in vitro* nucleosome pull-down assays showed that all variants with Q substitutions abolished ChAM interaction with nucleosomes (**Fig. 2*E***). As anticipated from the change in electrostatic charge, all ChAM variants with K to Q substitutions also exhibited an impaired affinity for DNA, as determined by native electrophoretic mobility shift assay (EMSA) (**Fig. 2*F***). Collectively, these results confirmed that Q substitutions of the 7K-patch perturbed the ability of ChAM to bind both nucleosomes and naked DNA; this variant is hence considered to behave as a ChAM null.

Acetylation within the 7K-patch enhances ChAM nucleosome association

KAT2A/B associate with chromatin and facilitate transcription by acetylating histones (Nagy et al, 2010). Consistently, we found that the level of acetylation in the GFP-ChAM fragment affinity purified from the chromatin-enriched fraction was notably higher than that from the cytoplasmic or the nuclear soluble fraction (**Fig. S2*A* and *B***). Our MS analysis of the chromatin-associated GFP-ChAM fragment identified acetylation of all seven lysine residues within the 7K-patch (**Fig. 3*A*,** marked with arrows). This observation appeared to be at odds with our

bioRxiv preprint doi: https://doi.org/10.1101/735811; this version posted January 21, 2020. The copyright holder for this preprint (which was not certified by peer review) is the author/funder. All rights reserved. No reuse allowed without permission.

observation that acetyl-mimetic Q substitutions disabled ChAM binding to nucleosomes (**Fig. 2*D* and *E***). Since the side chain of glutamine is significantly shorter than the corresponding acetyl-lysine side chain (**Fig. S2*C***), we questioned whether the K to Q substitutions accurately mimic the properties of acetylated ChAM. Hence, synthetic peptides corresponding the minimal ChAM (PALB2 residues 395-450) containing acetyl-lysine at the evolutionarily conserved K436, K437 and/or K438, were generated and their biochemical properties were characterised. Nucleosome pull-down assays revealed a modest increase in nucleosome binding with acetylated ChAM peptides compared to their non-acetylated counterpart (**Fig. 3*B***). Importantly, when salmon sperm DNA was supplemented in excess to outcompete the electrostatic ChAM interaction with DNA, only acetylated ChAM, but not non-acetylated ChAM, maintained its ability to bind nucleosomes. This effect was most evident with the ChAM peptide containing acetyl-K438, which was detected in our original MS study of the endogenous HeLa KAT2A/B-acetylome (Fournier et al, 2016). As anticipated, lysine acetylation, which neutralises the positive charge on the lysine side chain, conferred reduced affinity for negatively charged DNA (**Fig. 3*C* and *D***). Together, these results demonstrate that acetylation within the 7K-patch enhances ChAM nucleosome binding while limiting its non-specific affinity for DNA.

PALB2 mobility increases upon deacetylation

Encouraged by the *in vitro* results using acetylated ChAM peptides, we further assessed whether lysine acetylation might equally facilitate PALB2 chromatin association *in vivo*. To evaluate the impact of native PALB2 acetylation, we down-regulated KAT2A/B and assessed PALB2 mobility as a surrogate measure of its

bioRxiv preprint doi: https://doi.org/10.1101/735811; this version posted January 21, 2020. The copyright holder for this preprint (which was not certified by peer review) is the author/funder. All rights reserved. No reuse allowed without permission.

chromatin association. To this end, a tandem FLAG- and EGFP-tagged full-length wild-type (WT) PALB2 (FE-PALB2) was conditionally expressed in a U2OS cell line in which endogenous *PALB2* can be down-regulated by a doxycycline-inducible short hairpin RNA (U2OS-shPALB2) **(Fig. S3*A*)**, and its mobility was assessed using fluorescence recovery after photobleaching (FRAP). This analysis revealed that KAT2A/B siRNA treatment indeed led to an increase in FE-PALB2 diffusion rate (reduced FRAP $t_{1/2}$; **Figs. 3*E*, *F*, S3*B* and *C***), concomitant with reduced levels of global acetylation (Fournier et al, 2016). Conversely, the inhibition of lysine deacetylases (KDAC), which increased the global level of lysine acetylation, decreased the diffusion rate of FE-PALB2 (increased FRAP $t_{1/2}$; **Figs. 3*G*, *H*, S3*D* and *E***). These results support the notion that PALB2 chromatin association is enhanced by KAT2A/B-mediated acetylation events.

PALB2 ChAM 7K-patch acetylation is required for the protection of genomic DNA during DNA replication

To directly investigate the role of the 7K-patch acetylation *in vivo*, we generated full-length PALB2 variants in which lysine residues within the 7K-patch were substituted by Q or arginine (R). Contrary to the K to Q null-substitutions, which nullifies the positive charge of lysine, K to R substitutions maintain the charge yet are unable to accept acetylation and hence mimic constitutively non-acetyl-lysine (**Fig. S2*C***). These PALB2 variants, named 7Q or 7R, as well as PALB2 WT or an empty vector (EV), were stably expressed as FLAG-fusions at equivalent levels in U2OS-shPALB2 cells (**Figs. 4*A* and S4*A***). Our subcellular fractionation analyses showed a reduced level of PALB2 7Q in the chromatin-enriched fraction compared to PALB2 WT and 7R (**Fig. 4*B* and *C***). In line with these observations, our FRAP

bioRxiv preprint doi: https://doi.org/10.1101/735811; this version posted January 21, 2020. The copyright holder for this preprint (which was not certified by peer review) is the author/funder. All rights reserved. No reuse allowed without permission.

analysis of the PALB2 variants, conditionally expressed as FE-fusions in U2OS-shPALB2, revealed an increase in PALB2 7Q diffusion kinetics compared to those of PALB2 WT and 7R (**Fig. 4*D* and *E***). A PALB2 variant with an internal deletion of ChAM, which abolishes its chromatin association (Bleuyard et al, 2012), similarly exhibited a significant increase in PALB2 diffusion rate (**Fig. S4*B-D***). Hence, we concluded that the increase in PALB2 mobility reflected the chromatin-free fraction of PALB2, which is controlled by its ChAM 7K-patch.

In light of our previous finding that steady-state PALB2 chromatin association is important for the protection of actively transcribed genes during DNA replication (Bleuyard et al, 2017a), we assessed cell cycle progression of U2OS-shPALB2 cells complemented with either PALB2 WT, 7Q and 7R. To this end, cells were arrested at G1/S boundary by double thymidine block, in the presence of doxycycline throughout (43 h), and were synchronously released into S phase. To our surprise, not only PALB2 7Q but also 7R showed slow progression of S-phase compared to WT complemented cells (**Fig. 5*A*, *B* and *C***). In line with this observation, PALB2 7Q or 7R-complemented cells displayed increased levels of the well-established DDR marker, serine 139 phosphorylated histone variant H2AX (γ-H2AX), upon doxycycline exposure (**Fig. 5*D* and *E***). While PALB2 7R appeared to maintain global chromatin association equivalent to PALB2 WT (**Fig. 4*B* and *C***), PALB2 function in gene protection requires its enriched association with a subset of actively transcribed genes (Bleuyard et al, 2017a). Markedly, our ChIP-qPCR revealed reduced enrichment of both PALB2 7Q and 7R at known PALB2-bound loci, namely the *ACTB, TCOF1* and *WEE1* genes (**Fig. S5**). Together, these results suggest that ChAM acetylation promotes PALB2 enrichment at active

bioRxiv preprint doi: https://doi.org/10.1101/735811; this version posted January 21, 2020. The copyright holder for this preprint (which was not certified by peer review) is the author/funder. All rights reserved. No reuse allowed without permission.

genes, which in turn protects these regions from DNA damage during DNA replication.

DNA damage triggers ChAM deacetylation and an increase in PALB2 mobility

So far, our analyses showed that ChAM acetylation promotes PALB2 association with nucleosomes/chromatin (**Fig. 6*A***), whereas PALB2 dissociates from active genes upon CPT treatment (Bleuyard et al, 2017b). These observations prompted us to further investigate whether ChAM acetylation is dynamically controlled during the DDR. Significantly, rapid deacetylation of ChAM, which was expressed exogenously in HEK293 cells, was detectable within 15 min following ionizing radiation (IR) and persisted for at least 2 h (**Fig. 6*B* and *C***). Furthermore, using the FRAP approach, we observed clear increases in diffusion rates of FE-PALB2 following DNA damage induced by IR, MMC or olaparib treatment, where DNA damaging efficiency was confirmed by γ-H2AX staining (**Figs. 6*D-G*, S6*A-D***). Compared to untreated control conditions, IR, MMC and olaparib treatment decreased FRAP $t_{1/2}$ by 22%, 36%, and 18%, respectively. Together, these results indicate that DNA damage triggers ChAM deacetylation and induces PALB2 mobilisation.

7K-patch-mediated PALB2 chromatin association is important for HR repair

Given that DNA damage triggers ChAM deacetylation and PALB2 mobilisation, we further evaluated the impact of the 7K-patch in the DDR. As expected, the depletion of endogenous PALB2 conferred impaired RAD51 foci formation both in undamaged and upon MMS or IR exposure (**Fig. S7*A***), which was rescued by PALB2 WT complementation (**Fig. 7*A* and *B***). Markedly, cells complemented with

bioRxiv preprint doi: https://doi.org/10.1101/735811; this version posted January 21, 2020. The copyright holder for this preprint (which was not certified by peer review) is the author/funder. All rights reserved. No reuse allowed without permission.

PALB2 7R were similarly able to restore MMS-induced RAD51 foci formation, but the 7Q variant failed to do so (**Fig. 7*A* and *B***). Consistent with this observation, PALB2 7Q-complemented cells also exhibited increased olaparib sensitivity compared to those complemented with PALB2 WT or 7R (**Fig. 7*C***). Given that increased sensitivity to PARP inhibition is a hallmark of HR deficiency, this finding suggested that the 7Q substitutions conferred HR defects. It is noteworthy that all PALB2 variants exhibited equivalent levels of interaction with BRCA2 or RAD51 (**Fig. S7*B***) and were recruited to sites of DNA damage with similar efficiency (**Fig. S7*C* and *D***). These findings indicated that lysine residues within the ChAM 7K-patch are indispensable for PALB2 function in HR, but that this mechanism is independent of PALB2 binding to BRCA2 or RAD51 or its recruitment to sites of DNA damage.

Discussion

In this study, we have demonstrated that reversible lysine acetylation controls the mode of PALB2 chromatin association: the 7K-patch in the C-terminal part of ChAM was acetylated by KAT2A/B in undamaged cells, and was important for normal damage-induced RAD51 recruitment and olaparib resistance. Crucially, ChAM acetylation enhances PALB2 binding to nucleosomes and limits non-specific interactions with DNA. DNA damage, however, triggers PALB2 deacetylation and increases the overall mobility of PALB2. Considering all our findings collectively, we propose the model shown in **Fig. 7*D***: KAT2A/B-mediated ChAM acetylation, jointly with MRG15, enforces PALB2 enrichment at undamaged transcriptionally active chromatin and hence protects these regions during DNA replication. DNA damage triggers ChAM deacetylation and a concomitant reduction in PALB2-

bioRxiv preprint doi: https://doi.org/10.1101/735811; this version posted January 21, 2020. The copyright holder for this preprint (which was not certified by peer review) is the author/funder. All rights reserved. No reuse allowed without permission.

MRG15 interaction (Bleuyard et al, 2017b), which releases PALB2 from chromatin and increases its mobility. In this way, PALB2 may become available to form functional HR complexes with BRCA1, which is otherwise less stably associated with PALB2 (Bleuyard et al, 2017b). Following recruitment of the entire HR complex to sites of DNA damage, deacetylated ChAM binding to exposed naked DNA may allow appropriate engagement of this complex with damaged DNA and hence promote RAD51 loading and HR repair.

The increase in PALB2 mobility during the DDR shown in this study is reminiscent of previous reports showing increased RAD51 mobility upon replication stress (Srivastava et al, 2009; Yu et al, 2003). Yu *et al*. showed that a fraction of RAD51, which is in complex with BRCA2, is immobile in unchallenged cells, but becomes mobile upon hydroxyurea-induced replicative stress (Yu et al, 2003). Notably, their data suggested that such increased RAD51 mobility was unlikely to be a consequence of altered interaction with BRCA2 upon replicative stress. Similarly, Jeyasekharan *et al*. reported increased BRCA2 mobility upon IR-induced DNA damage, which was induced in a manner dependent on the DNA damage signalling kinases ATM and ATR and coincided with active HR events (Jeyasekharan et al, 2010). Given that BRCA2 and PALB2 form a stable complex (B2P2) together with a fraction of RAD51 and that their interaction is important for HR repair, we suggest that the B2P2 complex and associated RAD51 are mobilised together upon genotoxic stress.

The mechanisms that regulate the mobilisation and localisation of HR factors remain incompletely understood but undoubtedly involve PTMs. We propose that variable modes of PTM-mediated chromatin association synergistically govern the recruitment of repair factors to defined regions of

bioRxiv preprint doi: https://doi.org/10.1101/735811; this version posted January 21, 2020. The copyright holder for this preprint (which was not certified by peer review) is the author/funder. All rights reserved. No reuse allowed without permission.

chromatin. In undamaged cells, PALB2 is enriched at actively transcribed chromatin through KAT2A/B-mediated ChAM acetylation and H3K36me^3-mediated MRG15 interaction, while maintaining transient chromatin interaction. This transient mode of association may allow a severance mechanism, in which PALB2 continuously monitors the presence of DNA damage across these regions. Indeed, cells expressing PALB2 7R exhibited an increase in the basal level of γ–H2AX compared to those expressing PALB2 WT, underlining the importance of PALB2 acetylation in unperturbed cells. Upon DNA damage, however, ChAM is deacetylated and, as a consequence, PALB2 affinity for undamaged chromatin is reduced. We suggest that damage-induced ChAM deacetylation allows its recruitment to sites of DNA damage through interaction with BRCA1, fulfilling its function in promoting HR repair. Intriguingly, cells expressing the non-acetylatable PALB2 7R variant exhibited no detectable HR defects, which is in agreement with our finding that DNA damage triggers ChAM deacetylation. These observations highlight the importance of dynamic regulation of PALB2, where both acetylated and non-acetylated forms of PALB2 play critical roles in genome integrity control. Our work also suggests that caution should be exercised in the use of K to Q substitutions for functional studies of lysine acetylation. Robust *in vivo* assessment of acetylation events would ideally involve the development of a chemically modifiable residue that exhibits improved similarity to acetylated lysine in a reversible manner.

More broadly, lysine acetylation is known to control biological processes, such as transcription, based on the metabolic status of the cell (Lee et al, 2014). Therefore, a better appreciation of the role of lysine acetylation in the DDR could expand the scope of studies aiming to understand how reprogrammed metabolism

bioRxiv preprint doi: https://doi.org/10.1101/735811; this version posted January 21, 2020. The copyright holder for this preprint (which was not certified by peer review) is the author/funder. All rights reserved. No reuse allowed without permission.

could increase genome instability in cancer cells (Nowell, 1976). Since PTMs are essential for physiological homeostasis and metabolites are necessary cofactors for the deposition of these PTMs, we envision that reprogrammed metabolism in cancer cells could alter the PTM landscape of DDR proteins and hence contribute to genome instability. Considering that glucose concentration in the growth medium can influence the level of protein acetylation in cells (Lee et al, 2014), it will be important to understand whether PALB2 function could be affected by cellular metabolic status. Indeed, our preliminary results demonstrated that extracellular glucose concentration affect PALB2 dynamics, as reducing glucose level in the growth medium increases PALB2 dynamics. It is therefore reasonable to speculate that, in tumour cells with reprogrammed metabolism, protein properties such as chromatin association could be detrimentally altered. Future studies assessing aberrant PALB2 lysine acetylation in cancer tissues and whether KDAC or bromodomain inhibitors, currently in clinical trials for cancer therapy, or alteration of glucose metabolic pathways would modulate PALB2 acetylation may offer therapeutic potentials. Furthermore, deciphering the metabolic regulation of the DDR and DNA repair could highlight additional cellular pathways that might be targeted for cancer therapy, possibly in combination with existing therapies that otherwise may give rise to resistance.

Author contributions

M.F. and F.E. conceived the study and designed the experimental strategies; M.F., J-Y.B, A.M.C., J.E., and S.H. performed the experiments; J-Y.B, S.S., and L.T. contributed to reagents and analytical tools; M.F. and J.E. analysed data; M.F., J.Y.B,

bioRxiv preprint doi: https://doi.org/10.1101/735811; this version posted January 21, 2020. The copyright holder for this preprint (which was not certified by peer review) is the author/funder. All rights reserved. No reuse allowed without permission.

A.M.C., S.S., and F.E. contributed to text and figures; M.F. and F.E. wrote the manuscript.

Acknowledgements

FE is supported by a Wellcome Trust Senior Research Fellowship in Basic Biomedical Science (101009/Z/13/Z) and is thankful for support from the Edward P Abraham Research Fund. SJS is supported by the Francis Crick Institute which receives its core funding from Cancer Research UK (FC001156), the UK Medical Research Council (FC001156), and the Wellcome Trust (FC001156). LT receives funding from the European Research Council (ERC) Advanced Grant (ERC-2013-340551, Birtoaction). We are also grateful to Nicola O'Reilly (Francis Crick Institute Peptide Chemistry Technology Platform) for synthesis of ChAM peptides, Andrew Jefferson and Carina Mónico (Micron Oxford Advanced Bioimaging) for assistance with microscopy, Christine Ralf (Sir William Dunn School) for technical support in generating constructs, and Chris Norbury (Sir William Dunn School) for critical reading of the manuscript.

Competing interests

The authors declare no financial and non-financial competing interests on this study.

Data availability

The mass spectrometry proteomics data have been deposited to the ProteomeXchange Consortium via the PRIDE (Perez-Riverol et al, 2019) partner repository with the dataset identifier PXD014678 and PXD014681.

bioRxiv preprint doi: https://doi.org/10.1101/735811; this version posted January 21, 2020. The copyright holder for this preprint (which was not certified by peer review) is the author/funder. All rights reserved. No reuse allowed without permission.

Figure legends

Figure 1. KAT2A/B acetylates PALB2 within a 7K-patch in its ChAM domain.

A. PALB2 lysine residues identified as acceptors of KAT2A/B-dependent acetylation *in vivo* and *in vitro* by tandem MS analyses are shown in blue and black, respectively. The acetylated lysine residues within the ChAM are highlighted in red. Full-length PALB2 (FL, 200kDa) and fragments 1 to 4 used for *in vitro* acetylation assays are also shown. 1: PALB2 1-320 (61.2kDa), 2: 295-610 (60.6kDa), 3: 580-900 (61.2 kDa) and 4: 867-1186 (61.1kDa). ***B.*** PALB2 FL and fragments 1 to 4 were acetylated *in vitro* by KAT2B with ^{14}C-labelled acetyl-CoA, and following SDS-PAGE, acetylated proteins and total proteins were detected by ^{14}C-autoradiography and Coomassie blue staining, respectively. RAD51 was not identified as a target of KAT2A/B *in vivo* (Fournier et al, 2016) and was used as a negative control. ***C.*** A heat map of acetylated lysine residues, as identified by quantitative MS analysis of *in vitro* acetylated PALB2 FL or fragment 2 by KAT2B, KAT2A or a catalytically inactive KAT2A (KAT2A-ED). The abundance of each acetyl-lysine was evaluated as previously described (Fournier et al, 2016). ***D.*** ChAM protein sequences from twelve PALB2 orthologues were aligned using MUSCLE and visualised using ClustalW default colour-coding. Lysine residues acetylated by KAT2A and KAT2B *in vitro* are respectively highlighted by red and green circles. Hs (*Homo sapiens*, human), Pt (*Pan troglodytes*, chimpanzee), Pp (*Pan paniscus*, bonobo), Bt (*Bos taurus*, cow), Ml (*Myotis lucifugus*, little brown bat), Ss (*Sus scrofa*, wild boar), Ec (*Equus caballus*, horse), Cl (*Canis lupus familiaris*, dog), Am (*Ailuropoda melanoleuca*, giant panda), Oa (*Ovis aries*, sheep), Gg (*Gallus gallus*, red junglefowl), Tg (*Taeniopygia guttata*, zebra finch).

bioRxiv preprint doi: https://doi.org/10.1101/735811; this version posted January 21, 2020. The copyright holder for this preprint (which was not certified by peer review) is the author/funder. All rights reserved. No reuse allowed without permission.

Figure 2. The 7K-patch promotes ChAM nucleosome association.

A. Diagram showing the full-length (FL) PALB2, GFP-ChAM fragments #1 to #5 and GST-ChAM variants used in this study. ChAM C-terminal lysine-rich patch (7K-patch, residues 436-449) is highlighted in red. ***B.*** Western blotting assessing the chromatin enrichment of GFP-ChAM fragments transiently expressed in HEK293T cells. Empty GFP vector (EV) was used as a negative control. Whole cell extract was also prepared to compare GFP-ChAM fragments expression levels. Lamin A and histone H3 were used as controls for the cellular fractionation. ***C.*** *In vitro* nucleosome binding assay using GFP and GFP-ChAM fragments. Partially purified human nucleosomes captured by GFP and GFP-ChAM fragments immobilised on beads were detected by anti-histone H3 western blot and Ponceau S staining. ***D.*** Coomassie blue staining of GST and GST-ChAM variants purified from *E.coli* and separated by SDS-PAGE. ***E.*** *In vitro* binding assays using immobilised GST-ChAM variants and purified HeLa mononucleosomes. GST was used as a negative control. The nucleosome binding efficiency was assessed by anti-histone H3 western blot. ***F.*** Electrophoretic mobility shift assay (EMSA) using pBluescript plasmid DNA (pBS) and purified GST-ChAM variants. Three DNA conformations are indicated to the right: supercoiled (s.c.), linear (l.), and nicked (n.).

Figure 3. Acetylation within the 7K-patch enhances ChAM nucleosome association.

A. *In vivo* acetylated lysine residues in chromatin-associated ChAM, detected by tandem MS analysis, are highlighted by arrows. Synthetic biotin-ChAM peptides non-acetylated (WT) or acetylated at single lysine residues 436 (436-ac), 437

bioRxiv preprint doi: https://doi.org/10.1101/735811; this version posted January 21, 2020. The copyright holder for this preprint (which was not certified by peer review) is the author/funder. All rights reserved. No reuse allowed without permission.

(437-ac), and 438 (438-ac), or all three lysine residues (All 3-ac) are shown. ***B.*** *In vitro* nucleosome binding assays for the synthetic biotin-ChAM peptides. After incubation with purified HeLa polynucleosomes in the absence or presence of 5 μg salmon sperm DNA, biotin-ChAM peptides were pulled-down by streptavidin beads (Strep pulldown), and associated nucleosome was detected by anti-histone H3 western blot. ***C.*** EMSA using 300 ng pBluescript plasmid DNA and increasing amount of indicated biotin-ChAM peptides, i.e. 2.97 μM (light gray circle), 5.94 μM (dark gray circle) and 29.7 μM (black circle). Three DNA conformations are indicated: supercoiled (s.c.), linear (l.), and nicked (n.). ***D.*** As in *C*, except using the indicated biotin-ChAM peptides. ***E-F.*** FRAP assay of FE-PALB2 in U2OS cells in which KAT2A and KAT2B were depleted by siRNA (siKAT2A/siKAT2B). Non-treated (NT) and negative control siRNA (siCntl) treated cells were used as controls. ***G-H***. As in *E-F*, except cells were treated with a cocktail of lysine deacetylase inhibitors (KDACi, 5 mM sodium butyrate, 5 μM trichostatin A and 5 mM nicotinamide) or DMSO as a control. For each condition, representative images of live cells before bleaching (pre-bleaching) and during a 37.5 s recovery period (post-bleaching) are shown together with half-recovery time plots for at least 20 cells. Dashed circles indicate bleached areas. Statistical analyses were performed using GraphPad Prism 7.02 and *p*-values are for the unpaired Student's *t*-test (** $p < 0.0035$, *** $p < 0.0006$, and **** $p < 0.0001$).

Figure 4. PALB2 ChAM 7K-patch mediate global chromatin association.

A. Western blot analysis of U2OS-shPALB2 cells constitutively expressing FLAG (EV) or FLAG-PALB2 variants. Where indicated, cells were treated with 2 μg/mL doxycycline (+dox) to deplete endogenous PALB2. Lamin A was used as a loading

bioRxiv preprint doi: https://doi.org/10.1101/735811; this version posted January 21, 2020. The copyright holder for this preprint (which was not certified by peer review) is the author/funder. All rights reserved. No reuse allowed without permission.

control. ***B-C.*** Subcellular distribution of FLAG-PALB2 variants in cytoplasmic (Cyt), nuclear soluble (Nuc) and chromatin-enriched (Chr) fractions upon doxycycline-induced PALB2 depletion. Histone H3 was used as a control for cellular fractionation. Protein levels, detected by western blotting, were quantified by ImageJ. PALB2 levels in the chromatin fraction were normalised against PALB2 levels in whole-cell extracts shown in *A* and expressed as a percentage of the WT in *C*. Statistical analyses were performed using GraphPad Prism 7.02, and *p*-values are for the unpaired Student's *t*-test (**** $p < 0.0001$, ns = non-specific). ***D-E***. FRAP analysis of FE-PALB2 WT, 7R and 7Q conditionally expressed in U2OS-shPALB2 cells in which endogenous PALB2 was depleted *via* doxycycline exposure. Representative images before bleaching (pre-bleaching) and during the recovery period (post-bleaching) are shown in *D*, where dashed circles indicate bleached areas. Half-recovery time plots for at least 20 cells per cell line are shown in *E*. Statistical analyses were performed using GraphPad Prism 7.02 and *p*-values are for the unpaired Student's *t*-test (**** $p < 0.0001$).

Figure 5. PALB2 ChAM 7K-patch acetylation is required to maintain genome stability during replication.

A. DNA content of U2OS-shPALB2 cell lines stably expressing FLAG (EV) and FLAG-PALB2 variants, as assessed by flow cytometry (FACS) analysis of cells stained with propidium iodide (PI). Samples were prepared under three different conditions: asynchronous (As), synchronised at G1/S by double thymidine block (0 h) and at 3 hour after thymidine release (3 h). ***B-C.*** Histogram showing the percentage of U2OS-shPALB2 EV, FLAG-PALB2 WT, 7Q and 7R cells in S (DNA content between 2N and 4N) and G2 (DNA content 4N) phases of the cell cycle,

bioRxiv preprint doi: https://doi.org/10.1101/735811; this version posted January 21, 2020. The copyright holder for this preprint (which was not certified by peer review) is the author/funder. All rights reserved. No reuse allowed without permission.

based on the quantification of FACS profiles shown in *A*. ***D.*** γ-H2AX levels in U2OS-shPALB2 expressing the FLAG (EV) or FLAG-PALB2 WT, 7Q and 7R upon doxycycline (dox)-induced endogenous PALB2 depletion were detected by western blot. Total H2AX was used as a loading control. ***E.*** Quantification of γ-H2AX and H2AX levels shown in *D*, performed by densitometry analysis in ImageJ. Histogram shows the ratios of γ-H2AX versus H2AX levels.

Figure 6. DNA damage triggers ChAM deacetylation and PALB2 mobilization. ***A.*** Depiction of PALB2 acetylation and nucleosome binding, controlled by KAT2A/B and KDACs. ***B.*** HEK293 cells transiently expressing GFP-tagged ChAM were treated with 4 Gy IR, and affinity-purified GFP-ChAM was assessed using anti-GFP and anti-acetyl-lysine (pan-AcK) antibodies. γ-H2AX signal in whole cell lysate was detected to monitor DNA damage. ***C.*** Histogram showing the relative level of ChAM acetylation following irradiation. The levels of acetylated and total GFP-ChAM were quantified by ImageJ, and the ratio of acetyl/total GFP-ChAM was normalised against that of the pre-irradiation sample (time 0). Error bars indicate standard deviation of three independent experiments (n=3). ***D-E.*** The mobility of FE-PALB2 in U2OS-shPALB2 was monitored by FRAP. Cells were examined under non-treated conditions (NT) or treated with 4 Gy IR or 1 mM MMC. ***F-G.*** As in *D-E*, except cells were treated with the PARP inhibitor olaparib or DMSO as a control. For each condition, representative images of live cells before bleaching (pre-bleaching) and during a 37.5 s recovery period (post-bleaching) are shown together with half-recovery time plots for at least 20 cells. Dashed circles indicate bleached areas. Statistical analyses were performed using GraphPad Prism 7.02

bioRxiv preprint doi: https://doi.org/10.1101/735811; this version posted January 21, 2020. The copyright holder for this preprint (which was not certified by peer review) is the author/funder. All rights reserved. No reuse allowed without permission.

and *p*-values are for the unpaired Student's *t*-test (** $p < 0.0035$, *** $p < 0.0006$, and **** $p < 0.0001$).

Figure 7. 7K-patch-mediated PALB2 chromatin association is important for HR repair.

A. Representative images of IR-induced RAD51 foci in U2OS-shPALB2 cells stably expressing FLAG (EV) and FLAG-PALB2 variants, following doxycycline-induced endogenous PALB2 depletion and 4 Gy IR treatment. DAPI was used for nuclear staining and γ-H2AX as a DNA damage marker. ***B.*** Quantification of the number of RAD51 foci per cell, shown in *A* (n ≥ 62). Statistical analyses were performed using GraphPad Prism 7.02 and *p*-values are for the unpaired Student's *t*-test (**** $p < 0.0001$). ***C.*** Cell survival upon olaparib treatment of U2OS-shPALB2 cells stably expressing FLAG (EV) or FLAG-PALB2 variants, as assessed by WST-1 assay after five days of olaparib exposure. Where indicated, endogenous PALB2 was depleted by doxycycline exposure. ***D***. Model for PALB2 acetylation function in the maintenance of genome stability. *Left*: MRG15 and KAT2A/B-mediated ChAM acetylation jointly promote PALB2 enrichment at undamaged transcriptionally active chromatin. DNA damage triggers ChAM deacetylation and releases PALB2 from chromatin. This allows PALB2 to interact with BRCA1, which in turn recruits the entire HR complex to sites of DNA damage. ChAM binding to naked DNA through the 7K-patch may promote RAD51 loading and HR repair. *Right*: The 7K-patch null mutant with K to Q substitutions is more freely diffusible, and although it can be recruited to sites of DNA damage, it fails to engage with damaged DNA, leading to defective HR.

bioRxiv preprint doi: https://doi.org/10.1101/735811; this version posted January 21, 2020. The copyright holder for this preprint (which was not certified by peer review) is the author/funder. All rights reserved. No reuse allowed without permission.

Figure S1. PALB2 is directly acetylated by KAT2A and 2B.

A-B. *In vitro* acetylation of PALB2 by KAT2B (*A*) or KAT2A and a catalytically inactive KAT2A-ED (*B*). Purified PALB2 full-length and fragments 1 to 4 (Fig. 1*A*) were incubated with either purified KAT2B, KAT2A or KAT2A-ED in the presence of acetyl-CoA, followed by SDS-PAGE. Total and acetylated proteins were visualized by Ponceau S staining and anti-acetyl lysine (pan-AcK) western blot, respectively. Acetylated PALB2 fragment 2 by KAT2B or KAT2A is highlighted with red dashed boxes.

Figure S2. Chromatin-associated ChAM is highly acetylated *in vivo.*

A. Depiction of experimental procedures for subcellular fractionation of HEK293 cells transiently expressing GFP-ChAM variants. Chromatin enriched GFP-ChAM was detected by WB (Fig. 2*B*), or following benzonase treatment, affinity purified using GFP-trap and was analysed for acetylation by MS (Fig. 3*A*). For nucleosome binding assay, shown in Fig 2*C*, nucleosomes were partially purified from separate, non-transfected HEK293, and incubated with GFP-ChAM purified from cytoplasmic fraction of transfected HEK293. ***B***. Subcellular distribution of GFP-ChAM overexpressed in HEK293 cells, in cytoplasmic (Cyt), nuclear soluble (Nuc) and chromatin-enriched (Chr) fractions. Histone H3 was used as a control for cellular fractionation. GFP-ChAM and acetylated GFP-ChAM were respectively detected by anti-GFP and anti-acetyl-lysine (pan-AcK) antibodies. ***C.*** Depiction of lysine (K), acetyl-lysine (K-ac), arginine (R) and glutamine (Q) structures, showing differences in size and charge for each residue.

Figure S3. PALB2 mobility increases upon deacetylation.

bioRxiv preprint doi: https://doi.org/10.1101/735811; this version posted January 21, 2020. The copyright holder for this preprint (which was not certified by peer review) is the author/funder. All rights reserved. No reuse allowed without permission.

A. Depiction of cell lines used for FRAP assays of full-length PALB2. U2OS Flp-In T-REx, harboring inducible shRNA targeting 3'UTR of endogenous PALB2 (U2OS-shPALB2) was used as parental cells. FE-PALB2 under tetO promoter, integrated at a defined FRT site, was induced by doxycycline exposure. ***B.*** Diagram of experimental procedure, assessing the impact of KAT2A/B using FRAP against FE-PALB2. KAT2A protein levels were measured by western blot analysis of U2OS-shPALB2 FE-PALB2 cells treated with siRNA targeting KAT2A and KAT2B (siKAT2A/siKAT2B) or scramble small interfering RNA (siCntl) (negative control) for 48 or 72 h. Tubulin was used as a loading control. ***C***. Relative fluorescence intensity of FE-PALB2 in WT, siCntl, and siKAT2A/B treated cells, related to FRAP analysis shown in Fig. 3*E* and *F*. ***D***. Diagram of experimental procedure, assessing the impact of KDAC inhibition using FRAP against FE-PALB2. Level of pan-acetylated histones in U2OS-shPALB2 FE-PALB2 cells treated with DMSO or deacetylases inhibitors (KDACi) is shown. Ponceau S staining of proteins after transfer onto nitrocellulose membrane was used as a loading control. ***E***. Relative fluorescence intensity of FE-PALB2 in mock and KDACi treated cells, related to FRAP analysis shown in Fig. 3*G* and *H*.

Figure S4. PALB2 ChAM 7K-patch is required to maintain genome stability.

A. Depiction of cell lines used in this study. U2OS-shPALB2 was used as parental cells. FE-PALB2 variants under tetO promoter or FLAG-PALB2 variants under CMV promoter were integrated at a defined FRT site. ***B-D***. FRAP analysis of FE-PALB2 wild-type (WT) or harboring an internal deletion of the ChAM (ΔChAM) conditionally induced in U2OS-shPALB2. Images of FE-PALB2 in live cells before bleaching (pre-bleaching) and during the recovery time after bleaching, plots of

bioRxiv preprint doi: https://doi.org/10.1101/735811; this version posted January 21, 2020. The copyright holder for this preprint (which was not certified by peer review) is the author/funder. All rights reserved. No reuse allowed without permission.

half-time recovery times (s) after photobleaching and relative fluorescence intensity are shown in *C*, *D* and *E*, respectively.

Figure S5. PALB2 ChAM 7K-patch is required to maintain genome stability.

ChIP-qPCR analysis defecting FLAG-PALB2 WT, 7Q and 7R enrichment at known PALB2-bound loci (Bleuyard et al, 2017a), namely the coding regions of *ACTB* ***(A)***, *TCOF1* ***(B)*** and *WEE1* (***C***) genes.

Figure S6. PALB2 mobility increases upon genotoxic stress.

A. Diagrams of experimental procedures, assessing the impact of IR, MMC and olaparib using FRAP against FE-PALB2. ***B***. γ-H2AX levels in untreated or damaged cells (4 Gy IR, 1 mM MMC, or 2.5 μM olaparib) as measured by anti-γ-H2AX immunofluorescence staining. ***C***. Relative fluorescence intensity of FE-PALB2 in either undamaged or DNA damaging conditions (4 Gy IR or 1 mM MMC) measured after photobleaching of cells shown in Fig. 6*D* and *E*. ***D***. As in C, except cells were treated with DMSO vehicle or 2.5 μM olaparib, related to Fig. 6*F* and *G*.

Figure S7. PALB2 ChAM 7K-patch promotes HR upon DNA damage.

A. Number of RAD51 foci per cell in U2OS-shPALB2 without depletion of endogenous PALB2 (white circles) or upon depletion (black circles), in either untreated or DNA damaging conditions (1 mM MMC or 4 Gy IR). ***B.*** FLAG-PALB2 was pulled-down from U2OS-shPALB2 cells stably expressing either FLAG-tagged PALB2 variants, upon doxycycline-induced endogenous PALB2 depletion. Cells expressing only the FLAG-tag (EV) were used a negative control. BRCA2 and RAD51 interaction with PALB2 was assessed by western blot. ***C.*** Analysis of FE-

bioRxiv preprint doi: https://doi.org/10.1101/735811; this version posted January 21, 2020. The copyright holder for this preprint (which was not certified by peer review) is the author/funder. All rights reserved. No reuse allowed without permission.

PALB2 variants recruitment to DNA damage sites induced by laser micro-irradiation. Dashed boxes indicate irradiated areas. ***D.*** Quantitation of the amount of FE-PALB2 variants recruited to laser damage sites. The relative fluorescence intensity at laser damage sites was calculated by dividing the fluorescence intensity of the damaged area over the time course experiment by the fluorescence intensity of the non-damaged region of the nucleus and normalisation using the pre-damaged fluorescence value as a reference.

References

Ahlskog JK, Larsen BD, Achanta K, Sorensen CS (2016) ATM/ATR-mediated phosphorylation of PALB2 promotes RAD51 function. *EMBO Rep* **17:** 671-681

Bleuyard JY, Buisson R, Masson JY, Esashi F (2012) ChAM, a novel motif that mediates PALB2 intrinsic chromatin binding and facilitates DNA repair. *EMBO Rep* **13:** 135-141

Bleuyard JY, Butler RM, Esashi F (2017a) Perturbation of PALB2 function by the T413S mutation found in small cell lung cancer. *Wellcome Open Res* **2:** 110

Bleuyard JY, Fournier M, Nakato R, Couturier AM, Katou Y, Ralf C, Hester SS, Dominguez D, Rhodes D, Humphrey TC, Shirahige K, Esashi F (2017b) MRG15-mediated tethering of PALB2 to unperturbed chromatin protects active genes from genotoxic stress. *Proc Natl Acad Sci U S A* **114:** 7671-7676

Buisson R, Niraj J, Rodrigue A, Ho CK, Kreuzer J, Foo TK, Hardy EJ, Dellaire G, Haas W, Xia B, Masson JY, Zou L (2017) Coupling of Homologous Recombination and the Checkpoint by ATR. *Mol Cell* **65:** 336-346

Cardona A, Saalfeld S, Schindelin J, Arganda-Carreras I, Preibisch S, Longair M, Tomancak P, Hartenstein V, Douglas RJ (2012) TrakEM2 software for neural circuit reconstruction. *PLoS One* **7:** e38011

Dantuma NP, van Attikum H (2016) Spatiotemporal regulation of posttranslational modifications in the DNA damage response. *EMBO J* **35:** 6-23

Fournier M, Orpinell M, Grauffel C, Scheer E, Garnier JM, Ye T, Chavant V, Joint M, Esashi F, Dejaegere A, Gonczy P, Tora L (2016) KAT2A/KAT2B-targeted acetylome reveals a role for PLK4 acetylation in preventing centrosome amplification. *Nature Comm* **7:** 13227

bioRxiv preprint doi: https://doi.org/10.1101/735811; this version posted January 21, 2020. The copyright holder for this preprint (which was not certified by peer review) is the author/funder. All rights reserved. No reuse allowed without permission.

Guo Y, Feng W, Sy SM, Huen MS (2015) ATM-dependent Phosphorylation of the Fanconi Anemia Protein PALB2 Promotes the DNA Damage Response. *J Biol Chem* **290:** 27545-27556

Hayakawa T, Zhang F, Hayakawa N, Ohtani Y, Shinmyozu K, Nakayama J, Andreassen PR (2010) MRG15 binds directly to PALB2 and stimulates homology-directed repair of chromosomal breaks. *J Cell Sci* **123:** 1124-1130

Jeyasekharan AD, Ayoub N, Mahen R, Ries J, Esposito A, Rajendra E, Hattori H, Kulkarni RP, Venkitaraman AR (2010) DNA damage regulates the mobility of Brca2 within the nucleoplasm of living cells. *Proc Natl Acad Sci U S A* **107:** 21937-21942

Jones S, Hruban RH, Kamiyama M, Borges M, Zhang X, Parsons DW, Lin JC, Palmisano E, Brune K, Jaffee EM, Iacobuzio-Donahue CA, Maitra A, Parmigiani G, Kern SE, Velculescu VE, Kinzler KW, Vogelstein B, Eshleman JR, Goggins M, Klein AP (2009) Exomic sequencing identifies PALB2 as a pancreatic cancer susceptibility gene. *Science* **324:** 217

Lee JV, Carrer A, Shah S, Snyder NW, Wei S, Venneti S, Worth AJ, Yuan ZF, Lim HW, Liu S, Jackson E, Aiello NM, Haas NB, Rebbeck TR, Judkins A, Won KJ, Chodosh LA, Garcia BA, Stanger BZ, Feldman MD, Blair IA, Wellen KE (2014) Akt-dependent metabolic reprogramming regulates tumor cell histone acetylation. *Cell Metab* **20:** 306-319

Nagy Z, Riss A, Fujiyama S, Krebs A, Orpinell M, Jansen P, Cohen A, Stunnenberg HG, Kato S, Tora L (2010) The metazoan ATAC and SAGA coactivator HAT complexes regulate different sets of inducible target genes. *Cell Mol Life Sci* **67:** 611-628

Nowell PC (1976) The clonal evolution of tumor cell populations. *Science* **194:** 23-28

O'Donovan PJ, Livingston DM (2010) BRCA1 and BRCA2: breast/ovarian cancer susceptibility gene products and participants in DNA double-strand break repair. *Carcinogenesis* **31:** 961-967

Orthwein A, Noordermeer SM, Wilson MD, Landry S, Enchev RI, Sherker A, Munro M, Pinder J, Salsman J, Dellaire G, Xia B, Peter M, Durocher D (2015) A mechanism for the suppression of homologous recombination in G1 cells. *Nature* **528:** 422-426

Perez-Riverol Y, Csordas A, Bai J, Bernal-Llinares M, Hewapathirana S, Kundu DJ, Inuganti A, Griss J, Mayer G, Eisenacher M, Perez E, Uszkoreit J, Pfeuffer J, Sachsenberg T, Yilmaz S, Tiwary S, Cox J, Audain E, Walzer M, Jarnuczak AF, Ternent T, Brazma A, Vizcaino JA (2019) The PRIDE database and related tools and resources in 2019: improving support for quantification data. *Nucleic Acids Res* **47:** D442-D450

bioRxiv preprint doi: https://doi.org/10.1101/735811; this version posted January 21, 2020. The copyright holder for this preprint (which was not certified by peer review) is the author/funder. All rights reserved. No reuse allowed without permission.

Rahman N, Seal S, Thompson D, Kelly P, Renwick A, Elliott A, Reid S, Spanova K, Barfoot R, Chagtai T, Jayatilake H, McGuffog L, Hanks S, Evans DG, Eccles D, Breast Cancer Susceptibility C, Easton DF, Stratton MR (2007) PALB2, which encodes a BRCA2-interacting protein, is a breast cancer susceptibility gene. *Nat Genet* **39:** 165-167

Reid S, Schindler D, Hanenberg H, Barker K, Hanks S, Kalb R, Neveling K, Kelly P, Seal S, Freund M, Wurm M, Batish SD, Lach FP, Yetgin S, Neitzel H, Ariffin H, Tischkowitz M, Mathew CG, Auerbach AD, Rahman N (2007) Biallelic mutations in PALB2 cause Fanconi anemia subtype FA-N and predispose to childhood cancer. *Nature Genet* **39:** 162-164

Schneider CA, Rasband WS, Eliceiri KW (2012) NIH Image to ImageJ: 25 years of image analysis. *Nat Methods* **9:** 671-675

Srivastava V, Modi P, Tripathi V, Mudgal R, De S, Sengupta S (2009) BLM helicase stimulates the ATPase and chromatin-remodeling activities of RAD54. *J Cell Sci* **122:** 3093-3103

Sy SM, Huen MS, Chen J (2009a) MRG15 is a novel PALB2-interacting factor involved in homologous recombination. *J Biol Chem* **284:** 21127-21131

Sy SM, Huen MS, Chen J (2009b) PALB2 is an integral component of the BRCA complex required for homologous recombination repair. *Proc Natl Acad Sci U S A* **106:** 7155-7160

Tanner KG, Langer MR, Denu JM (2000) Kinetic mechanism of human histone acetyltransferase P/CAF. *Biochemistry* **39:** 11961-11969

Wellen KE, Hatzivassiliou G, Sachdeva UM, Bui TV, Cross JR, Thompson CB (2009) ATP-citrate lyase links cellular metabolism to histone acetylation. *Science* **324:** 1076-1080

Xia B, Dorsman JC, Ameziane N, de Vries Y, Rooimans MA, Sheng Q, Pals G, Errami A, Gluckman E, Llera J, Wang W, Livingston DM, Joenje H, de Winter JP (2007) Fanconi anemia is associated with a defect in the BRCA2 partner PALB2. *Nat Genet* **39:** 159-161

Xia B, Sheng Q, Nakanishi K, Ohashi A, Wu J, Christ N, Liu X, Jasin M, Couch FJ, Livingston DM (2006) Control of BRCA2 cellular and clinical functions by a nuclear partner, PALB2. *Mol Cell* **22:** 719-729

Yata K, Bleuyard JY, Nakato R, Ralf C, Katou Y, Schwab RA, Niedzwiedz W, Shirahige K, Esashi F (2014) BRCA2 coordinates the activities of cell-cycle kinases to promote genome stability. *Cell Rep* **7:** 1547-1559

Yu DS, Sonoda E, Takeda S, Huang CL, Pellegrini L, Blundell TL, Venkitaraman AR (2003) Dynamic control of Rad51 recombinase by self-association and interaction with BRCA2. *Mol Cell* **12:** 1029-1041

Figure 1

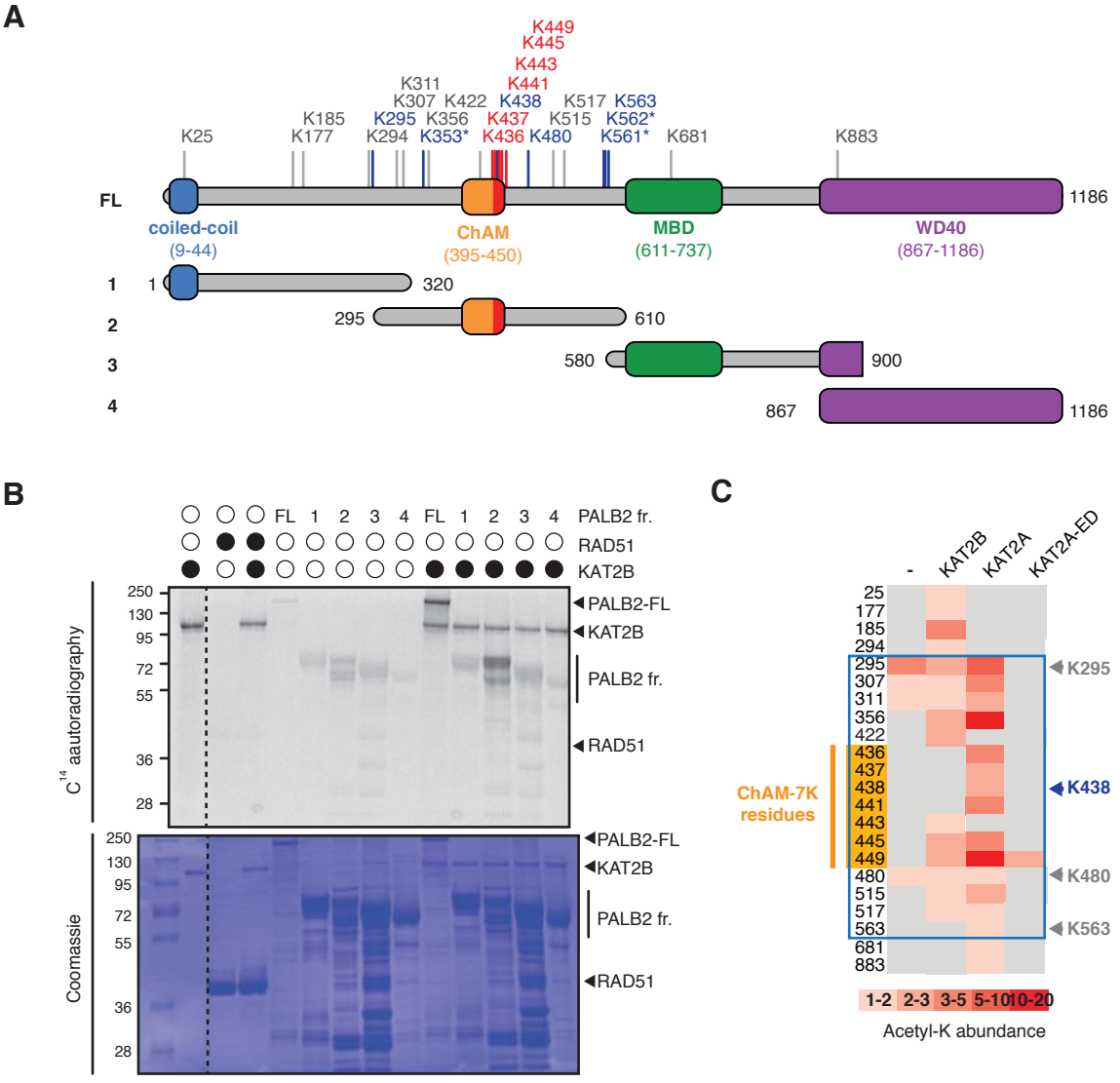
A
K449
K445
K443
K441
K438
K437
K436
K311
K307
K422
K517
K563
K562*
K561*
K185
K177
K295
K294
K356
K353*
K515
K480
K681
K883
K25
FL
1186
coiled-coil
(9-44)
ChAM
(395-450)
MBD
(611-737)
WD40
(867-1186)
1
1
320
2
295
610
3
580
900
4
867
1186
B
FL 1 2 3 4 FL 1 2 3 4
PALB2 fr.
RAD51
KAT2B
C14 aautoradiography
Coomassie
250
130
95
72
55
36
28
PALB2-FL
KAT2B
PALB2 fr.
RAD51
C
-
KAT2B
KAT2A
KAT2A-ED
25
177
185
294
295
307
311
356
422
436
437
438
441
443
445
449
480
515
517
563
681
883
K295
K438
K480
K563
ChAM-7K residues
1-2
2-3
3-5
5-10
10-20
Acetyl-K abundance
D
ChAM
7K-patch
KAT2B targets
KAT2A targets
HsPALB2
PtPALB2
PpPALB2
BtPALB2
MlPALB2
SsPALB2
EcPALB2
ClPALB2
AmPALB2
OaPALB2
GgPALB2
TgPALB2
K438: endogenous KAT2A/B target

Figure 2

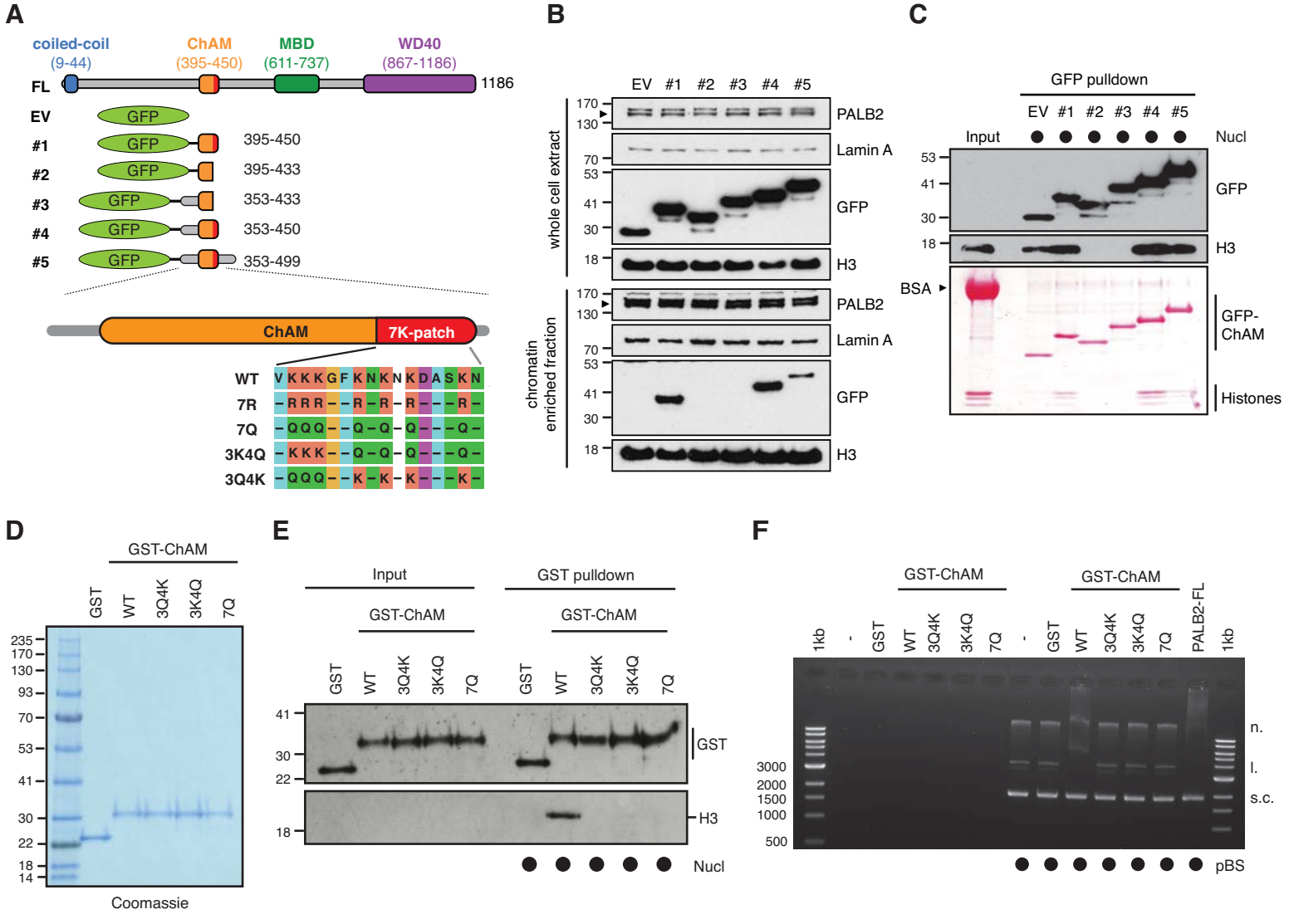
A
coiled-coil (9-44)
ChAM (395-450)
MBD (611-737)
WD40 (867-1186)
FL
1186
EV
#1 395-450
#2 395-433
#3 353-433
#4 353-450
#5 353-499
GFP
ChAM
7K-patch
WT V K K K G F K N K N K D A S K N
7R – R R R – – R – R – R – – – R –
7Q – Q Q Q – – Q – Q – Q – – – Q –
3K4Q – K K K – – Q – Q – Q – – – Q –
3Q4K – Q Q Q – – K – K – K – – – K –
B
EV #1 #2 #3 #4 #5
whole cell extract
chromatin enriched fraction
PALB2
Lamin A
GFP
H3
170
130
70
53
41
30
18
C
GFP pulldown
EV #1 #2 #3 #4 #5
Input
Nucl
GFP
H3
BSA
GFP-ChAM
Histones
D
GST-ChAM
GST
WT
3Q4K
3K4Q
7Q
235
170
130
93
70
53
41
30
22
18
14
Coomassie
E
Input
GST pulldown
GST-ChAM
GST
WT
3Q4K
3K4Q
7Q
41
30
22
18
H3
Nucl
F
GST-ChAM
1kb
-
GST
WT
3Q4K
3K4Q
7Q
PALB2-FL
3000
2000
1500
1000
500
n.
l.
s.c.
pBS

bioRxiv preprint doi: https://doi.org/10.1101/735811; this version posted January 21, 2020. The copyright holder for this preprint (which was not certified by peer review) is the author/funder. All rights reserved. No reuse allowed without permission.

Figure 3

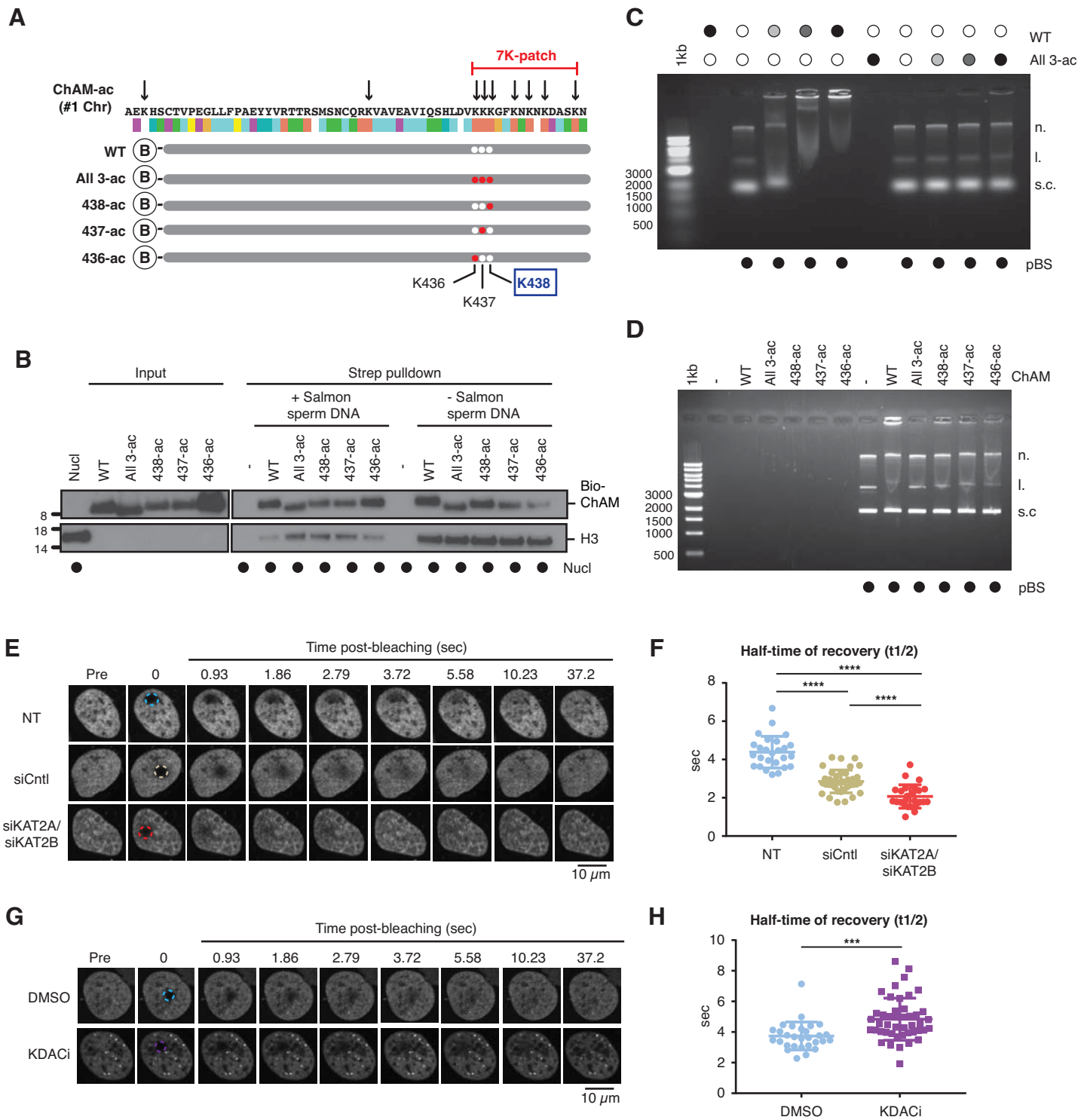

Figure 4

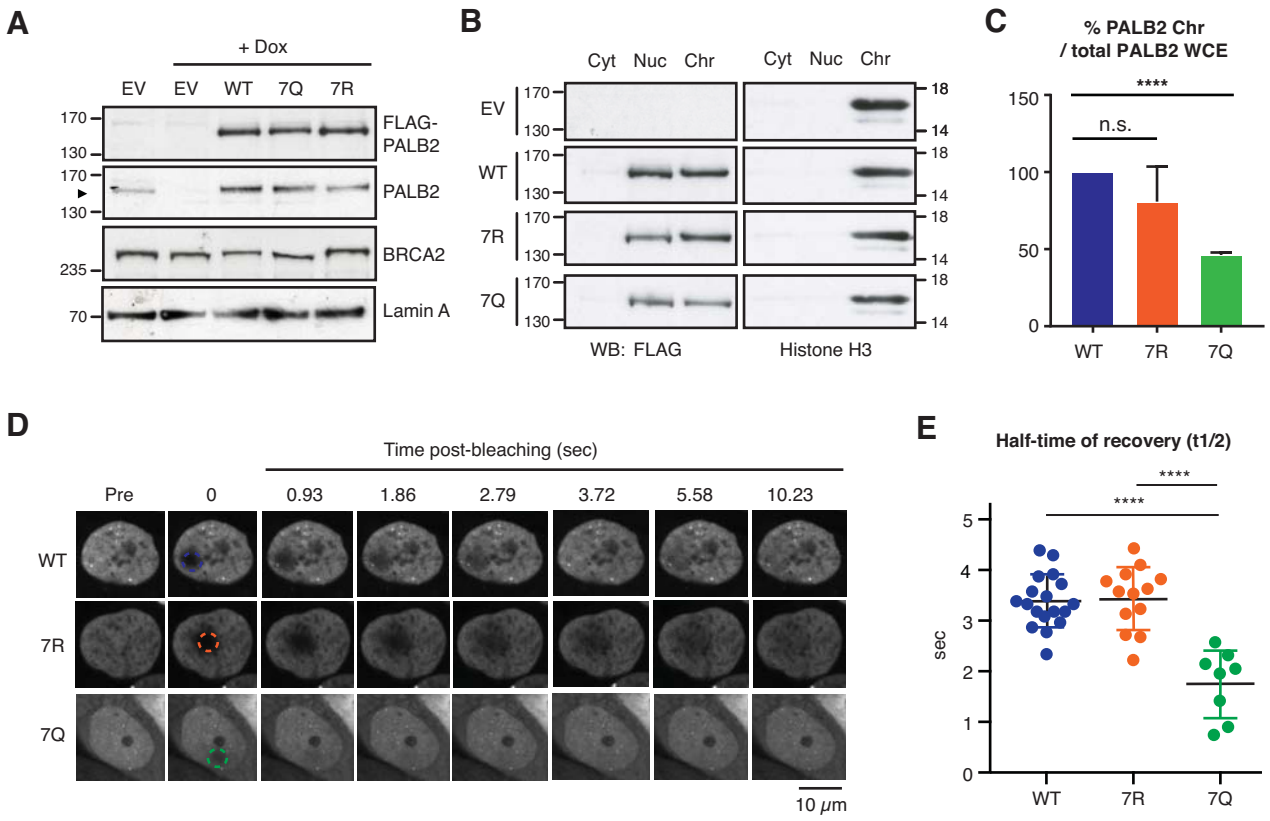
A
+ Dox
EV
EV
WT
7Q
7R
170
130
FLAG-PALB2
170
130
PALB2
235
BRCA2
70
Lamin A
B
Cyt
Nuc
Chr
Cyt
Nuc
Chr
EV
WT
7R
7Q
170
130
18
14
WB: FLAG
Histone H3
C
% PALB2 Chr / total PALB2 WCE
****
n.s.
150
100
50
0
WT
7R
7Q
D
Time post-bleaching (sec)
Pre
0
0.93
1.86
2.79
3.72
5.58
10.23
WT
7R
7Q
10 μm
E
Half-time of recovery (t1/2)
****
****
sec
5
4
3
2
1
0
WT
7R
7Q

bioRxiv preprint doi: https://doi.org/10.1101/735811; this version posted January 21, 2020. The copyright holder for this preprint (which was not certified by peer review) is the author/funder. All rights reserved. No reuse allowed without permission.

Figure 5

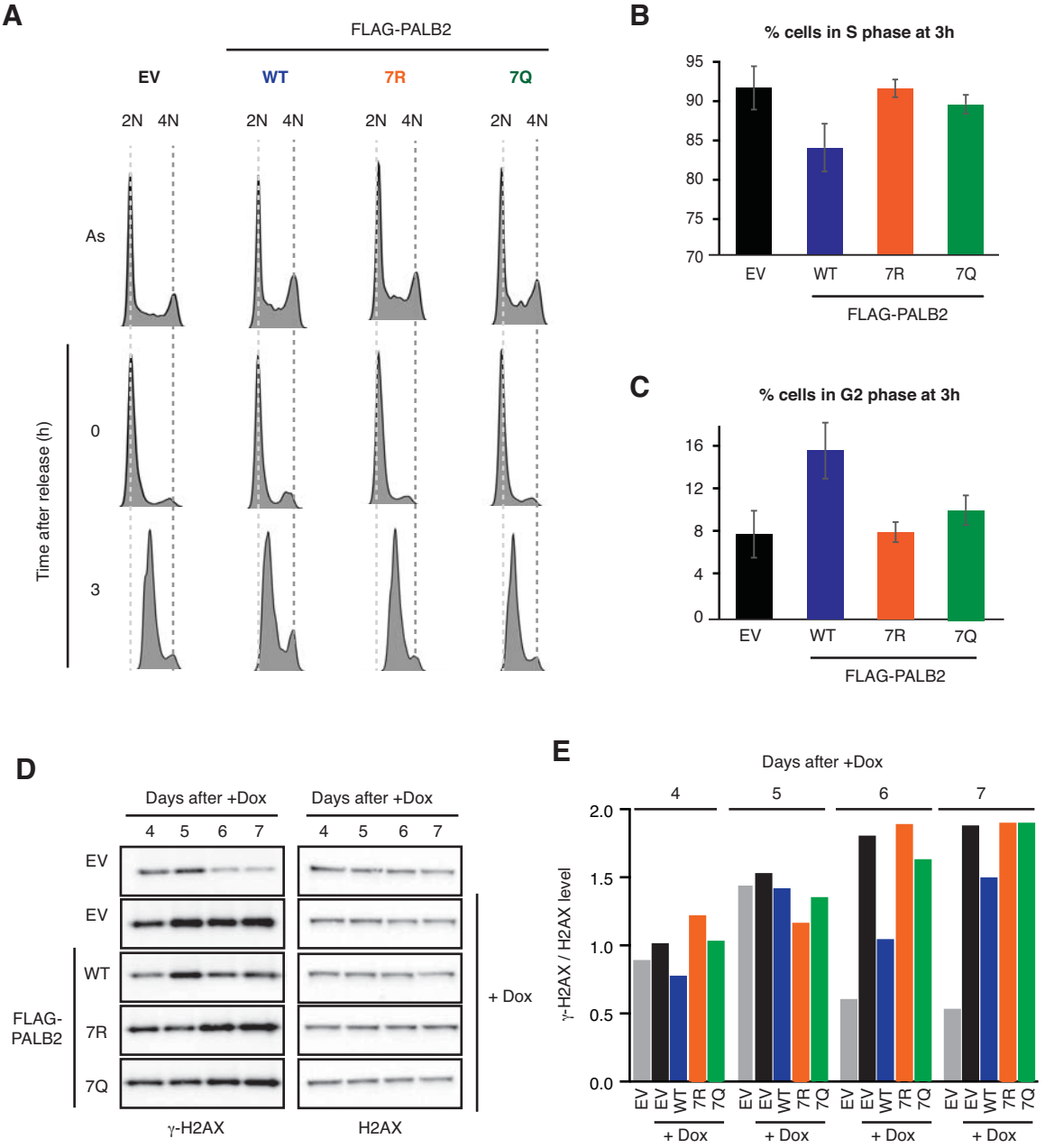

bioRxiv preprint doi: https://doi.org/10.1101/735811; this version posted January 21, 2020. The copyright holder for this preprint (which was not certified by peer review) is the author/funder. All rights reserved. No reuse allowed without permission.

Figure 6

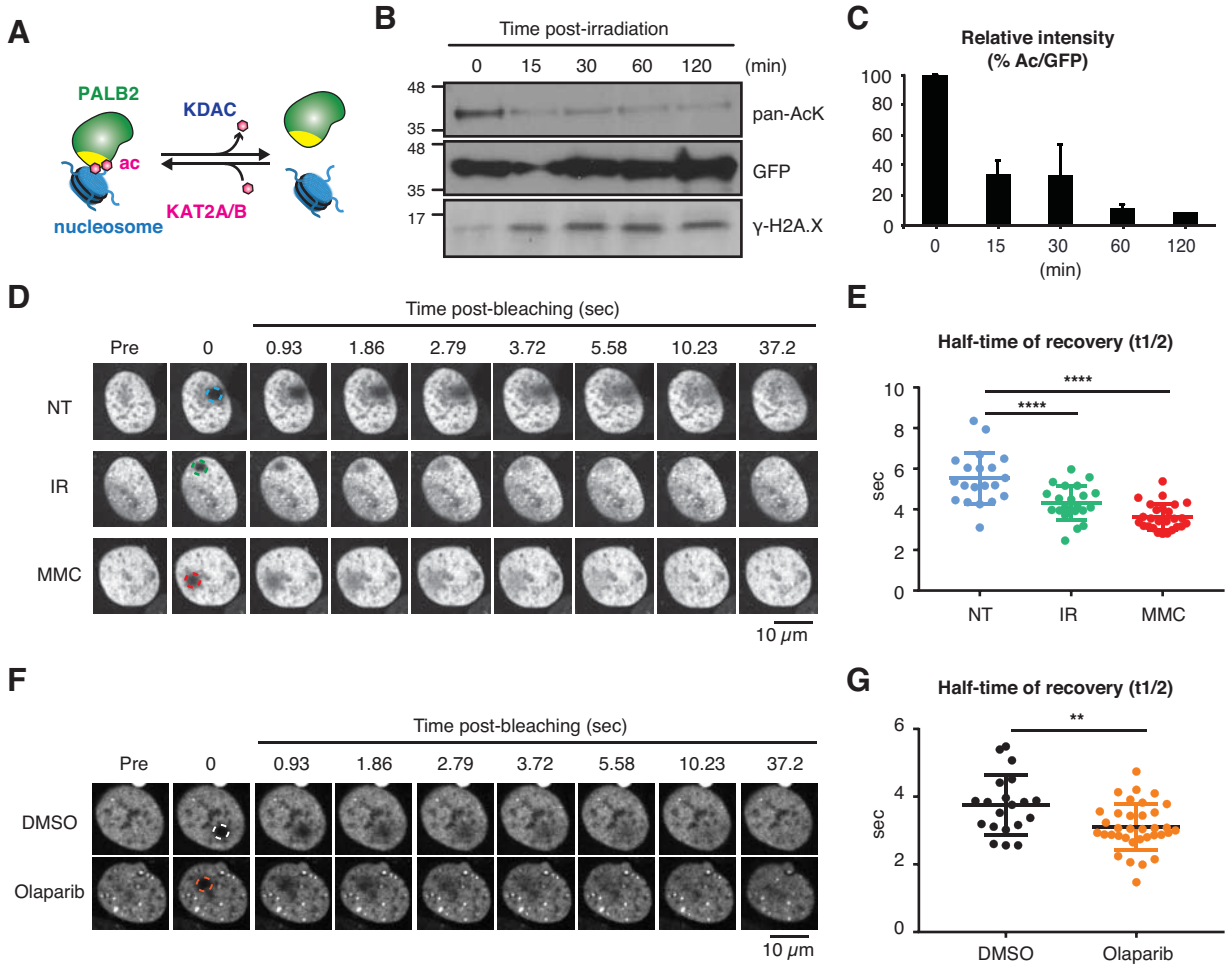

Figure 7

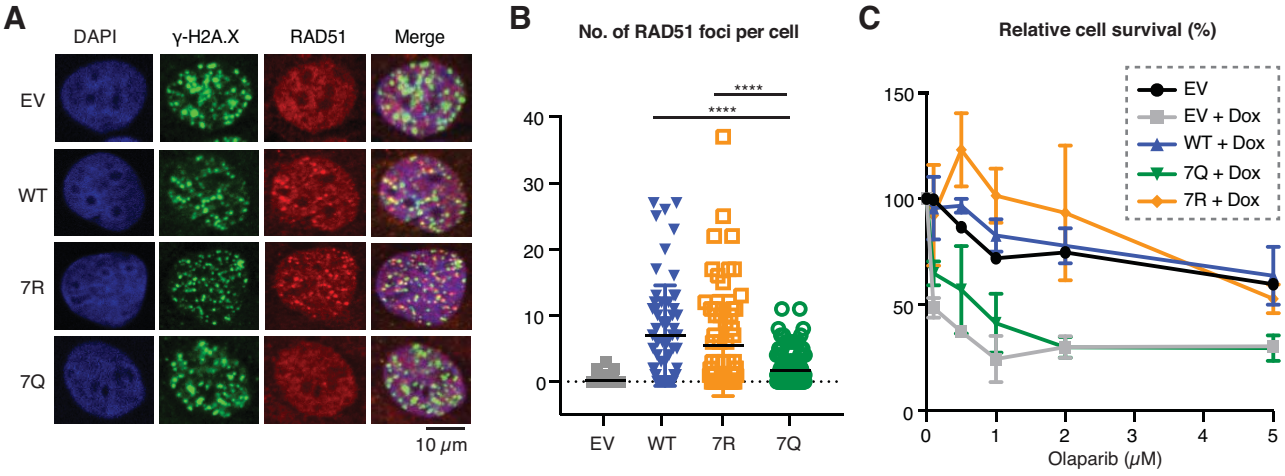
A
DAPI
γ-H2A.X
RAD51
Merge
EV
WT
7R
7Q
10 μm
B
No. of RAD51 foci per cell
****
****
40
30
20
10
0
EV
WT
7R
7Q
C
Relative cell survival (%)
150
100
50
0
0
1
2
3
4
5
Olaparib (μM)
EV
EV + Dox
WT + Dox
7Q + Dox
7R + Dox

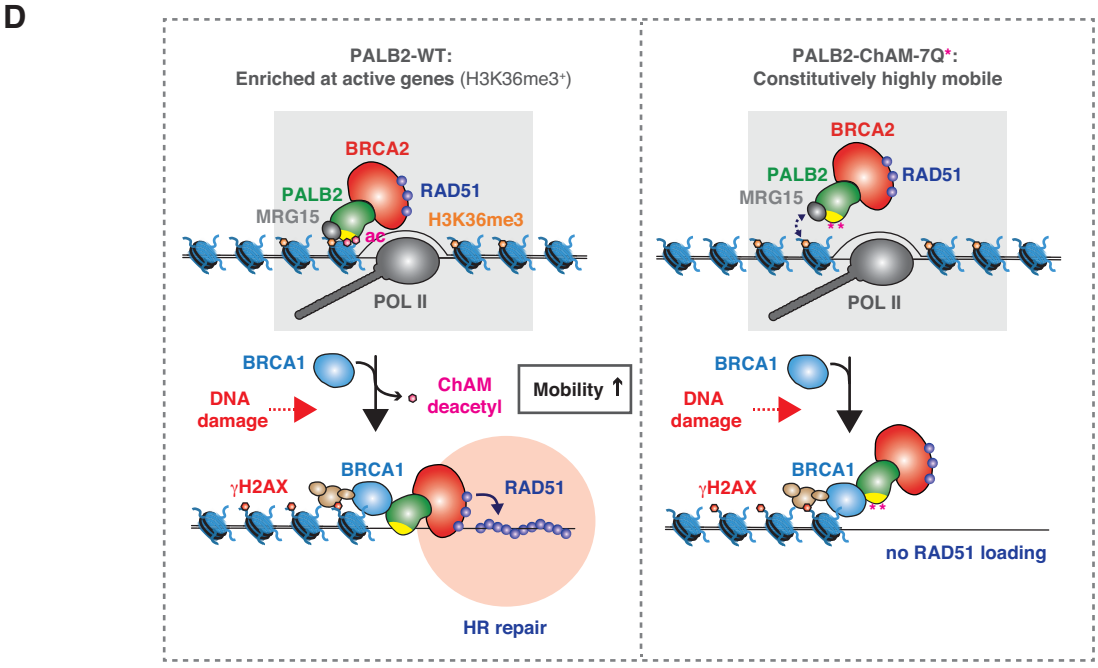
D
PALB2-WT:
Enriched at active genes (H3K36me3+)
BRCA2
PALB2
RAD51
MRG15
H3K36me3
ac
POL II
BRCA1
DNA damage
ChAM deacetyl
Mobility ↑
γH2AX
BRCA1
RAD51
HR repair
PALB2-ChAM-7Q*:
Constitutively highly mobile
BRCA2
PALB2
RAD51
MRG15
POL II
BRCA1
DNA damage
γH2AX
BRCA1
no RAD51 loading

bioRxiv preprint doi: https://doi.org/10.1101/735811; this version posted January 21, 2020. The copyright holder for this preprint (which was not certified by peer review) is the author/funder. All rights reserved. No reuse allowed without permission.

Figure S1

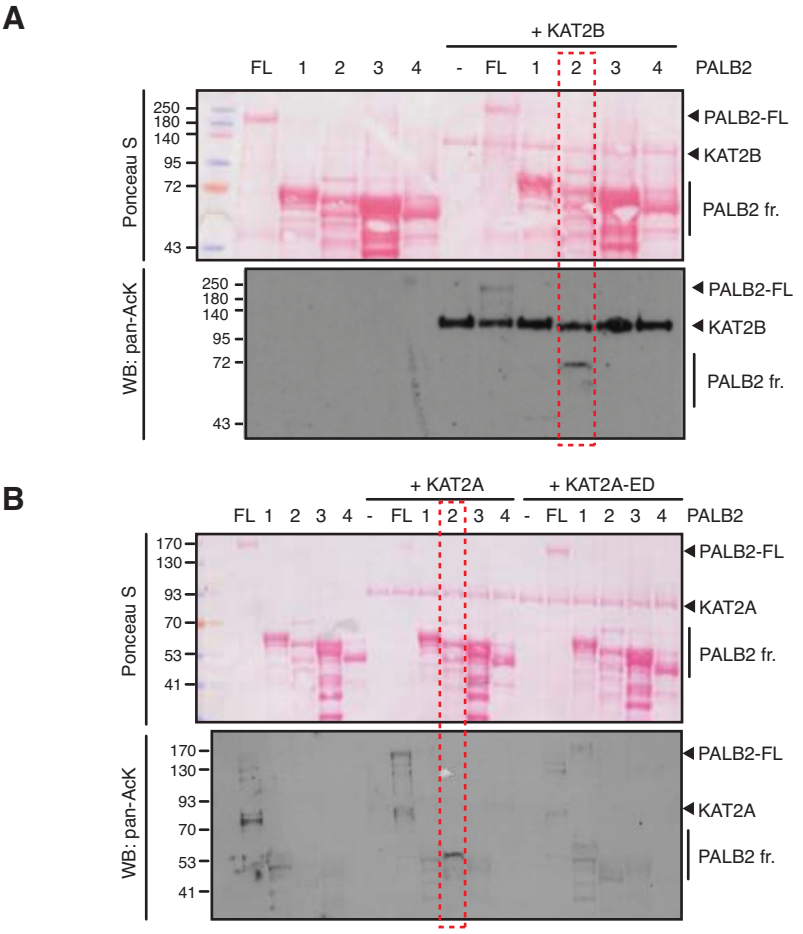

Figure S2

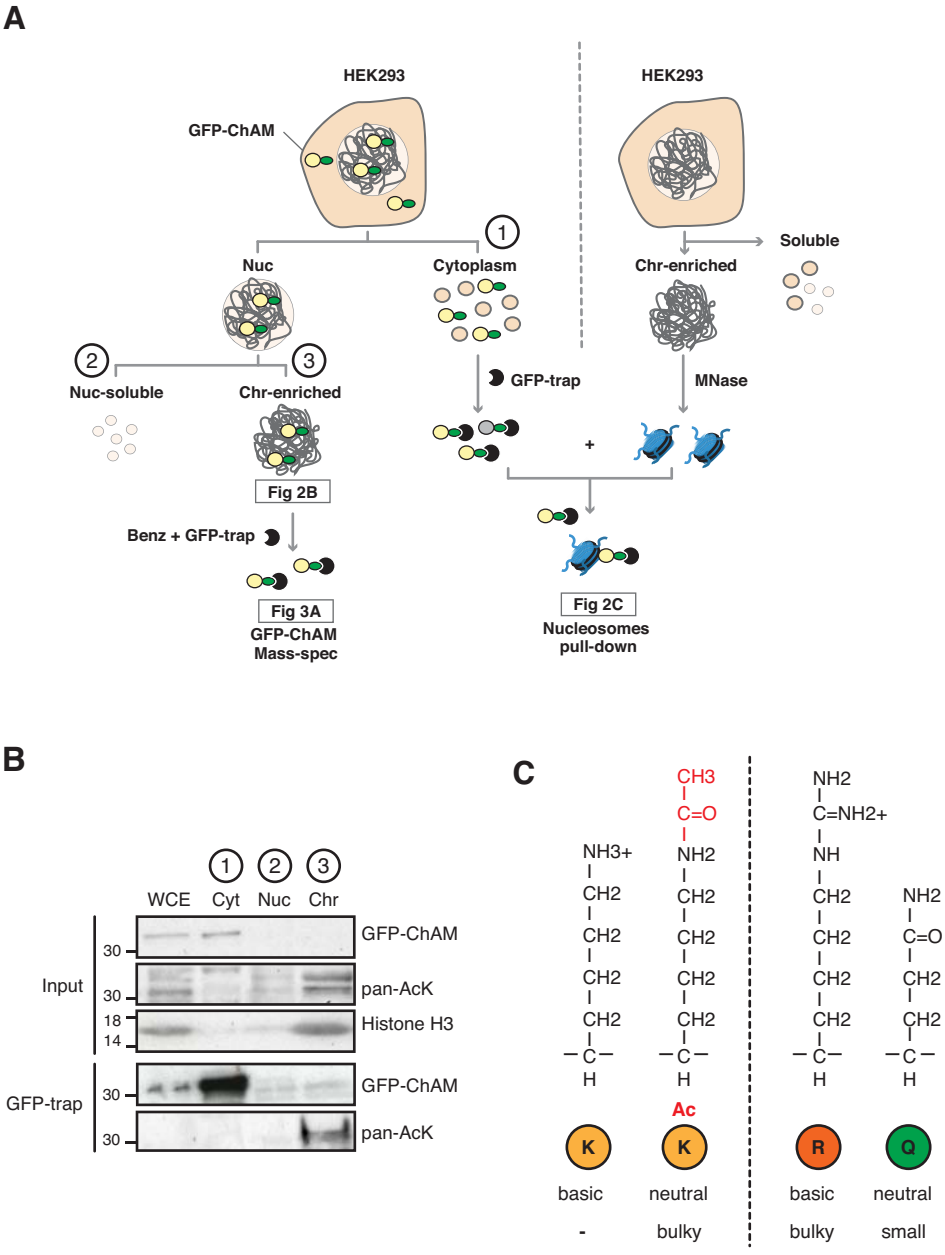
A
HEK293
GFP-ChAM
Nuc
Cytoplasm
Nuc-soluble
Chr-enriched
Fig 2B
Benz + GFP-trap
Fig 3A
GFP-ChAM
Mass-spec
GFP-trap
HEK293
Chr-enriched
Soluble
MNase
Fig 2C
Nucleosomes
pull-down
B
WCE
Cyt
Nuc
Chr
Input
GFP-trap
GFP-ChAM
pan-AcK
Histone H3
C
basic
neutral
basic
neutral
-
bulky
bulky
small
Ac

Figure S3

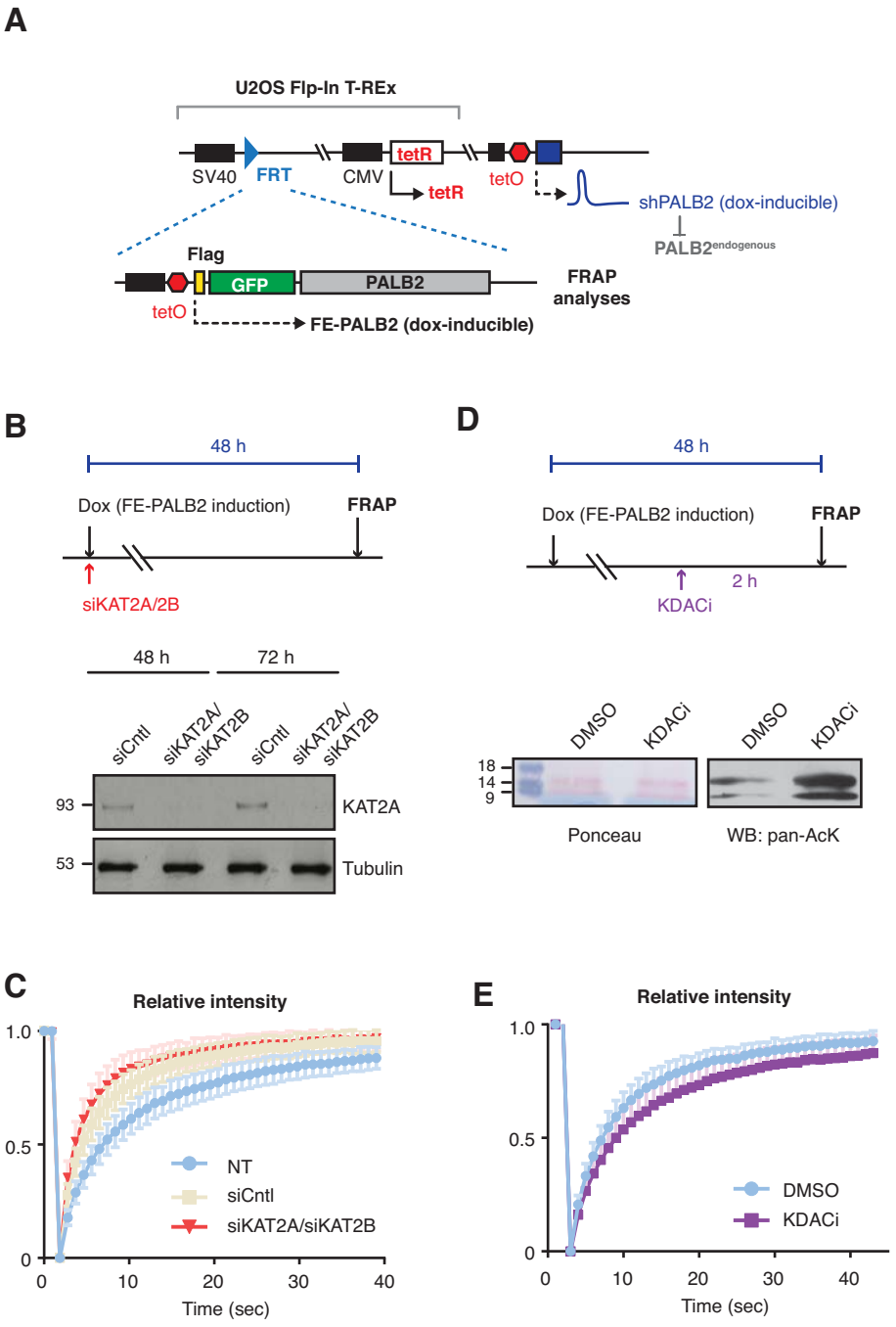
A
U2OS Flp-In T-REx
SV40
FRT
CMV
tetR
tetR
tetO
shPALB2 (dox-inducible)
PALB2endogenous
Flag
GFP
PALB2
tetO
FE-PALB2 (dox-inducible)
FRAP analyses
B
48 h
Dox (FE-PALB2 induction)
FRAP
siKAT2A/2B
48 h
72 h
siCntl
siKAT2A/ siKAT2B
siCntl
siKAT2A/ siKAT2B
93
KAT2A
53
Tubulin
D
48 h
Dox (FE-PALB2 induction)
FRAP
2 h
KDACi
DMSO
KDACi
DMSO
KDACi
18
14
9
Ponceau
WB: pan-AcK
C
Relative intensity
1.0
0.5
0
0
10
20
30
40
Time (sec)
NT
siCntl
siKAT2A/siKAT2B
E
Relative intensity
1.0
0.5
0
0
10
20
30
40
Time (sec)
DMSO
KDACi

Figure S4

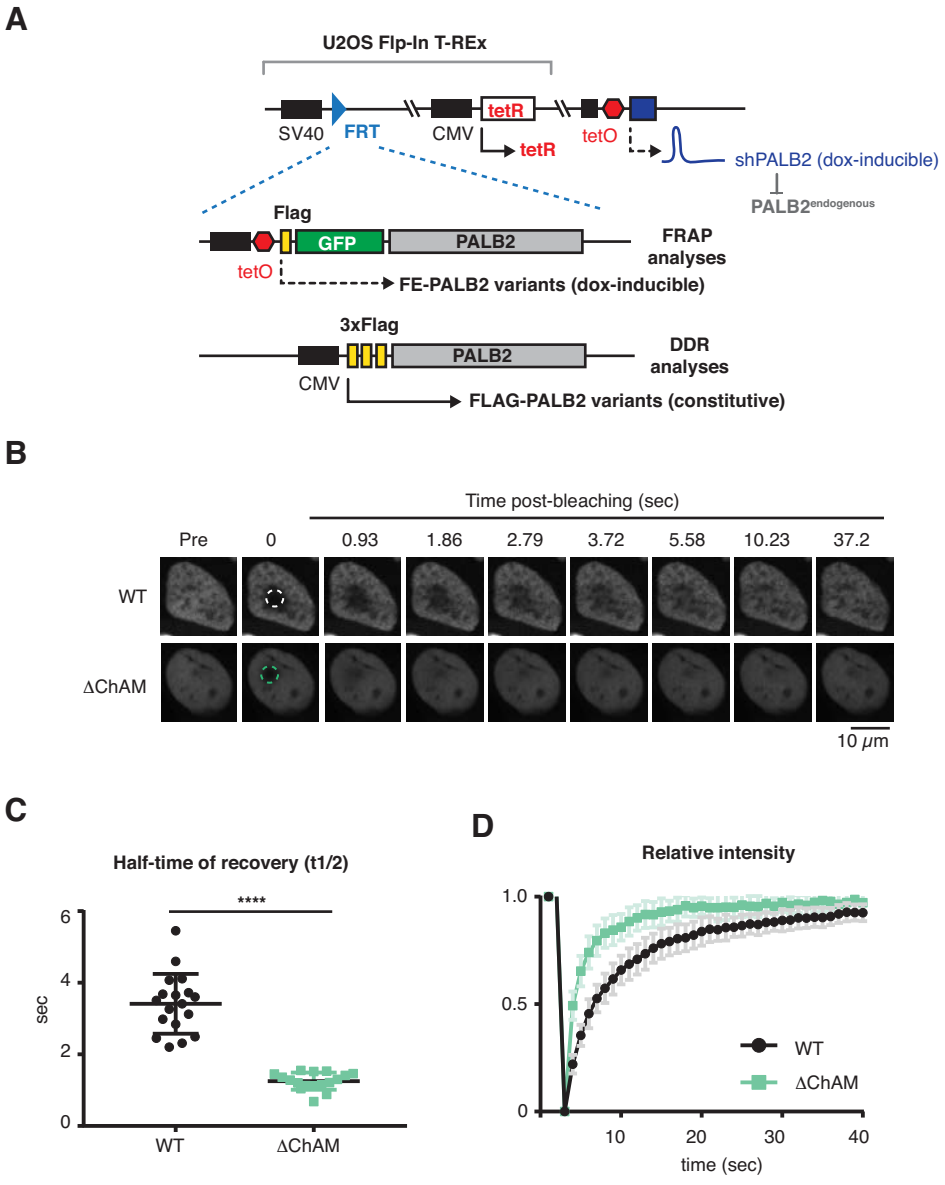
A
U2OS Flp-In T-REx
SV40
FRT
CMV
tetR
tetR
tetO
shPALB2 (dox-inducible)
PALB2endogenous
Flag
GFP
PALB2
FRAP analyses
tetO
FE-PALB2 variants (dox-inducible)
3xFlag
PALB2
DDR analyses
CMV
FLAG-PALB2 variants (constitutive)
B
Time post-bleaching (sec)
Pre
0
0.93
1.86
2.79
3.72
5.58
10.23
37.2
WT
ΔChAM
10 μm
C
Half-time of recovery (t1/2)
****
sec
6
4
2
0
WT
ΔChAM
D
Relative intensity
1.0
0.5
0
10
20
30
40
time (sec)
WT
ΔChAM

Figure S5

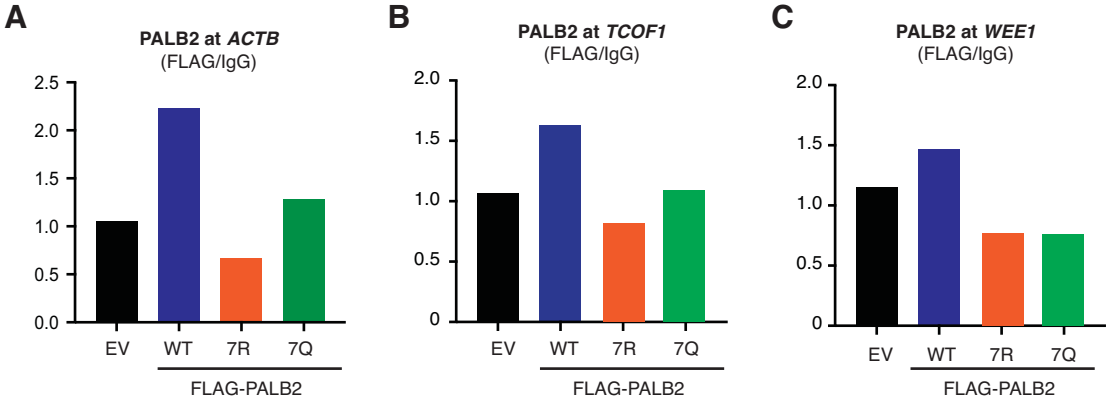
A
PALB2 at ACTB
(FLAG/IgG)
2.5
2.0
1.5
1.0
0.5
0.0
EV
WT
7R
7Q
FLAG-PALB2
B
PALB2 at TCOF1
(FLAG/IgG)
2.0
1.5
1.0
0.5
0
EV
WT
7R
7Q
FLAG-PALB2
C
PALB2 at WEE1
(FLAG/IgG)
2.0
1.5
1.0
0.5
0
EV
WT
7R
7Q
FLAG-PALB2

Figure S6

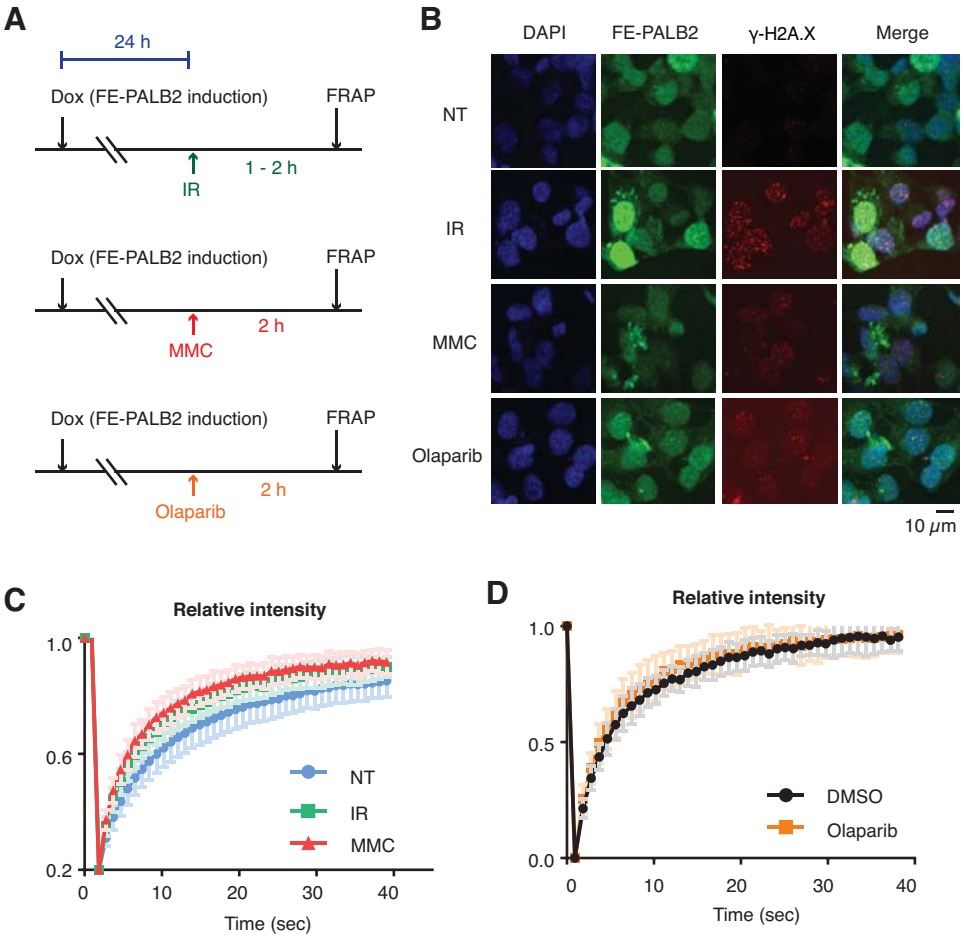
A
24 h
Dox (FE-PALB2 induction)
FRAP
IR
1 - 2 h
Dox (FE-PALB2 induction)
FRAP
MMC
2 h
Dox (FE-PALB2 induction)
FRAP
Olaparib
2 h
B
DAPI
FE-PALB2
γ-H2A.X
Merge
NT
IR
MMC
Olaparib
10 μm
C
Relative intensity
1.0
0.6
0.2
0
10
20
30
40
Time (sec)
NT
IR
MMC
D
Relative intensity
1.0
0.5
0.0
0
10
20
30
40
Time (sec)
DMSO
Olaparib

Figure S7

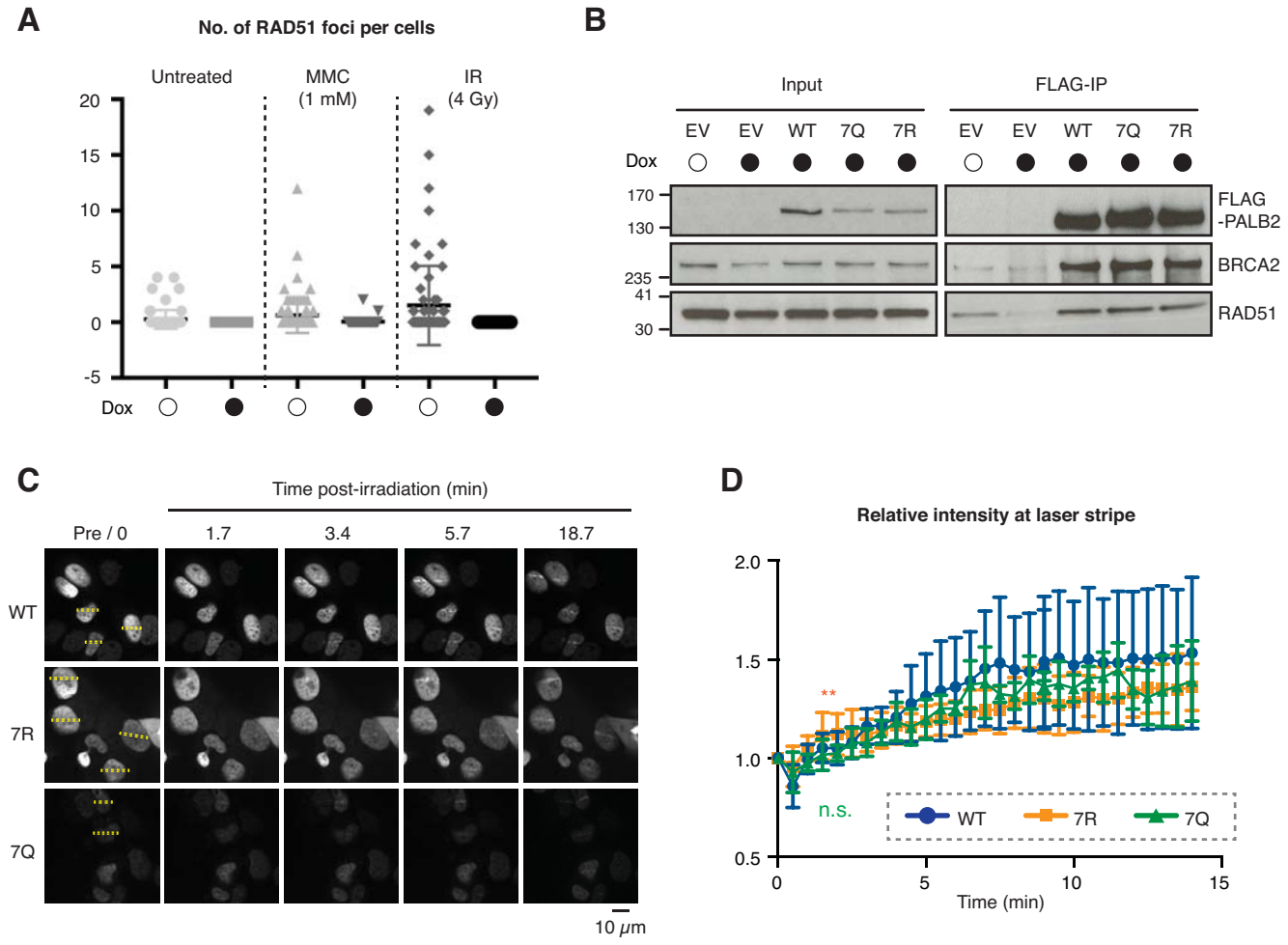
A
No. of RAD51 foci per cells
Untreated
MMC
(1 mM)
IR
(4 Gy)
20
15
10
5
0
-5
Dox
B
Input
FLAG-IP
EV
EV
WT
7Q
7R
EV
EV
WT
7Q
7R
Dox
170
130
235
41
30
FLAG
-PALB2
BRCA2
RAD51
C
Time post-irradiation (min)
Pre / 0
1.7
3.4
5.7
18.7
WT
7R
7Q
10 μm
D
Relative intensity at laser stripe
2.0
1.5
1.0
0.5
**
n.s.
WT
7R
7Q
0
5
10
15
Time (min)

bioRxiv preprint doi: https://doi.org/10.1101/735811; this version posted January 21, 2020. The copyright holder for this preprint (which was not certified by peer review) is the author/funder. All rights reserved. No reuse allowed without permission.

Supplemental Material and Methods

Plasmids

For bacterial expression, full-length PALB2 and fragments 1 to 4 were PCR amplified using primer pairs, numbered 1 and 2 (Fr. 1), 3 and 4 (Fr. 2), 5 and 6 (Fr. 3), or 7 and 8 (Fr. 4) listed in Table 1, from pCMV-SPORT6-PALB2 (IMAGE clone 6045564, Source BioSciences) and cloned into the BamHI/NotI sites of the pGEX-6P-1 vector (GE Healthcare). For mammalian expression, ChAM fragments of varied length were first PCR amplified using primer pairs, numbered 9 and 11 (#1), 9 and 12 (#2), 10 and 12 (#3), 10 and 11 (#4), or 10 and 13 (#5) listed in Table 1, and cloned into the BamHI/XhoI sites of the pENTR3C Gateway entry vector (Thermo Fisher Scientific). To generate GFP-fusion or GST-fusion expression vectors, ChAM fragments were then transferred from pENTR3C to pcDNA-DEST53 (GFP-fusions) or pDEST15 (GST-fusions) (Invitrogen) using Gateway cloning. PALB2 Q and R mutations were introduced in the pENTR3C-ChAM#1 or pENTR3C-PALB2 vectors by inverse PCR (5'-phosphorylated oligonucleotides containing the desired mutations were used to create blunt-ended products, which were then recircularised by intramolecular ligation). GST-ChAM missense variants 7Q, 3Q4K and 3K4Q were respectively generated using primer pairs, numbered 18 and 20 (7Q), 18 and 15 (3Q4K), or 14 and 20 (3K4Q) listed in Table 1. PALB2 7Q and 7R full length missense variants were respectively generated using primer pairs, numbered 18 and 19 (7Q), or 16 and 17 (7R) listed in Table 1. To generate N3xFLAG-fusion expression vectors, PALB2 variants were then transferred from pENTR3C to pcDNA5/FRT-GW/N3×FLAG (Bleuyard et al, 2017) using Gateway cloning.

bioRxiv preprint doi: https://doi.org/10.1101/735811; this version posted January 21, 2020. The copyright holder for this preprint (which was not certified by peer review) is the author/funder. All rights reserved. No reuse allowed without permission.

Chemical cell fractionation and whole-cell extract

HEK293T cells transiently expressing GFP-ChAM variants were collected using TrypLE Express reagent (Gibco), washed twice with ice-cold PBS and resuspended in Sucrose buffer (10 mM Tris-HCl pH 7.5, 20 mM KCl, 250 mM Sucrose, 2.5 mM $MgCl_2$, 10 mM benzamidine hydrochloride and P2714 protease inhibitor cocktail from Sigma-Aldrich), using 1 mL buffer per 100 mg of weighed cell pellet. After addition of Triton X-100 (Sigma) to a final concentration of 0.3% w/v, the cell suspensions were vortexed three times for 10 s with 1 min intervals. The intact nuclei were collected by centrifugation for 5 min at 500 x g, 4°C, and the supernatant collected as cytoplasmic fraction. The nuclei pellet was washed once with ice-cold sucrose buffer and resuspended in ice-cold NETN150 buffer (50 mM Tris-HCl pH 8.0, 150 mM NaCl, 2 mM EDTA, 0.5% NP-40, 10 mM benzamidine hydrochloride and P2714 protease inhibitor cocktail from Sigma), using 400 µL buffer per 100 mg of initial weighed cell pellet. After 30 min incubation on ice, the chromatin fraction was collected by centrifugation for 5 min at 500 x g, 4°C and the supernatant collected as nuclear soluble fraction. The chromatin pellet was washed once with ice-cold NETN150 buffer and finally solubilised for 1 h on ice in NETN150 buffer containing 2 mM $MgCl_2$ and 125 U/mL Benzonase nuclease (Merck Millipore), using 250 µL buffer per 100 mg of initial weighed cell pellet. Cytoplasmic, nuclear soluble and chromatin-enriched fractions were centrifuged for 30 min at 16,100 x g, 4°C to remove cell debris and insoluble material. For whole-cell extract, cells were directly lysed in NETN150 buffer containing 2 mM

bioRxiv preprint doi: https://doi.org/10.1101/735811; this version posted January 21, 2020. The copyright holder for this preprint (which was not certified by peer review) is the author/funder. All rights reserved. No reuse allowed without permission.

$MgCl_2$ and 125 U/mL Benzonase for 1 h on ice and centrifuged for 30 min at 16,100 x g, 4°C to remove cell debris and insoluble material.

Cell survival

In 96-wells plates, EUFA1341 cells complemented with FLAG-PALB2 WT and variants were exposed to increasing concentration of Olaparib (0-2 μM). After 4 days of incubation at 37°C, cell proliferation was measured using WST-1 reagent (Roche Applied Science) following manufacturer protocol.

Laser damage

To perform laser damage experiments, cells were plated onto cell view cell culture dishes (3.5mm) and analysed in phenol red-free medium (Leibovitz L15-medium, Gibco life technologies). Images analysis were performed on a spinning-disk confocal microscope (Ultra-View Vox, Perkin Elmer) mounted on an IX81 Olympus microscope with an Olympus 60x 1.4 oil PlanApo objective, in a controlled chamber at 37°C and 5% CO2 (TOKAI HIT stage top incubator). The fluorescence signal was detected using an EMCCD camera (ImagEM, Hamamatsu C9100-13). To perform laser damage experiments, cells were irradiated in the DAPI channel at maximum laser power with a single pulse for 90 ms, using a straight line crossing the whole cellular surface. After bleaching, GFP fluorescence recovery was monitored within the bleached area every 30 s for 5 min. Laser damage parameters were controlled using the Volocity software 6.0 (QuorumTechnologies). PALB2 recruitment at sites of laser damage was quantified in Fiji/Image G (Image / Stacks/ Plot Z-axis Profile) by measuring the EGFP fluorescence intensity within a region of interest at site of damage over

bioRxiv preprint doi: https://doi.org/10.1101/735811; this version posted January 21, 2020. The copyright holder for this preprint (which was not certified by peer review) is the author/funder. All rights reserved. No reuse allowed without permission.

fifteen minutes after laser-induced damage. Images were recorded every 30 s during this period. Fluorescence intensity at the damaged site over the time course experiment was corrected for background and overall loss of fluorescence intensity in the nucleus (non-damaged region of interest) and normalised to the pre-damaged value.

ChIP-qPCR

ChIP experiments were performed from $20x10^6$ cells as described previously (Bleuyard et al, 2017). FLAG antibody used to perform ChIP experiments is described in the antibodies section of Material and Methods. Quantitative real-time PCR (qPCR) experiments have been performed on a Rotorgene Q Real-Time PCR system (Qiagen) using the SensiFAST SYBR No-Rox kit (Bioline). Oligonucleotides used to perform qPCR against coding regions of *ACTB*, *TCOF1* and *WEE1* genes are listed in Table 1 (numbered 21 to 26).

Cell synchronisation

Cell synchronisation experiments were performed by double thymidine block as previously described (Esashi et al, 2005). Briefly, cells were first blocked in G1/S phase with 2 mM thymidine treatment for 18 hr, release in fresh media for 9 h and blocked again at G1/S phase with 2 mM thymidine treatment for 16 h. Subsequently, cells were release in fresh media and collected at 0 and 3 h after release for DNA content analysis by flow cytometry (FACS).

Cell cycle analysis by flow cytometry

bioRxiv preprint doi: https://doi.org/10.1101/735811; this version posted January 21, 2020. The copyright holder for this preprint (which was not certified by peer review) is the author/funder. All rights reserved. No reuse allowed without permission.

Cell cycle analysis was performed by DNA content measurement by propidium iodide (PI) staining followed by FACS analysis. After cell collection by centrifugation at 500 x g at 4°C, cells were fixed in 70% ethanol. After cell permeabilisation for 5 min on ice with 0.1% Triton contained in 0.1% BSA resuspended in PBS, DNA was stained for 3 h in the dark in a PI solution containing 0.1% BSA, 0.1 mg/ml of RNase and 2 ug/ml of PI. DNA content was analysed from 10000 cells on a FACS calibur machine (BD Calibur) and FACS data was analysed using FlowJo software V10.

Mass spectrometry

Protein sample digestion: proteins contained in solution were urea-denaturated in 4 M urea dissolved into 50 mM triethylammonium bicarbonate (TEAB), reduced with 10 mM tris-(2-carboxyethyl)phosphine (TCEP) for 30 min at room temperature, alkylated with 50 mM chloroacetamide for 30 min at room temperature in the dark, digested with endoproteinase Lys-C (Roche) for 2 h at 37°C, followed by trypsin digestion for 16 h at 37°C. Before trypsin digestion, the urea concentration was diluted down to 1 M into 50 mM TEAB and calcium chloride was added at 1 mM final. The digestion steps were performed in a Thermomixer compact (Eppendorf) shaking at 650 rpm. Trypsin digestion was stopped by adding 1% Trifluoroacetic acid (TFA) final. Digest samples were centrifuged for 30 min at 4°C to remove aggregates. Peptides mixtures were further desalted onto hand-made C18 tips, as following: the C18 tip was first washed twice with 100% acetonitrile after 5 min centrifugation at 2000rpms at room temperature. Peptides were further loaded onto the C18 tip by centrifugation at 4,000 rpm at room temperature. After two washing steps into

bioRxiv preprint doi: https://doi.org/10.1101/735811; this version posted January 21, 2020. The copyright holder for this preprint (which was not certified by peer review) is the author/funder. All rights reserved. No reuse allowed without permission.

0.1% TFA solution, desalted peptides were eluted into 50% acetonitrile/0.1% TFA solution and dried using a SpeedVac before LC-MS/MS analysis. All MS/MS spectra for acetylated PALB2 peptides are provided in the supplementary material.

Acetylated lysine abundance values were calculated as following: PALB2 acetylated peptides specifically identified in KAT2A, KAT2B and KAT2A mutant conditions were extracted and compared. Spectral counts for similar acetylated peptides identified across these three conditions were divided by the total PALB2 spectral counts identified in each condition, to normalise for experimental variation encountered between independent runs. This calculation was performed for each acetylated peptide identified, and normalised values were then summed up to define the acetylation abundance factor of PALB2 in each condition tested.

References

Bleuyard JY, Fournier M, Nakato R, Couturier AM, Katou Y, Ralf C, Hester SS, Dominguez D, Rhodes D, Humphrey TC, Shirahige K, Esashi F (2017) MRG15-mediated tethering of PALB2 to unperturbed chromatin protects active genes from genotoxic stress. *Proc Natl Acad Sci U S A* **114:** 7671-7676

Esashi F, Christ N, Gannon J, Liu Y, Hunt T, Jasin M, West SC (2005) CDK-dependent phosphorylation of BRCA2 as a regulatory mechanism for recombinational repair. *Nature* **434:** 598-604

bioRxiv preprint doi: https://doi.org/10.1101/735811; this version posted January 21, 2020. The copyright holder for this preprint (which was not certified by peer review) is the author/funder. All rights reserved. No reuse allowed without permission.

Table 1. List of oligonucleotides used in this study

Name	Sequence	No.
PALB2-F1_fo1	5'-atggatccatggacgagcctccc-3'	1
PALB2-F1_re1	5'-atgcggccgcattagaacttgtgggcag-3'	2
PALB2-F2_fo1	5'-atggatccgcacaaggcaaaaaaatg-3'	3
PALB2-F2_re1	5'-atgcggccgctgtgatactgagaaaagac-3'	4
PALB2-F3_fo1	5'-atggatccttatccttggatgatgatg-3'	5
PALB2-F3_re1	5'-atgcggccgcagctttccaaagagaaac-3'	6
PALB2-F4_fo1	5'-atggatcctgttccgtagatgtgag-3'	7
PALB2-F4_re1	5'-atgcggccgcttatgaatagtggtatacaaat-3'	8
PALB2_395_Fo	5'- actggatcctcttgcacagtgcctg-3'	9
PALB2_353_Fo	5'- actggatccaaatctttaaaatctcccagtg-3'	10
PALB2_450_Re	5'- tatctcgagttaatttttacttgcatccttattttta-3'	11
PALB2_433_Re	5'- tatctcgagttacaaatgactctgaatgacagc-3'	12
PALB2_499_Re	5'- tatctcgagttacaagtcattatcttcagtggg-3'	13
Patch 1-K-Rev	5'-tcagagtcatttggatgtcaagaaaaaaggttt-3'	14
Patch 2-WT-Fwd	5'-aaaaataaaaataaggatgcaagtaaaaat-3	15
Patch 1-R-Rev	5'-tcagagtcatttggatgtcaggagaagagggttt-3'	16
Patch 2-R-Fwd_FL	5'-agaaatagaaatagggatgcaagtagaaatttaaacctttccaat-3'	17
Patch 1-Q-Rev	5'-tcagagtcatttggatgtccagcaacaaggttt-3'	18
Patch 2-Q-Fwd_FL	5'-caaaatcaaaatcaggatgcaagtcaaaatttaaacctttccaat-3'	19
Patch 2-Q-Fwd_ChAM	5'-caaaatcaaaatcaggatgcaagtcaaaattgagcggccgcact-3'	20
Beta-Actin_in3-fo	5'-taacactggctcgtgtgacaa-3'	21
Beta-Actin_in3-re	5'-aagtgcaaagaacacggctaa-3'	22
Chr5_TCOF1_peak2_fo	5'-ctacccgatccctcaggtca-3'	23
Chr5_TCOF1_peak2_re	5'-tcagggctctatgaggggac-3'	24
Chr11_WEE1_mid_fo	5'-ggccgaggcttgaggtatatt-3'	25
Chr11_WEE1_mid_re	5'-ataaccccaaagaacacaggtca-3'	26

PALB2 K25-ac

Peptide Consensus View

Sequence: LAFLKR
K5-Acetyl (42.01057 Da)
Charge: +2, Monoisotopic m/z: 395.25293 Da (+0.2 mmu/+0.51 ppm), MH+: 789.49858 Da, RT: 66.22 min,

Extracted from: C:\Users\Proteomics\Desktop\Marjorie PD searches\PALB2_acetyl\C150302_PALB2+PCAF\C150302_001_1ul_150305043940_PALB2-FL+PCAF.raw #12058 RT: 66.22
FTMS, HCD, z=+2, Mono m/z=395.25293 Da, MH+=789.49858 Da, Match Tol.=0.05 Da

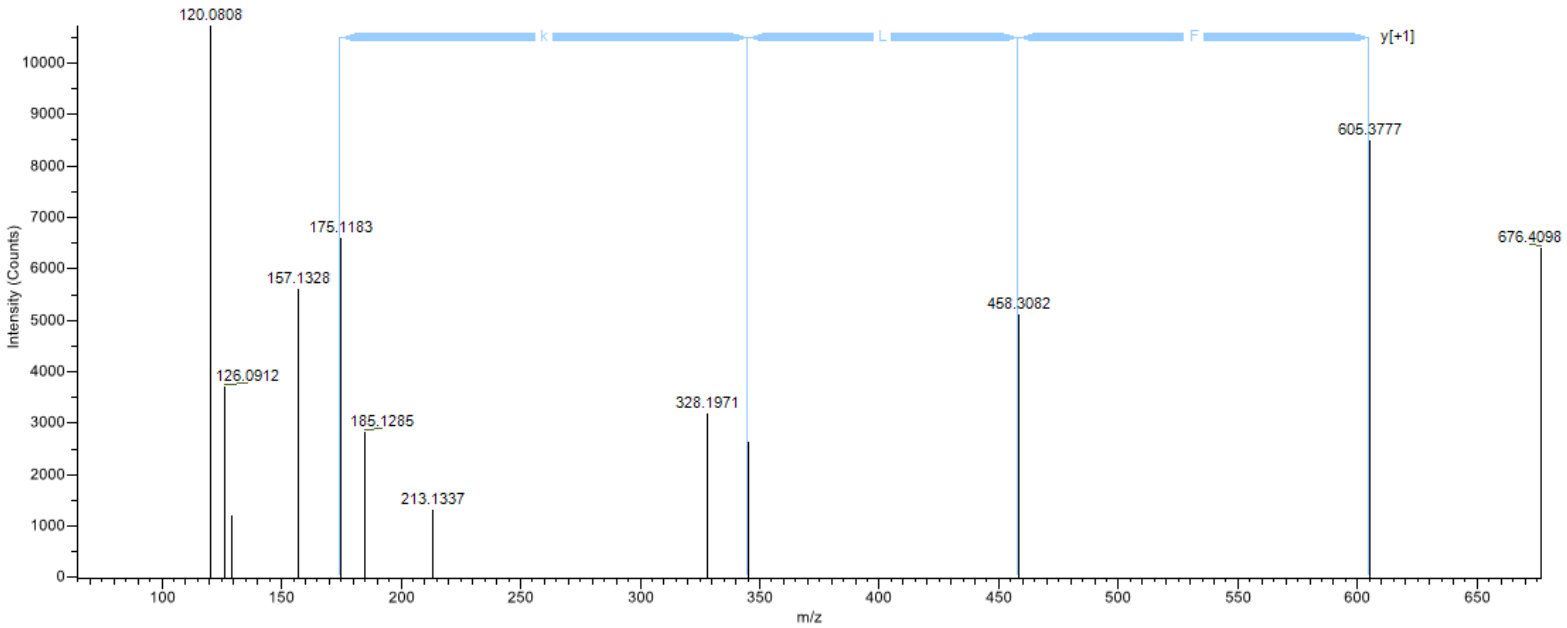

- [x] b
- [ ] b*
- [ ] b°
- [x] y
- [ ] y°
- [ ] y*
- [ ] Immonium

Hide Table

	(NH3+) -	A> <F	F> <L	L> <k	k>	R -
b (+1)	114.09135	185.12847	332.19689	445.28096	615.38649	771.48761
b*(+1)	97.06480	168.10192	315.17034	428.25441	598.35994	754.46106
b°(+1)	96.08078	167.11790	314.18632	427.27039	597.37593	753.47705
y (+1)	676.41411	605.37699	458.30857	345.22450	175.11896	789.49818
y*(+1)	659.38756	588.35044	441.28202	328.19795	158.09241	772.47163
y°(+1)	658.40354	587.36642	440.29800	327.21393	157.10840	771.48761

Value Type: Theo. Mass [Da]

L ⌈A⌋F ⌈L ⌈k ⌈R

z y
b c

Tolerance: Da Charge State: 1

PALB2 K177-ac

Peptide Consensus View

Sequence: LKEQEEISSKNPAR
K2-Acetyl (42.01057 Da)
Charge: +2, Monoisotopic m/z: 835.93756 Da (-1.51 mmu/-1.81 ppm), MH+: 1670.86785 Da, RT: 32.30 min,

Extracted from: C:\Users\Proteomics\Desktop\Marjorie PD searches\PALB2_acetyl\C150302_PALB2+PCAF\C150302_001_1ul_150305043940_PALB2-FL+PCAF.raw #5645 RT: 32.30
FTMS, HCD, z=+2, Mono m/z=835.93756 Da, MH+=1670.86785 Da, Match Tol.=0.05 Da

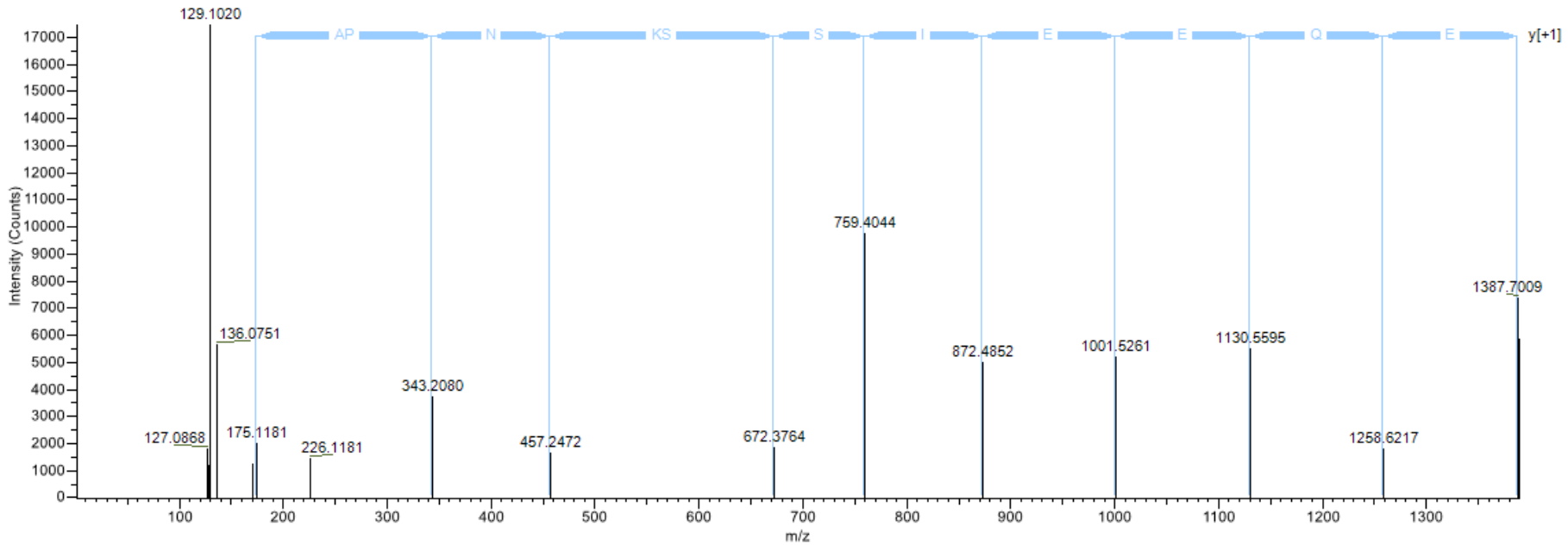

☑ b
☐ b*
☐ b°
☑ y
☐ y°
☐ y*
☐ Immonium

Hide Table

	(NH3+) - L>	k>	<E	E>	<Q	Q>	<E	E>	<E	E>	<I	I>	<S	S>	S>	<K	K>	<N	N>	<P	P>	<A	A>	<R	R - (COOH)
b (+1)	114.09135	284.19688	413.23948	541.29806	670.34066	799.38326	912.46733	999.49936	1086.53139	1214.62636	1328.66929	1425.72206	1496.75918	1652.86030
b*(+1)	97.06480	267.17033	396.21293	524.27151	653.31411	782.35671	895.44078	982.47281	1069.50484	1197.59981	1311.64274	1408.69551	1479.73263	1635.83375
b°(+1)	96.08078	266.18632	395.22892	523.28750	652.33010	781.37270	894.45677	981.48880	1068.52083	1196.61580	1310.65873	1407.71150	1478.74862	1634.84974
y (+1)	1557.78680	1387.68126	1258.63866	1130.58008	1001.53748	872.49488	759.41081	672.37878	585.34675	457.25178	343.20885	246.15608	175.11896	1670.87087
y*(+1)	1540.76025	1370.65471	1241.61211	1113.55353	984.51093	855.46833	742.38426	655.35223	568.32020	440.22523	326.18230	229.12953	158.09241	1653.84432
y°(+1)	1539.77623	1369.67070	1240.62810	1112.56952	983.52692	854.48432	741.40025	654.36822	567.33619	439.24122	325.19829	228.14552	157.10840	1652.86030

Value Type: Theo. Mass [Da]

L *k*ΓEΓQΓEΓEΓI ΓSΓS KΓNΓP AΓR

z y
b c

Tolerance: [redacted] Da Charge State: 1

PALB2 K185-ac

Peptide Consensus View

Sequence: LKEQEEISSKNPAR
K10-Acetyl (42.01057 Da)
Charge: +2, Monoisotopic m/z: 835.93848 Da (-0.6 mmu/-0.71 ppm), MH+: 1670.86968 Da, RT: 37.40 min,

Extracted from: C:\Users\Proteomics\Desktop\Marjorie PD searches\PALB2_acetyl\C150302_PALB2+PCAF\C150302_001_1ul_150305043940_PALB2-FL+PCAF.raw #6607 RT: 37.40
FTMS, HCD, z=+2, Mono m/z=835.93848 Da, MH+=1670.86968 Da, Match Tol.=0.05 Da

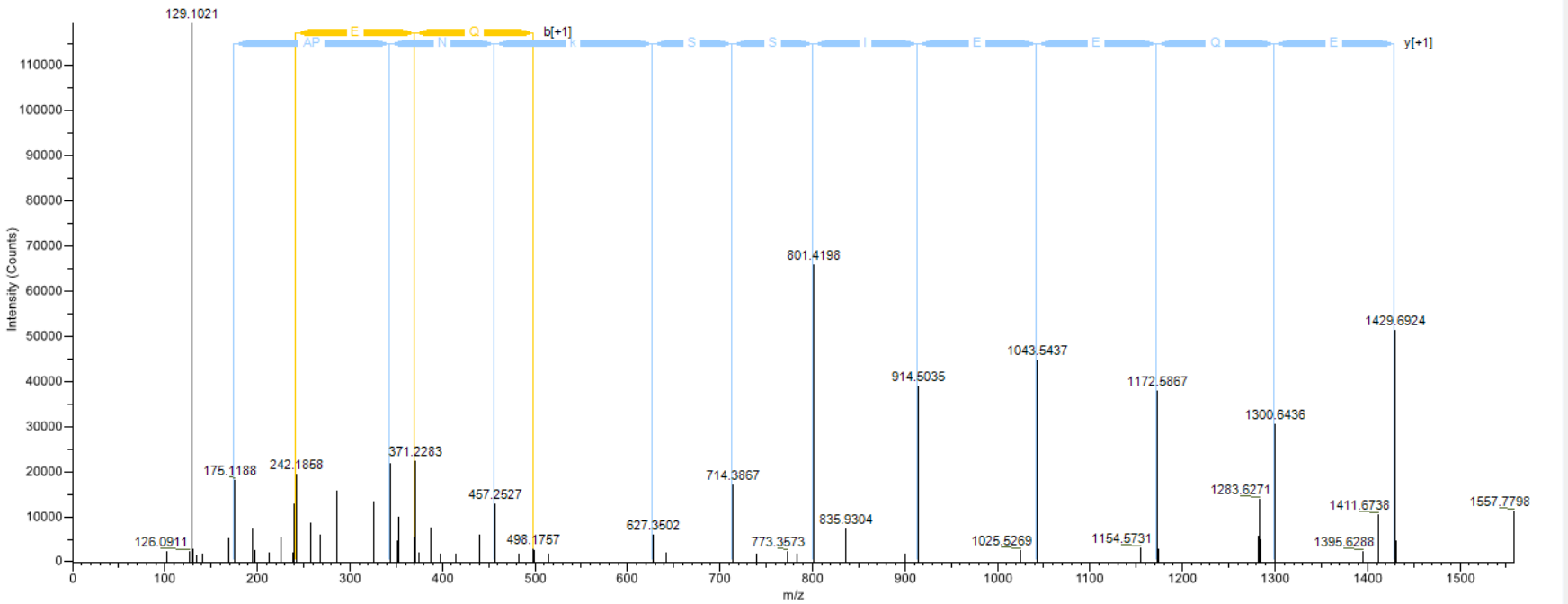

☑ b
☐ b*
☐ b°
☑ y
☐ y°
☐ y*
☐ Immonium

Hide Table

	(NH3+) - L>	K>	<E	E>	<Q	Q>	<E	E>	<E	E>	<I	I>	<S	S>	S>	<k	k>	<N	N>	<P	P>	<A	A>	<R	R - (COOH)
b (+1)	114.09135	242.18632	371.22892	499.28750	628.33010	757.37270	870.45677	957.48880	1044.52083	1214.62636	1328.66929	1425.72206	1496.75918	1652.86030
b*(+1)	97.06480	225.15977	354.20237	482.26095	611.30355	740.34615	853.43022	940.46225	1027.49428	1197.59981	1311.64274	1408.69551	1479.73263	1635.83375
b°(+1)	96.08078	224.17575	353.21835	481.27693	610.31953	739.36213	852.44620	939.47823	1026.51026	1196.61580	1310.65873	1407.71150	1478.74862	1634.84974
y (+1)	1557.78680	1429.69183	1300.64923	1172.59065	1043.54805	914.50545	801.42138	714.38935	627.35732	457.25178	343.20885	246.15608	175.11896	1670.87087
y*(+1)	1540.76025	1412.66528	1283.62268	1155.56410	1026.52150	897.47890	784.39483	697.36280	610.33077	440.22523	326.18230	229.12953	158.09241	1653.84432
y°(+1)	1539.77623	1411.68126	1282.63866	1154.58008	1025.53748	896.49488	783.41081	696.37878	609.34675	439.24122	325.19829	228.14552	157.10840	1652.86030

Value Type: Theo. Mass [Da]

L ⌈K⌋E⌋Q⌋E ⌈E ⌈I ⌈S ⌈S ⌈k ⌈N ⌈P A ⌈R

z y
b c

Tolerance: Da Charge State: 1

PALB2 K294-ac

Peptide Consensus View

Sequence: FTSPVSLEAQGKK
K12-Acetyl (42.01057 Da)
Charge: +2, Monoisotopic m/z: 717.38525 Da (-0.15 mmu/-0.21 ppm), MH+: 1433.76323 Da, RT: 70.61 min,

Extracted from: C:\Users\Proteomics\Desktop\Marjorie PD searches\PALB2_acetyl\C150302_PALB2+PCAF\C150302_001_1ul_150305043940_PALB2-FL+PCAF.raw #12895 RT: 70.61
FTMS, HCD, z=+2, Mono m/z=717.38525 Da, MH+=1433.76323 Da, Match Tol.=0.05 Da

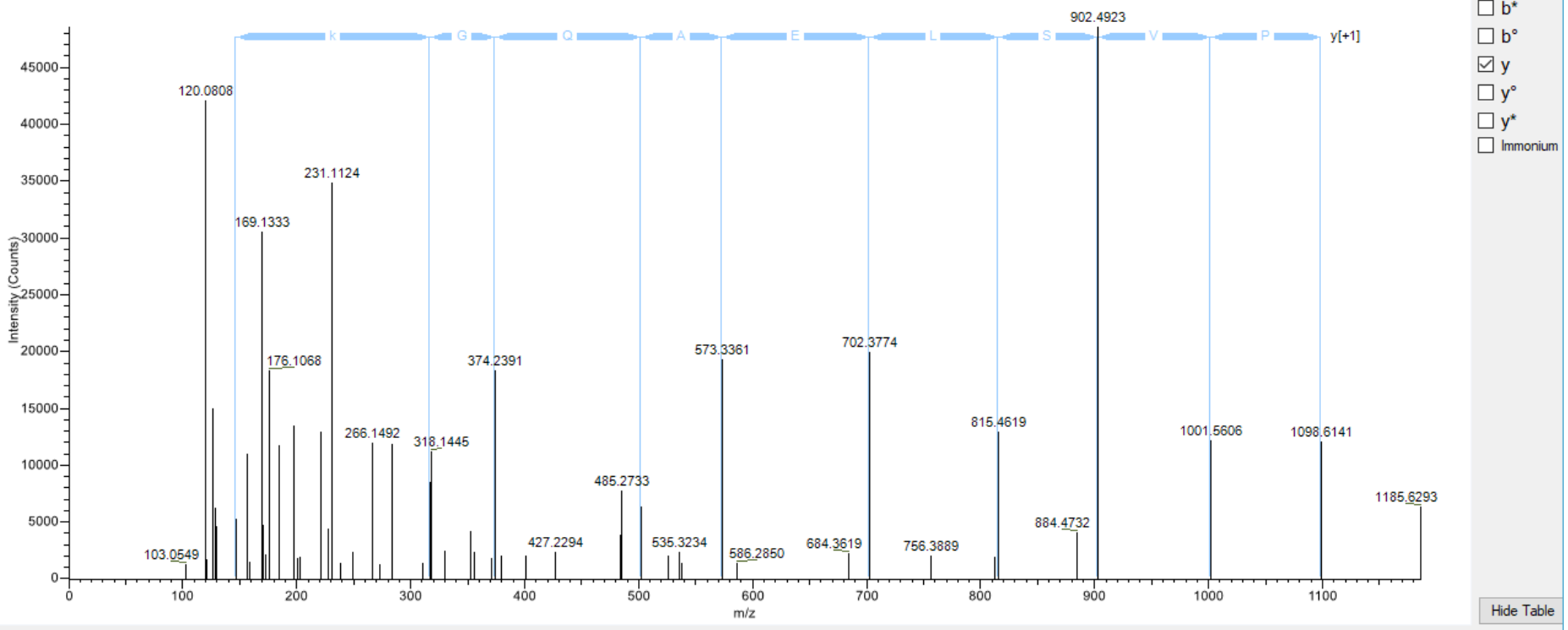

	(NH3+) - F>	T> <S	S> <P	P> <V	V>	S> <L	L> <E	E>	A>	Q> <G	G> <k	k> <K	K - (COOH)
b (+1)	148.07570	249.12338	336.15541	433.20818	532.27660	619.30863	732.39270	861.43530	932.47242	1060.53100	1117.55247	1287.65800	1415.75297
b*(+1)	131.04915	232.09683	319.12886	416.18163	515.25005	602.28208	715.36615	844.40875	915.44587	1043.50445	1100.52592	1270.63145	1398.72642
b°(+1)	130.06513	231.11281	318.14484	415.19761	514.26603	601.29806	714.38213	843.42473	914.46185	1042.52043	1099.54190	1269.64744	1397.74241
y (+1)	1286.69512	1185.64744	1098.61541	1001.56264	902.49422	815.46219	702.37812	573.33552	502.29840	374.23982	317.21835	147.11281	1433.76354
y*(+1)	1269.66857	1168.62089	1081.58886	984.53609	885.46767	798.43564	685.35157	556.30897	485.27185	357.21327	300.19180	130.08626	1416.73699
y°(+1)	1268.68455	1167.63687	1080.60484	983.55207	884.48365	797.45162	684.36755	555.32495	484.28783	356.22925	299.20778	129.10225	1415.75297

Value Type: Theo. Mass [Da]

F T S P V S L E A Q G k K

z y b c

Tolerance: Da Charge State: 1

PALB2 K295-ac

Peptide Consensus View

Sequence: KMTVSTDNLLVNK
K1-Acetyl (42.01057 Da)
Charge: +2, Monoisotopic m/z: 752.90540 Da (-0.26 mmu/-0.34 ppm), MH+: 1504.80351 Da, RT: 78.09 min,

Extracted from: C:\Users\Proteomics\Desktop\Marjorie PD searches\PALB2_acetyl\C150302_PALB2+PCAF\C150302_003_1ul_150305065254_PALB2-P2.2+PCAF.raw #14384 RT: 78.09
FTMS, HCD, z=+2, Mono m/z=752.90540 Da, MH+=1504.80351 Da, Match Tol.=0.05 Da

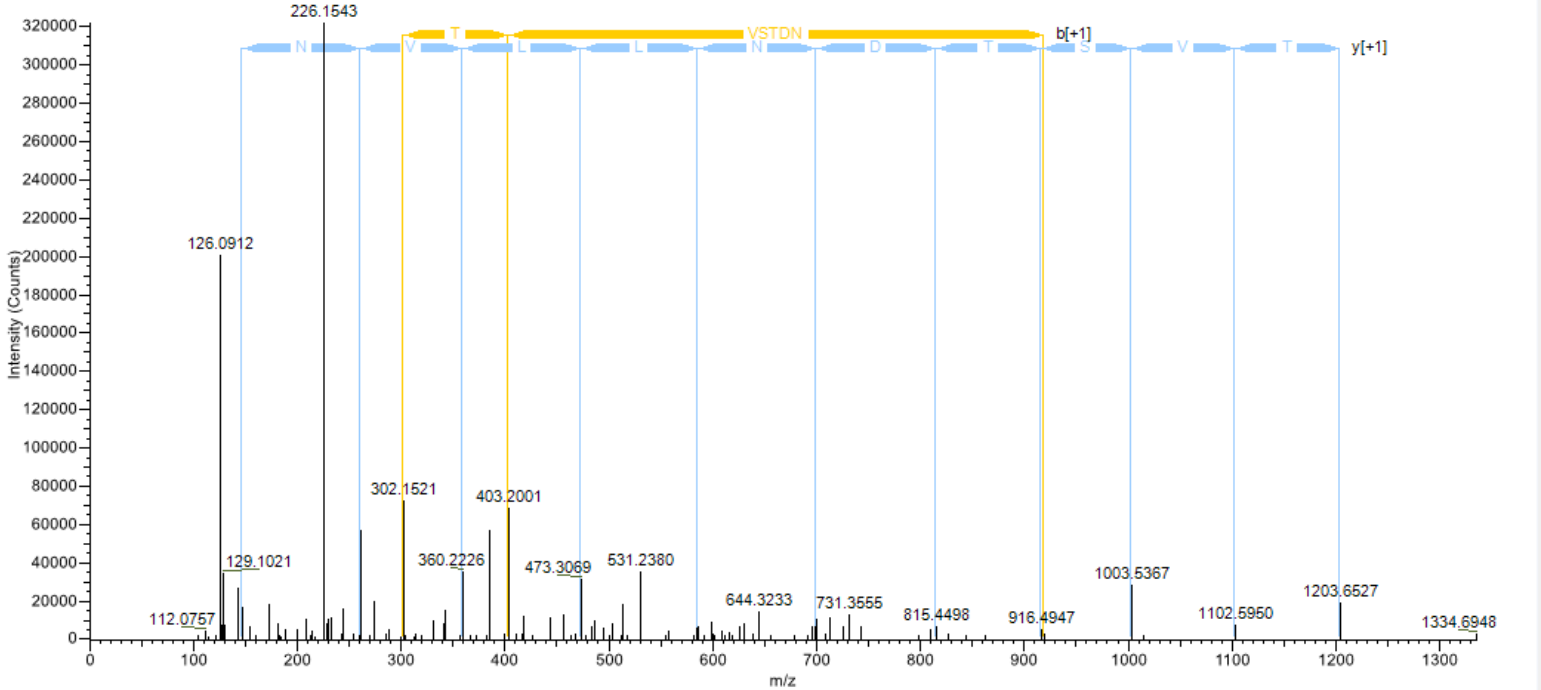

☑ b
☐ b*
☐ b°
☑ y
☐ y°
☐ y*
☐ Immonium

Hide Table

	(NH3+) - k>	M>	<T	T>	<V	V>	<S	S>	T>	D>	N>	L>	<L	L>	<V	V>	<N	N>	<K	K - (COOH)
b (+1)	171.11281	302.15331		403.20099		502.26941		589.30144	690.34912	805.37607	919.41900	1032.50307		1145.58714		1244.65556		1358.69849		1486.79346
b*(+1)	154.08626	285.12676		386.17444		485.24286		572.27489	673.32257	788.34952	902.39245	1015.47652		1128.56059		1227.62901		1341.67194		1469.76691
b°(+1)	153.10225	284.14275		385.19043		484.25885		571.29088	672.33856	787.36551	901.40844	1014.49251		1127.57658		1226.64500		1340.68793		1468.78290
y (+1)	1334.69849	1203.65799		1102.61031		1003.54189		916.50986	815.46218	700.43523	586.39230	473.30823		360.22416		261.15574		147.11281		1504.80403
y*(+1)	1317.67194	1186.63144		1085.58376		986.51534		899.48331	798.43563	683.40868	569.36575	456.28168		343.19761		244.12919		130.08626		1487.77748
y°(+1)	1316.68793	1185.64743		1084.59975		985.53133		898.49930	797.45162	682.42467	568.38174	455.29767		342.21360		243.14518		129.10225		1486.79346

Value Type: Theo. Mass [Da]

k M T V S T D N L L V N K

z y
b c

Tolerance: Da Charge State: 1

PALB2 K307-ac

Peptide Consensus View

Sequence: KMTVSTDNLLVNKAISK
K13-Acetyl (42.01057 Da)
Charge: +3, Monoisotopic m/z: 635.35419 Da (-1.4 mmu/-2.21 ppm), MH+: 1904.04801 Da, RT: 40.89 min,

Extracted from: C:\Users\Proteomics\Desktop\Marjorie PD searches\PALB2_acetyl\C150529_PALB2+GCN5+GCN5mut\C150529_019_PALB2 P2.2+GCN5.raw #9654 RT: 40.89
FTMS, HCD, z=+3, Mono m/z=635.35419 Da, MH+=1904.04801 Da, Match Tol.=0.05 Da

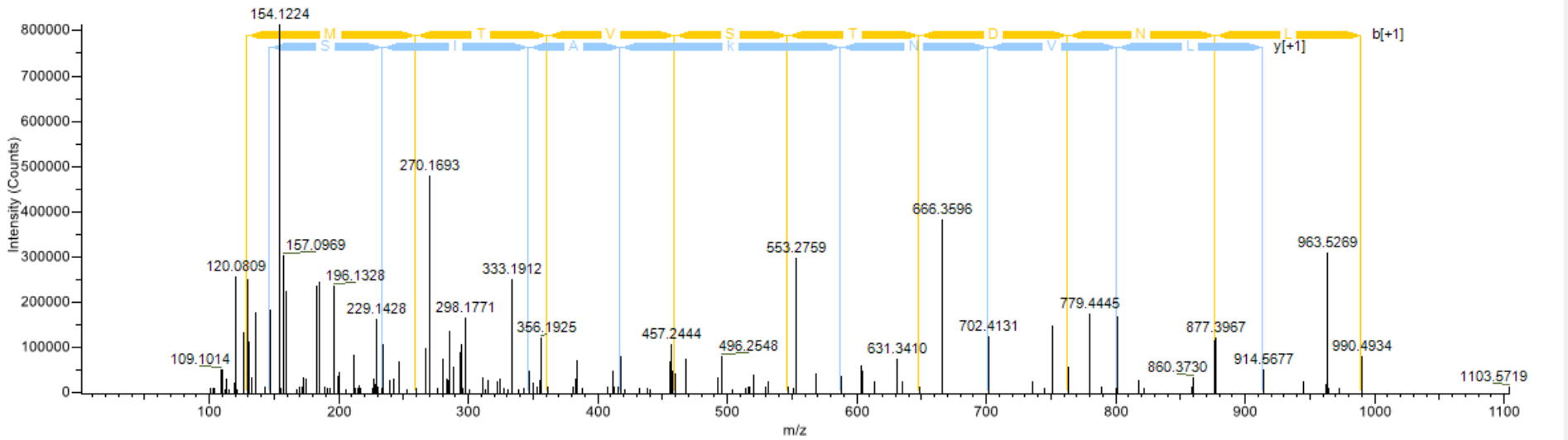

☑ b
☐ b*
☐ b°
☑ y
☐ y°
☐ y*
☐ Immonium

Hide Table

	(NH3+) -	M>	<T	T>	<V	V>	<S	S>	<T	T>	<D	D>	<N	N>	<L	L>	<L	L>	<V	V>	<N	N>	<k	k>	<A	A>	<I	I>	<S	S>
b (+1)	129.10225	260.14275		361.19043		460.25885		547.29088		648.33856		763.36551		877.40844		990.49251		1103.57658		1202.64500		1316.68793		1486.79346		1557.83058		1670.91465		1757.946
b*(+1)	112.07570	243.11620		344.16388		443.23230		530.26433		631.31201		746.33896		860.38189		973.46596		1086.55003		1185.61845		1299.66138		1469.76691		1540.80403		1653.88810		1740.920
b°(+1)	111.09168	242.13218		343.17986		442.24828		529.28031		630.32799		745.35494		859.39787		972.48194		1085.56601		1184.63443		1298.67736		1468.78290		1539.82002		1652.90409		1739.936
y (+1)	1775.95725	1644.91675		1543.86907		1444.80065		1357.76862		1256.72094		1141.69399		1027.65106		914.56699		801.48292		702.41450		588.37157		418.26603		347.22891		234.14484		147.112
y*(+1)	1758.93070	1627.89020		1526.84252		1427.77410		1340.74207		1239.69439		1124.66744		1010.62451		897.54044		784.45637		685.38795		571.34502		401.23948		330.20236		217.11829		130.086

Value Type: Theo. Mass [Da]

K M T V S T D N L L V N k A I S K

z y
b c

Tolerance: Da Charge State: 1

PALB2 K311-ac

Peptide Consensus View

Sequence: MTVSTDNLLVNKAISK
K16-Acetyl (42.01057 Da)
Charge: +2, Monoisotopic m/z: 888.48083 Da (-1.43 mmu/-1.61 ppm), MH+: 1775.95439 Da, RT: 43.82 min,

Extracted from: C:\Users\Proteomics\Desktop\Marjorie PD searches\PALB2_acetyl\C150529_PALB2+GCN5+GCN5mut\C150529_019_PALB2 P2.2+GCN5.raw #10566 RT: 43.82
FTMS, HCD, z=+2, Mono m/z=888.48083 Da, MH+=1775.95439 Da, Match Tol.=0.05 Da

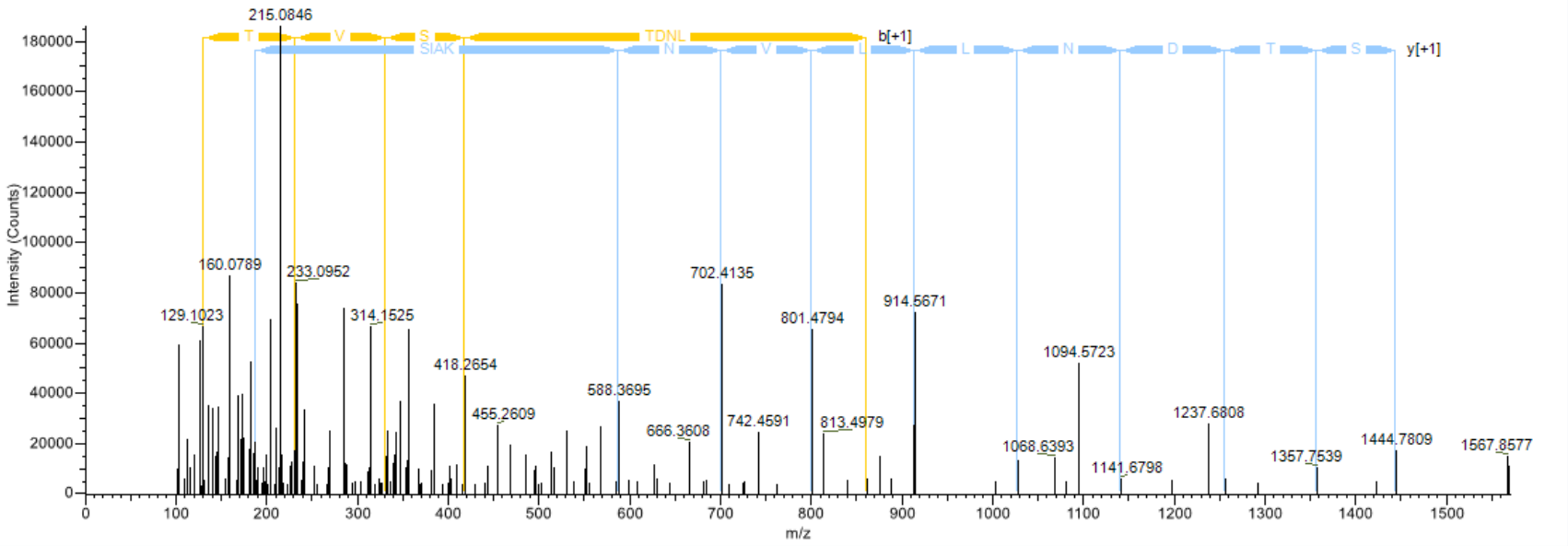

☑ b
☐ b*
☐ b°
☑ y
☐ y°
☐ y*
☐ Immonium

Hide Table

	(NH3+) -	T>	<V	V>	<S	S>	<T	T>	<D	D>	<N	N>	<L	L>	<L	L>	<V	V>	<N	N>	<K	K>	<A	A>	<I	I>	<S	S>	<k
b (+1)	132.04778	233.09546		332.16388		419.19591		520.24359		635.27054		749.31347		862.39754		975.48161		1074.55003		1188.59296		1316.68793		1387.72505		1500.80912		1587.8411
b*(+1)	115.02123	216.06891		315.13733		402.16936		503.21704		618.24399		732.28692		845.37099		958.45506		1057.52348		1171.56641		1299.66138		1370.69850		1483.78257		1570.8146
b°(+1)	114.03721	215.08489		314.15331		401.18534		502.23302		617.25997		731.30290		844.38697		957.47104		1056.53946		1170.58239		1298.67736		1369.71448		1482.79855		1569.8305
y (+1)	1644.91675	1543.86907		1444.80065		1357.76862		1256.72094		1141.69399		1027.65106		914.56699		801.48292		702.41450		588.37157		460.27660		389.23948		276.15541		189.1233
y*(+1)	1627.89020	1526.84252		1427.77410		1340.74207		1239.69439		1124.66744		1010.62451		897.54044		784.45637		685.38795		571.34502		443.25005		372.21293		259.12886		172.0968

Value Type: Theo. Mass [Da]

M T V S T D N L L V N K A I S k

Tolerance: Da Charge State: 1

PALB2 K356-ac

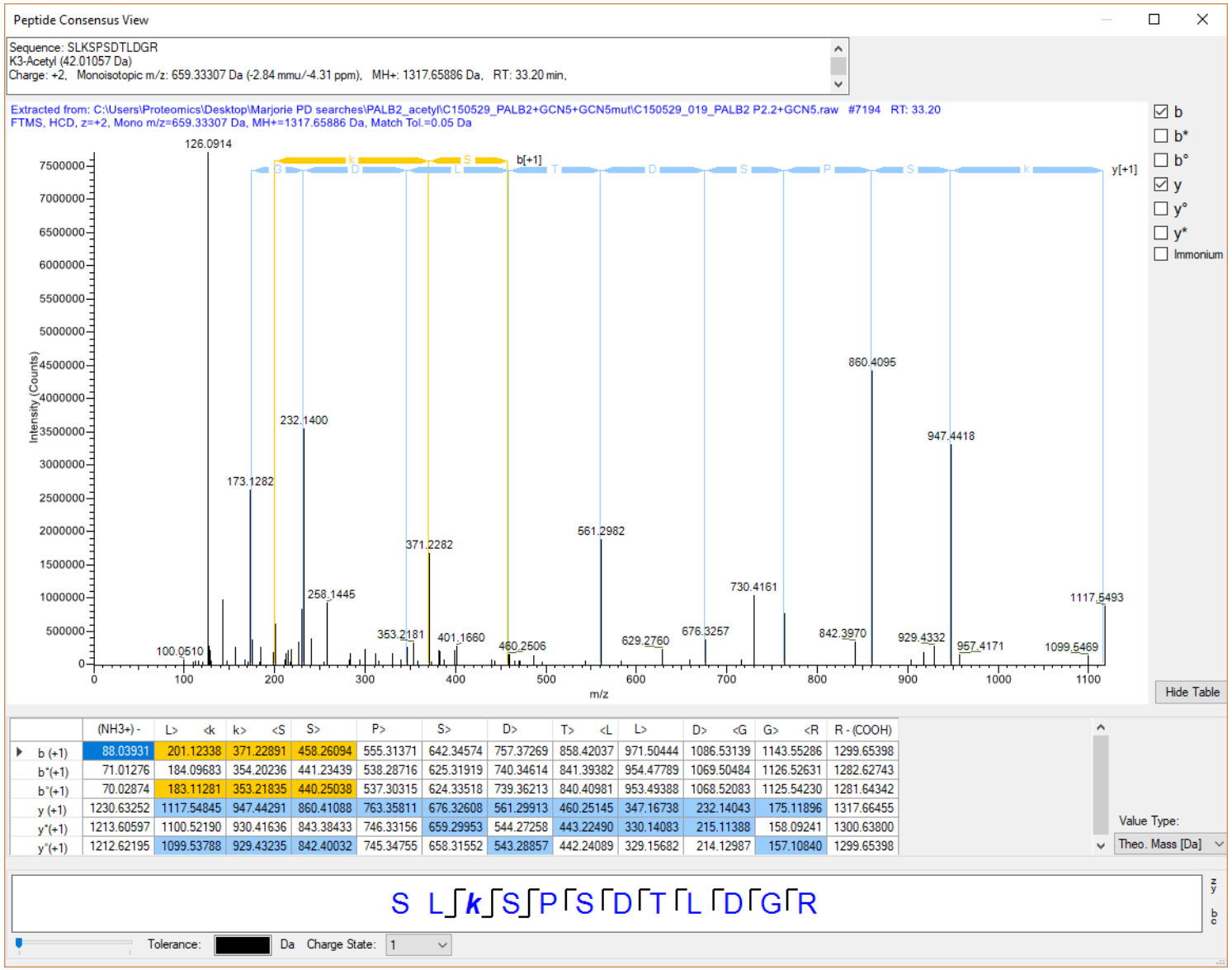

	(NH3+) -	L> <k	k> <S	S>	P>	S>	D>	T> <L	L>	D> <G	G> <R	R - (COOH)
b (+1)	88.03931	201.12338	371.22891	458.26094	555.31371	642.34574	757.37269	858.42037	971.50444	1086.53139	1143.55286	1299.65398
b*(+1)	71.01276	184.09683	354.20236	441.23439	538.28716	625.31919	740.34614	841.39382	954.47789	1069.50484	1126.52631	1282.62743
b°(+1)	70.02874	183.11281	353.21835	440.25038	537.30315	624.33518	739.36213	840.40981	953.49388	1068.52083	1125.54230	1281.64342
y (+1)	1230.63252	1117.54845	947.44291	860.41088	763.35811	676.32608	561.29913	460.25145	347.16738	232.14043	175.11896	1317.66455
y*(+1)	1213.60597	1100.52190	930.41636	843.38433	746.33156	659.29953	544.27258	443.22490	330.14083	215.11388	158.09241	1300.63800
y°(+1)	1212.62195	1099.53788	929.43235	842.40032	745.34755	658.31552	543.28857	442.24089	329.15682	214.12987	157.10840	1299.65398

PALB2 K393-ac

Peptide Consensus View

Sequence: SLSLEATSPLSAEKHSCTVPEGLLFPAEYYVR
K14-Acetyl (42.01057 Da), C17-Carbamidomethyl (57.02146 Da)
Charge: +3, Monoisotopic m/z: 1198.59985 Da (+0.55 mmu/+0.46 ppm), MH+: 3593.78501 Da, RT: 38.25 min,

Extracted from: D:\Data_D_90362\Marjorie Fournier\C130424_037.raw #12306 RT: 38.25
FTMS, HCD, z=+3, Mono m/z=1198.59985 Da, MH+=3593.78501 Da, Match Tol.=0.05 Da

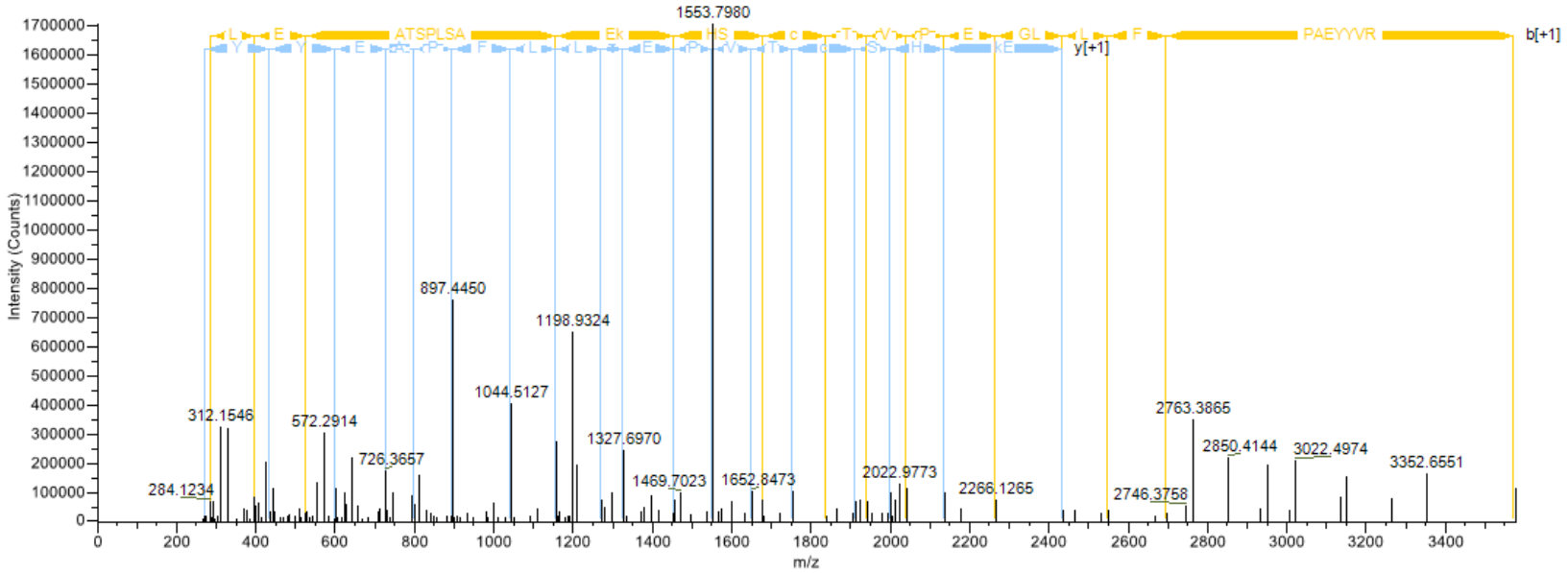

☑ b
☐ b*
☐ b°
☑ y
☐ y°
☐ y*
☐ Immonium

Hide Table

	(NH3+) -	L>	<S	S>	<L	L>	<E	E>	<A	A>	<T	T>	<S	S>	<P	P>	<L	L>	<S	S>	<A	A>	<E	E>	<k	k>	<H	H
b (+1)	88.03931	201.12338		288.15541		401.23948		530.28208		601.31920		702.36688		789.39891		886.45168		999.53575		1086.56778		1157.60490		1286.64750		1456.75303		15
b*(+1)	71.01276	184.09683		271.12886		384.21293		513.25553		584.29265		685.34033		772.37236		869.42513		982.50920		1069.54123		1140.57835		1269.62095		1439.72648		15
b°(+1)	70.02874	183.11281		270.14484		383.22891		512.27151		583.30863		684.35631		771.38834		868.44111		981.52518		1068.55721		1139.59433		1268.63693		1438.74247		15
y (+1)	3506.75133	3393.66726		3306.63523		3193.55116		3064.50856		2993.47144		2892.42376		2805.39173		2708.33896		2595.25489		2508.22286		2437.18574		2308.14314		2138.03761		20
y*(+1)	3489.72478	3376.64071		3289.60868		3176.52461		3047.48201		2976.44489		2875.39721		2788.36518		2691.31241		2578.22834		2491.19631		2420.15919		2291.11659		2121.01106		19

Value Type: Theo. Mass [Da]

S L S L E A T S P L S A E k H S c T V P E G L L F P A E Y Y V R

z y
b c

Tolerance: Da Charge State: 1

PALB2 K422-ac

Peptide Consensus View

Sequence: KVAVEAVIQSHLDVK
K1-Acetyl (42.01057 Da)
Charge: +2, Monoisotopic m/z: 839.48108 Da (+0.7 mmu/+0.84 ppm), MH+: 1677.95488 Da, RT: 32.23 min,

Extracted from: D:\Data_D_90362\Marjorie Fournier\C130424_037.raw #10144 RT: 32.23
FTMS, HCD, z=+2, Mono m/z=839.48108 Da, MH+=1677.95488 Da, Match Tol.=0.05 Da

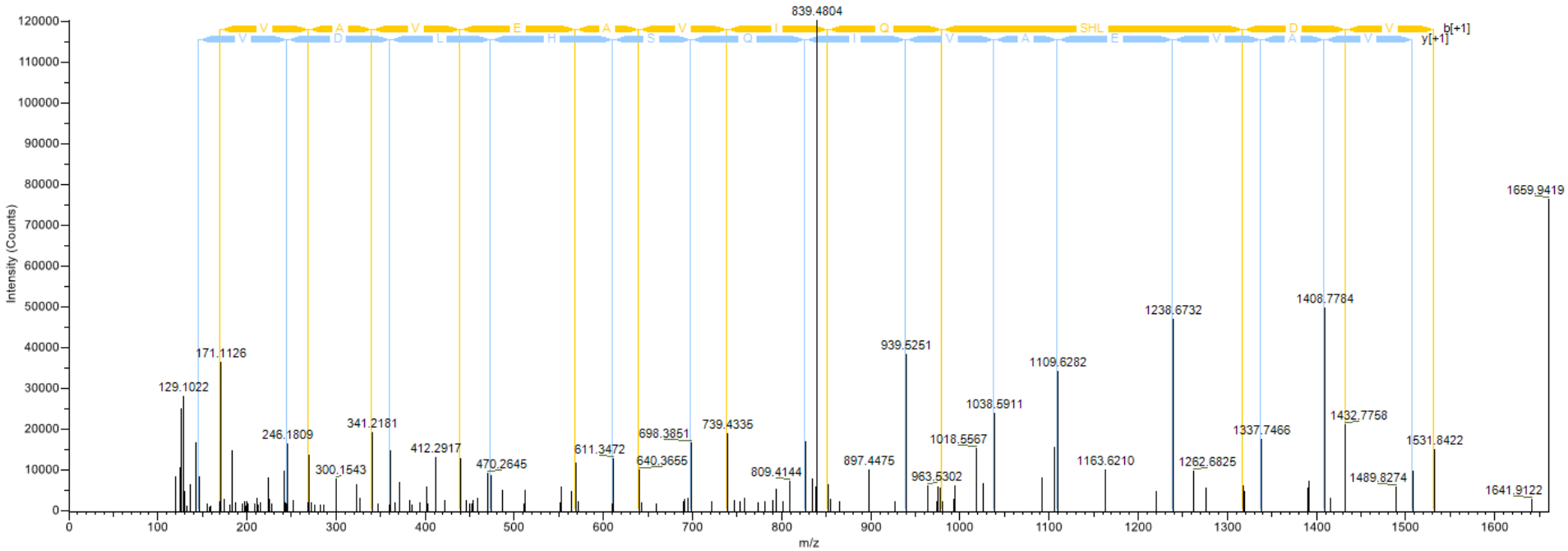

	(NH3+) - k>	V>	<A	A>	<V	V>	<E	E>	<A	A>	<V	V>	<I	I>	<Q	Q>	S>	<H	H>	<L	L>	<D	D>	<V	V>	<K	K - (COOH)
b (+1)	171.11281	270.18123		341.21835		440.28677		569.32937		640.36649		739.43491		852.51898		980.57756	1067.60959		1204.66850		1317.75257		1432.77952		1531.84794		1659.94291
b*(+1)	154.08626	253.15468		324.19180		423.26022		552.30282		623.33994		722.40836		835.49243		963.55101	1050.58304		1187.64195		1300.72602		1415.75297		1514.82139		1642.91636
b°(+1)	153.10225	252.17067		323.20779		422.27621		551.31881		622.35593		721.42435		834.50842		962.56700	1049.59903		1186.65794		1299.74201		1414.76896		1513.83738		1641.93235
y (+1)	1507.84794	1408.77952		1337.74240		1238.67398		1109.63138		1038.59426		939.52584		826.44177		698.38319	611.35116		474.29225		361.20818		246.18123		147.11281		1677.95348
y*(+1)	1490.82139	1391.75297		1320.71585		1221.64743		1092.60483		1021.56771		922.49929		809.41522		681.35664	594.32461		457.26570		344.18163		229.15468		130.08626		1660.92693
y°(+1)	1489.83738	1390.76896		1319.73184		1220.66342		1091.62082		1020.58370		921.51528		808.43121		680.37263	593.34060		456.28169		343.19762		228.17067		129.10225		1659.94291

Value Type: Theo. Mass [Da]

k⌡V⌡A⌡V⌡E⌡A⌡V⌡I ⌡Q⌡S⌈H⌈L⌡D⌡V⌡K⌋

z y
b c

Tolerance: Da Charge State: 1

PALB2 K436-ac

Peptide Consensus View

Sequence: VAVEAVIQSHLDVKKK
K14-Acetyl (42.01057 Da)
Charge: +3, Monoisotopic m/z: 602.68726 Da (-0.41 mmu/-0.68 ppm), MH+: 1806.04721 Da, RT: 29.57 min,

Extracted from: D:\Data_D_90362\Marjorie Fournier\C130424_037.raw #9228 RT: 29.57
FTMS, HCD, z=+3, Mono m/z=602.68726 Da, MH+=1806.04721 Da, Match Tol.=0.05 Da

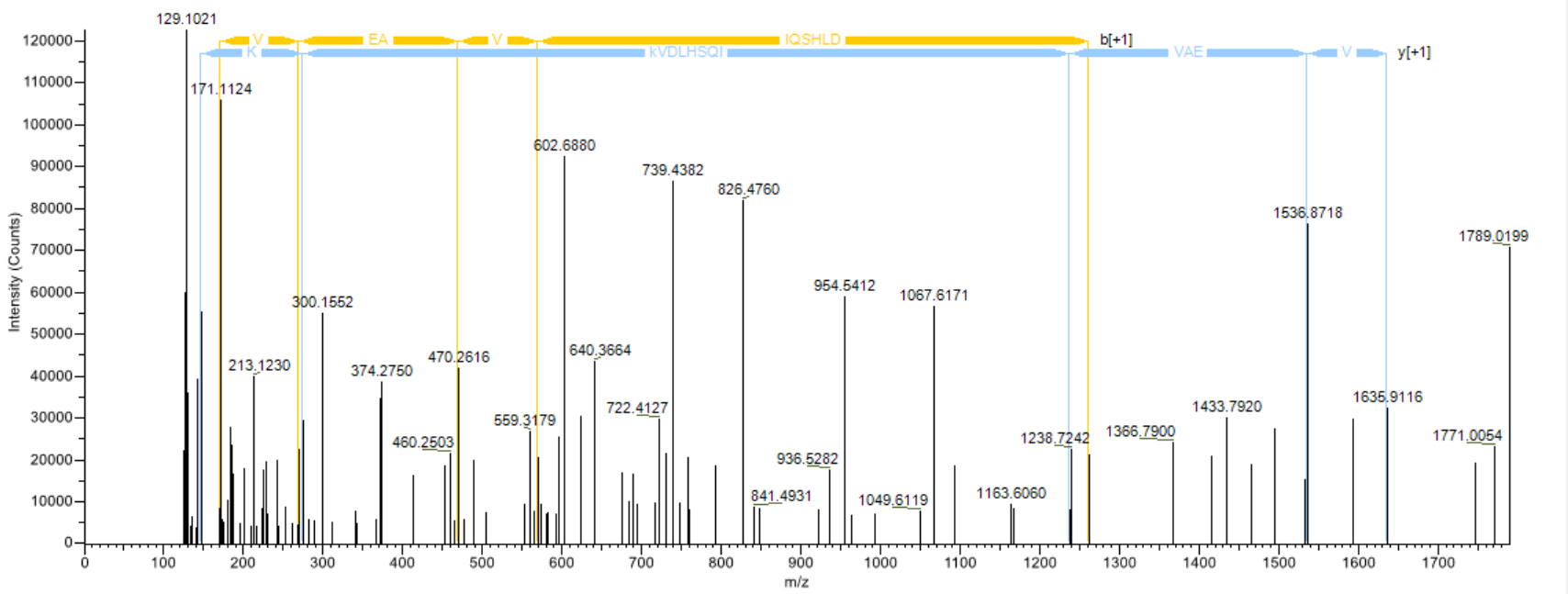

☑ b
☐ b*
☐ b°
☑ y
☐ y°
☐ y*
☐ Immonium

Hide Table

	(NH3+) -	A>	<V	V>	<E	E>	<A	A>	<V	V>	<I	I>	<Q	Q>	S>	H>	<L	L>	<D	D>	<V	V>	<k	k>	<K	K>	<K	K
b (+1)	100.07570	171.11282		270.18124		399.22384		470.26096		569.32938		682.41345		810.47203	897.50406	1034.56297		1147.64704		1262.67399		1361.74241		1531.84794		1659.94291		17
b*(+1)	83.04915	154.08627		253.15469		382.19729		453.23441		552.30283		665.38690		793.44548	880.47751	1017.53642		1130.62049		1245.64744		1344.71586		1514.82139		1642.91636		17
b°(+1)	82.06513	153.10225		252.17067		381.21327		452.25039		551.31881		664.40288		792.46146	879.49349	1016.55240		1129.63647		1244.66342		1343.73184		1513.83738		1641.93235		17
y (+1)	1706.98003	1635.94291		1536.87449		1407.83189		1336.79477		1237.72635		1124.64228		996.58370	909.55167	772.49276		659.40869		544.38174		445.31332		275.20778		147.11281		18
y*(+1)	1689.95348	1618.91636		1519.84794		1390.80534		1319.76822		1220.69980		1107.61573		979.55715	892.52512	755.46621		642.38214		527.35519		428.28677		258.18123		130.08626		17

Value Type:
Theo. Mass [Da]

V A⌡V⌡E A⌡V⌡I Q S H L D⌡V ***k***⌈K⌈K

z
y
b
c

Tolerance: Da Charge State: 1

PALB2 K437-ac

Peptide Consensus View

Sequence: VAVEAVIQSHLDVKK
K15-Acetyl (42.01057 Da)
Charge: +2, Monoisotopic m/z: 839.48108 Da (+0.7 mmu/+0.84 ppm), MH+: 1677.95488 Da, RT: 32.23 min,

Extracted from: D:\Data_D_90362\Marjorie Fournier\C130424_037.raw #10144 RT: 32.23
FTMS, HCD, z=+2, Mono m/z=839.48108 Da, MH+=1677.95488 Da, Match Tol.=0.05 Da

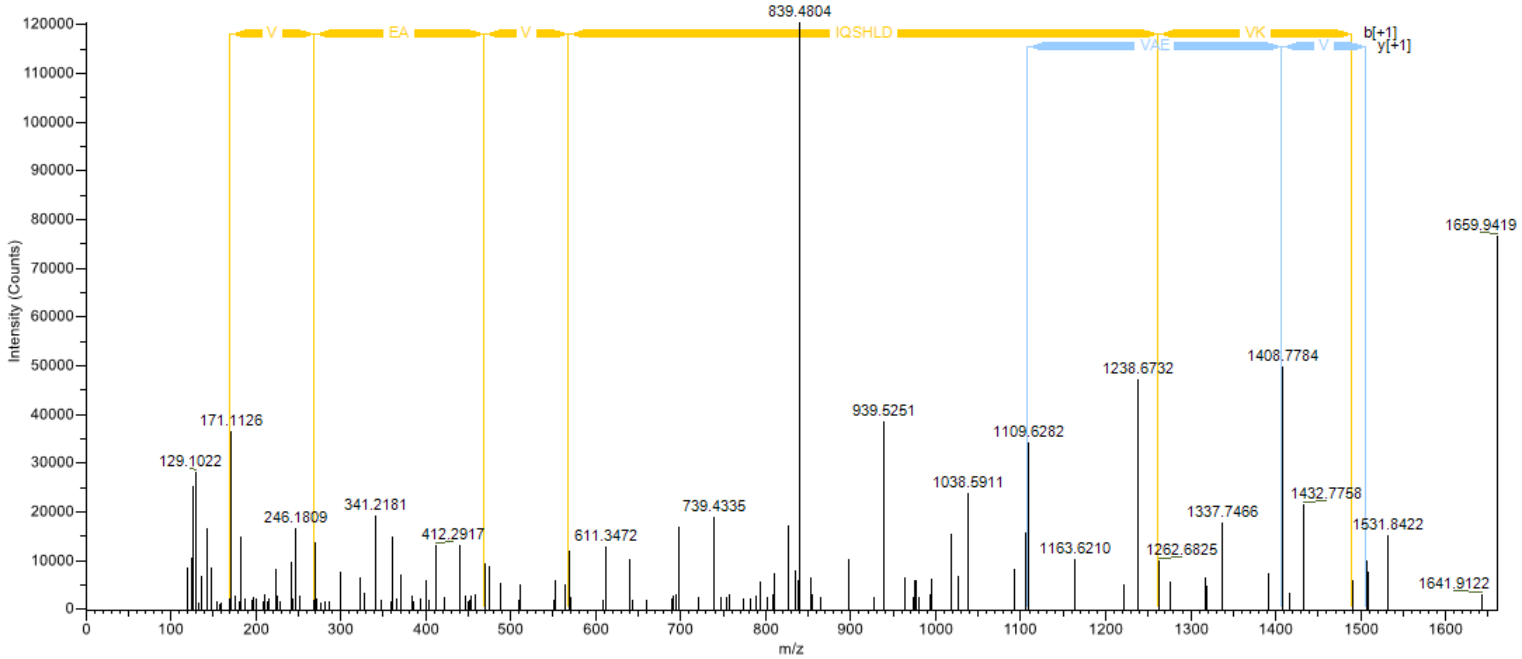

- [x] b
- [ ] b*
- [ ] b°
- [x] y
- [ ] y°
- [ ] y*
- [ ] Immonium

Hide Table

	(NH3+) -	A>	<V	V>	<E	E>	<A	A>	<V	V>	<I	I>	<Q	Q>	S>	H>	<L	L>	<D	D>	<V	V>	<K	K>	<k	k - (COOH)
b (+1)	100.07570	171.11282		270.18124		399.22384		470.26096		569.32938		682.41345		810.47203	897.50406	1034.56297		1147.64704		1262.67399		1361.74241		1489.83738		1659.9429
b*(+1)	83.04915	154.08627		253.15469		382.19729		453.23441		552.30283		665.38690		793.44548	880.47751	1017.53642		1130.62049		1245.64744		1344.71586		1472.81083		1642.9163
b°(+1)	82.06513	153.10225		252.17067		381.21327		452.25039		551.31881		664.40288		792.46146	879.49349	1016.55240		1129.63647		1244.66342		1343.73184		1471.82681		1641.9323
y (+1)	1578.88506	1507.84794		1408.77952		1279.73692		1208.69980		1109.63138		996.54731		868.48873	781.45670	644.39779		531.31372		416.28677		317.21835		189.12338		1677.9534
y°(+1)	1561.85851	1490.82139		1391.75297		1262.71037		1191.67325		1092.60483		979.52076		851.46218	764.43015	627.37124		514.28717		399.26022		300.19180		172.09683		1660.9269

Value Type: Theo. Mass [Da]

V A V E A V I Q S H L D V K k

Tolerance: Da Charge State: 1

PALB2 K438-ac

Peptide Consensus View

Sequence: KGFKNK
K1-Acetyl (42.01057 Da)
Charge: +2, Monoisotopic m/z: 382.22653 Da (-0.17 mmu/-0.46 ppm), MH+: 763.44579 Da, RT: 12.95 min,

Extracted from: D:\Data_D_90362\Marjorie Fournier\C130424_037.raw #3057 RT: 12.95
FTMS, HCD, z=+2, Mono m/z=382.22653 Da, MH+=763.44579 Da, Match Tol.=0.05 Da

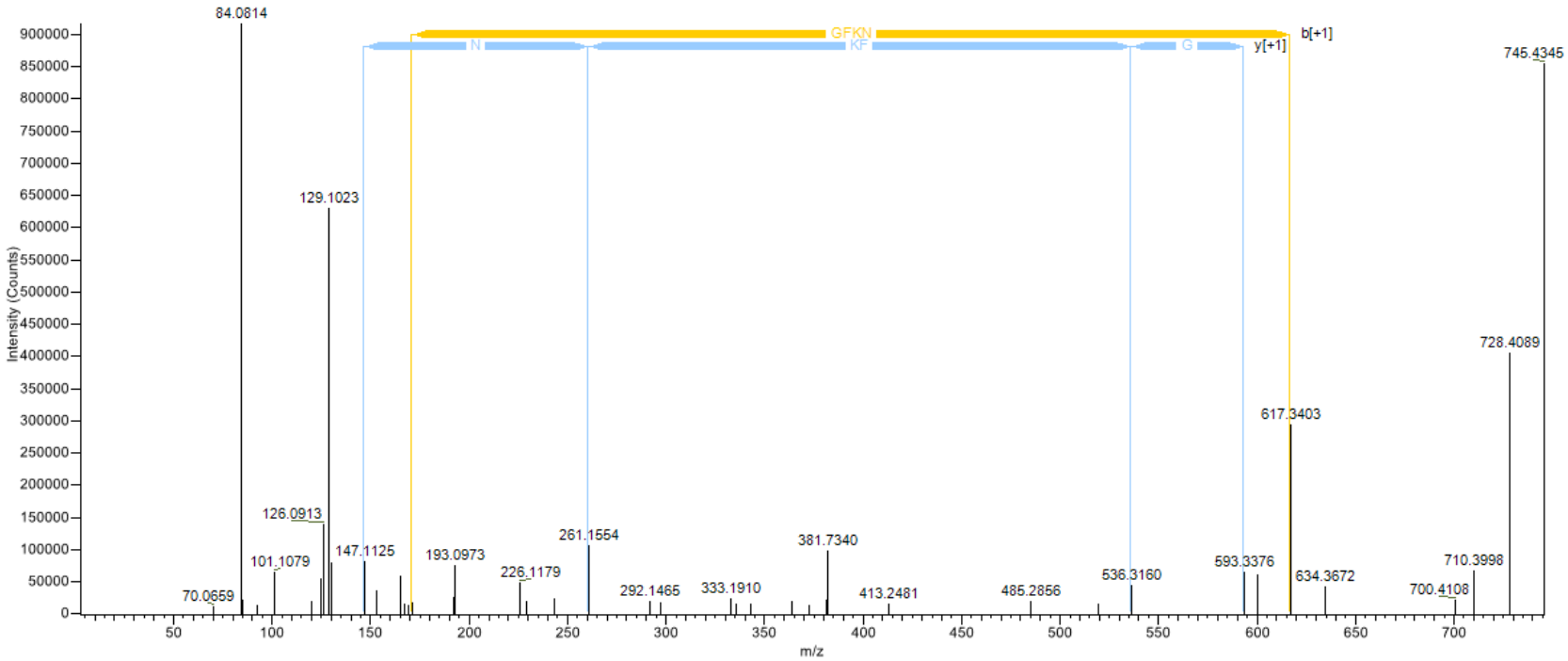

☑ b
☐ b*
☐ b°
☑ y
☐ y°
☐ y*
☐ Immonium

Hide Table

	(NH3+) -	G>	F> <K	K>	N>	K -
b (+1)	171.11281	228.13428	375.20270	503.29767	617.34060	745.43557
b*(+1)	154.08626	211.10773	358.17615	486.27112	600.31405	728.40902
b°(+1)	153.10225	210.12372	357.19214	485.28711	599.33004	727.42501
y (+1)	593.34060	536.31913	389.25071	261.15574	147.11281	763.44614
y*(+1)	576.31405	519.29258	372.22416	244.12919	130.08626	746.41959
y°(+1)	575.33004	518.30857	371.24015	243.14518	129.10225	745.43557

Value Type: Theo. Mass [Da]

k⌡G⌠F K⌠N⌡K⌡

z y
b c

Tolerance: Da Charge State: 1

PALB2 K441-ac

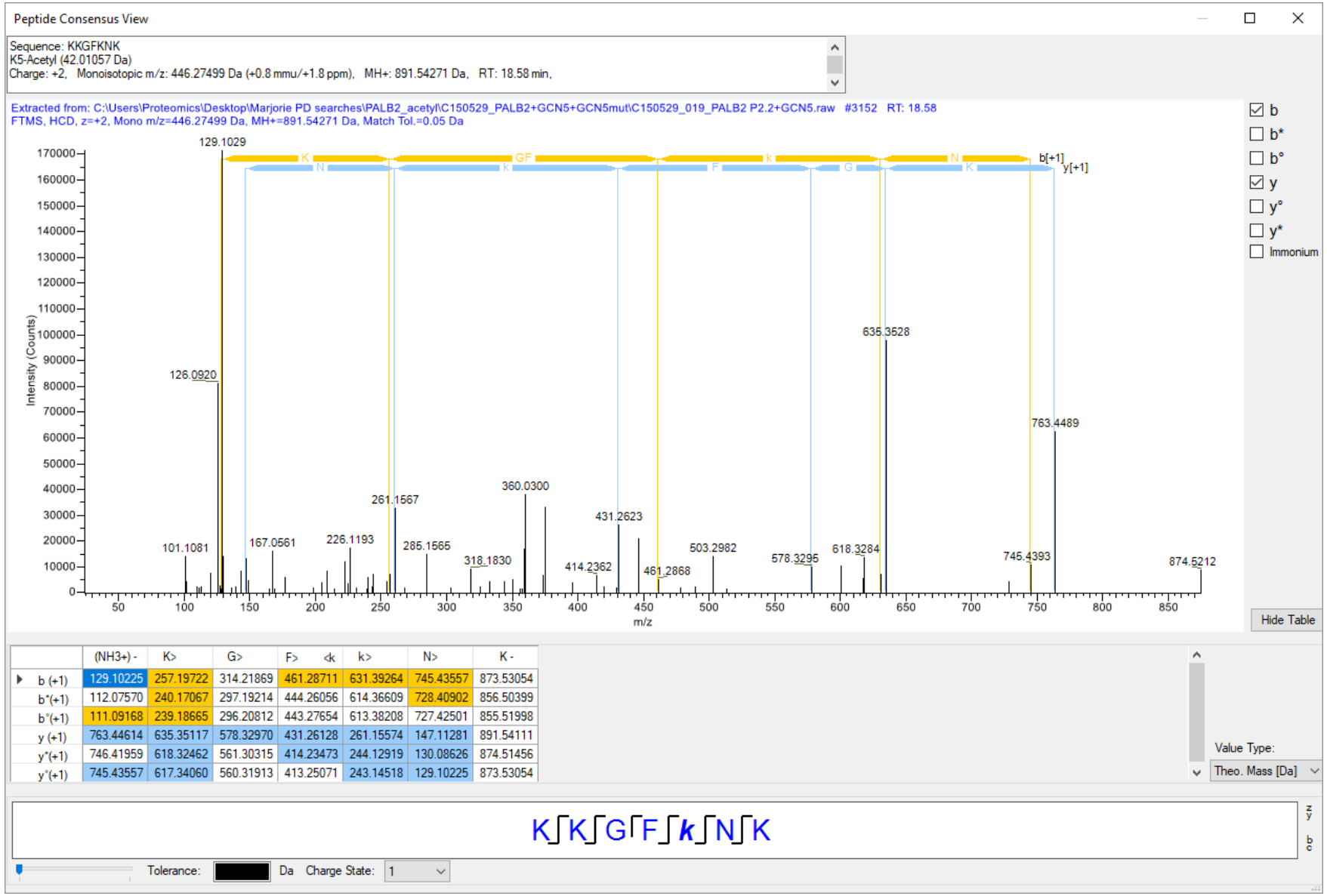

	(NH3+) -	K>	G>	F> <k	k>	N>	K -
b (+1)	129.10225	257.19722	314.21869	461.28711	631.39264	745.43557	873.53054
b*(+1)	112.07570	240.17067	297.19214	444.26056	614.36609	728.40902	856.50399
b°(+1)	111.09168	239.18665	296.20812	443.27654	613.38208	727.42501	855.51998
y (+1)	763.44614	635.35117	578.32970	431.26128	261.15574	147.11281	891.54111
y*(+1)	746.41959	618.32462	561.30315	414.23473	244.12919	130.08626	874.51456
y°(+1)	745.43557	617.34060	560.31913	413.25071	243.14518	129.10225	873.53054

PALB2 K443-ac

Peptide Consensus View

Sequence: NKNKDASKNLNLSNEETDQSEIR
K2-Acetyl (42.01057 Da)
Charge: +4, Monoisotopic m/z: 673.08118 Da (+0.1 mmu/+0.15 ppm), MH+: 2689.30288 Da, RT: 50.02 min,

Extracted from: C:\Users\Proteomics\Desktop\Marjorie PD searches\PALB2_acetyl\C150302_PALB2+PCAF\C150302_003_1ul_150305065254_PALB2-P2.2+PCAF.raw #9024 RT: 50.02
FTMS, HCD, z=+4, Mono m/z=673.08118 Da, MH+=2689.30288 Da, Match Tol.=0.05 Da

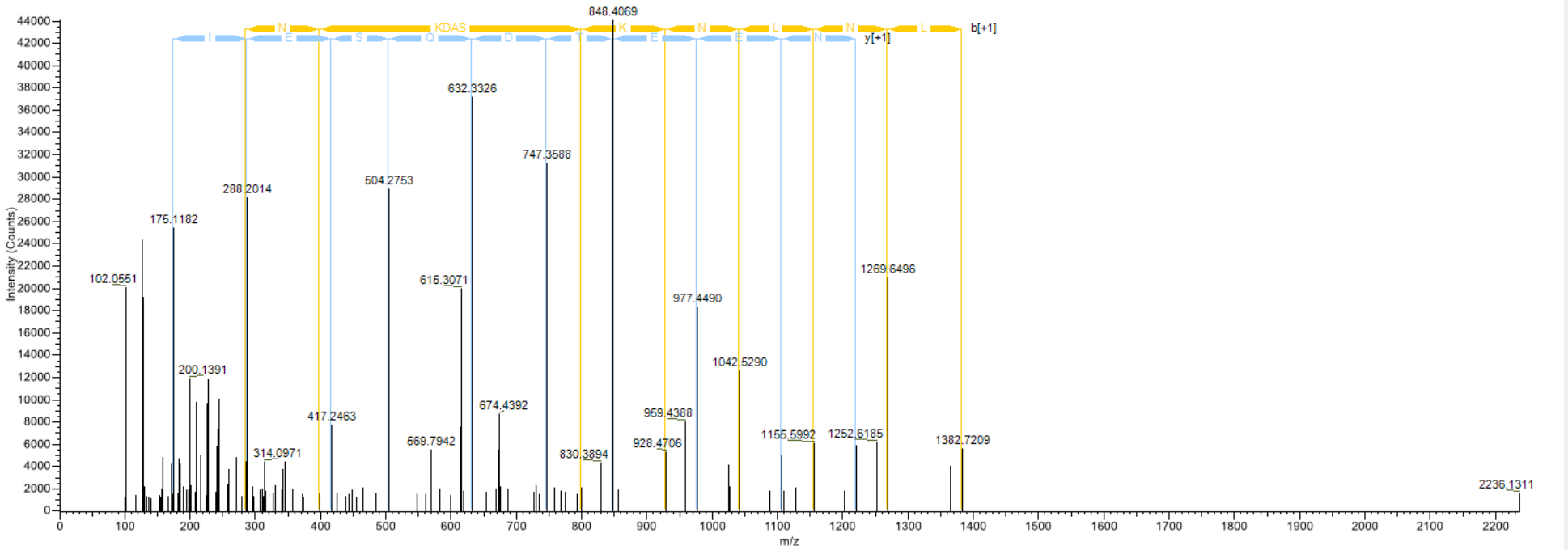

Hide Table

	(NH3+) -	k>	<N	N>	<K	K>	<D	D>	<A	A>	<S	S>	<K	K>	<N	N>	<L	L>	<N	N>	<L	L>	<S	S>	<N	N>	<E	E>	<E	E>	<T	T>	<D	D>	<Q	Q>	<S	S>
b (+1)	115.05021	285.15574	399.19867	527.29364	642.32059	713.35771	800.38974	928.48471	1042.52764	1155.61171	1269.65464	1382.73871	1469.77074	1583.81367	1712.85627	1841.89887	1942.94655	2057.97350	2186.03208	2273.0
b°(+1)	98.02366	268.12919	382.17212	510.26709	625.29404	696.33116	783.36319	911.45816	1025.50109	1138.58516	1252.62809	1365.71216	1452.74419	1566.78712	1695.82972	1824.87232	1925.92000	2040.94695	2169.00553	2256.0
b*(+1)	97.03964	267.14518	381.18811	509.28308	624.31003	695.34715	782.37918	910.47415	1024.51708	1137.60115	1251.64408	1364.72815	1451.76018	1565.80311	1694.84571	1823.88831	1924.93599	2039.96294	2168.02152	2255.0
y (+1)	2575.25954	2405.15400	2291.11107	2163.01610	2047.98915	1976.95203	1889.92000	1761.82503	1647.78210	1534.69803	1420.65510	1307.57103	1220.53900	1106.49607	977.45347	848.41087	747.36319	632.33624	504.27766	417.2
y*(+1)	2558.23299	2388.12745	2274.08452	2145.98955	2030.96260	1959.92548	1872.89345	1744.79848	1630.75555	1517.67148	1403.62855	1290.54448	1203.51245	1089.46952	960.42692	831.38432	730.33664	615.30969	487.25111	400.2

Value Type: Theo. Mass [Da]

N k N K D A S K N L N L S N E E T D Q S E I R

Tolerance: Da Charge State: 1

PALB2 K445-ac

Peptide Consensus View

Sequence: NKNKDASKNLNLSNEETDQSEIR
K4-Acetyl (42.01057 Da)
Charge: +3, Monoisotopic m/z: 897.10272 Da (-2.95 mmu/-3.29 ppm), MH+: 2689.29361 Da, RT: 29.55 min,

Extracted from: C:\Users\Proteomics\Desktop\Marjorie PD searches\PALB2_acetyl\C150703_PALB2+GCN5+GCN5mut\Qex02_SVH_150703_MarjorieFournier_4_PALB2-P2.2+GCN5.raw #8480 RT: 29.55
FTMS, HCD, z=+3, Mono m/z=897.10272 Da, MH+=2689.29361 Da, Match Tol.=0.05 Da

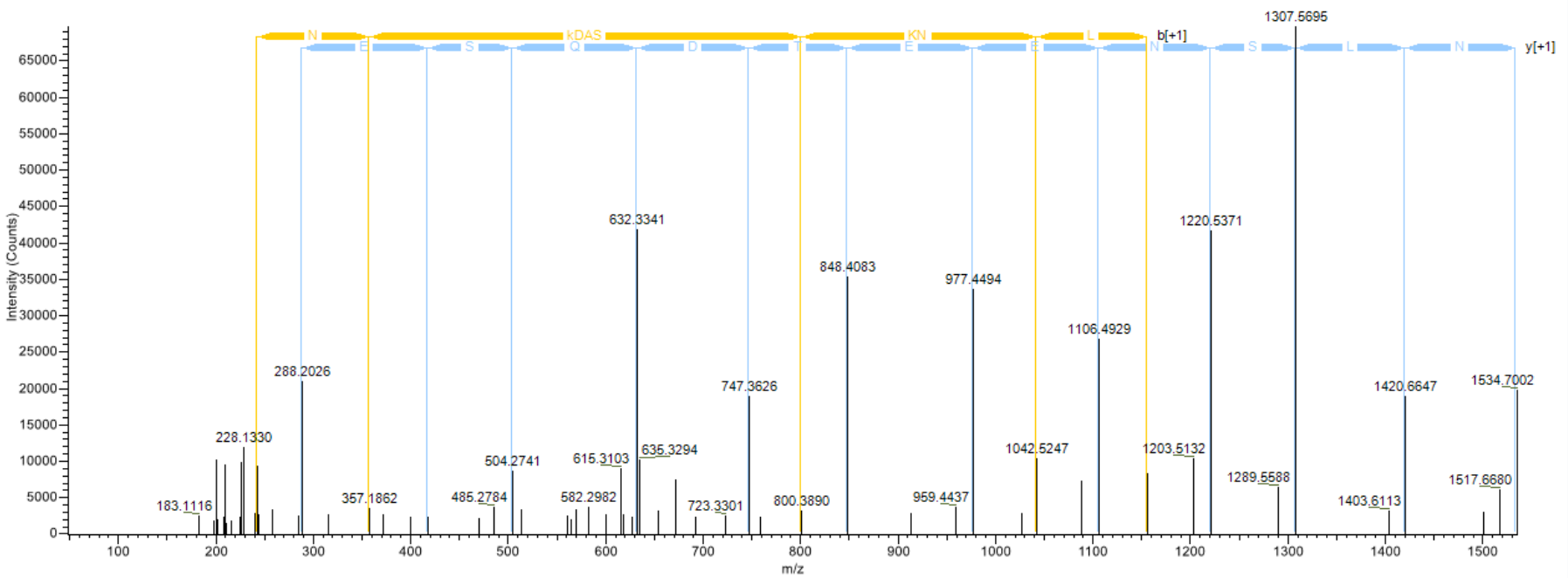

☑ b
☐ b*
☐ b°
☑ y
☐ y°
☐ y*
☐ Immonium

Hide Table

	(NH3+) -	K>	<N	N>	<k	k>	<D	D>	<A	A>	<S	S>	<K	K>	<N	N>	<L	L>	<N	N>	<L	L>	<S	S>	<N	N>	<E	E>	<E	E>	<T	T>	<D
b (+1)	115.05021	243.14518		357.18811		527.29364		642.32059		713.35771		800.38974		928.48471		1042.52764		1155.61171		1269.65464		1382.73871		1469.77074		1583.81367		1712.85627		1841.89887		1942.9465
b*(+1)	98.02366	226.11863		340.16156		510.26709		625.29404		696.33116		783.36319		911.45816		1025.50109		1138.58516		1252.62809		1365.71216		1452.74419		1566.78712		1695.82972		1824.87232		1925.9200
b°(+1)	97.03964	225.13461		339.17754		509.28308		624.31003		695.34715		782.37918		910.47415		1024.51708		1137.60115		1251.64408		1364.72815		1451.76018		1565.80311		1694.84571		1823.88831		1924.9359
y (+1)	2575.25954	2447.16457		2333.12164		2163.01610		2047.98915		1976.95203		1889.92000		1761.82503		1647.78210		1534.69803		1420.65510		1307.57103		1220.53900		1106.49607		977.45347		848.41087		747.3631
y*(+1)	2558.23299	2430.13802		2316.09509		2145.98955		2030.96260		1959.92548		1872.89345		1744.79848		1630.75555		1517.67148		1403.62855		1290.54448		1203.51245		1089.46952		960.42692		831.38432		730.3366

Value Type: Theo. Mass [Da]

N K N k D A S K N L N L S N E E T D Q S E I R

Tolerance: Da Charge State: 1

PALB2 K449-ac

Peptide Consensus View

Sequence: NKDASKNLNLSNEETDQSEIR
K6-Acetyl (42.01057 Da)
Charge: +3, Monoisotopic m/z: 816.39063 Da (-2.42 mmu/-2.96 ppm), MH+: 2447.15732 Da, RT: 33.82 min,

Extracted from: C:\Users\Proteomics\Desktop\Marjorie PD searches\PALB2_acetyl\C150703_PALB2+GCN5+GCN5mut\Qex02_SVH_150703_MarjorieFournier_4_PALB2-P2.2+GCN5.raw #10392 RT: 33.82
FTMS, HCD, z=+3, Mono m/z=816.39063 Da, MH+=2447.15732 Da, Match Tol.=0.05 Da

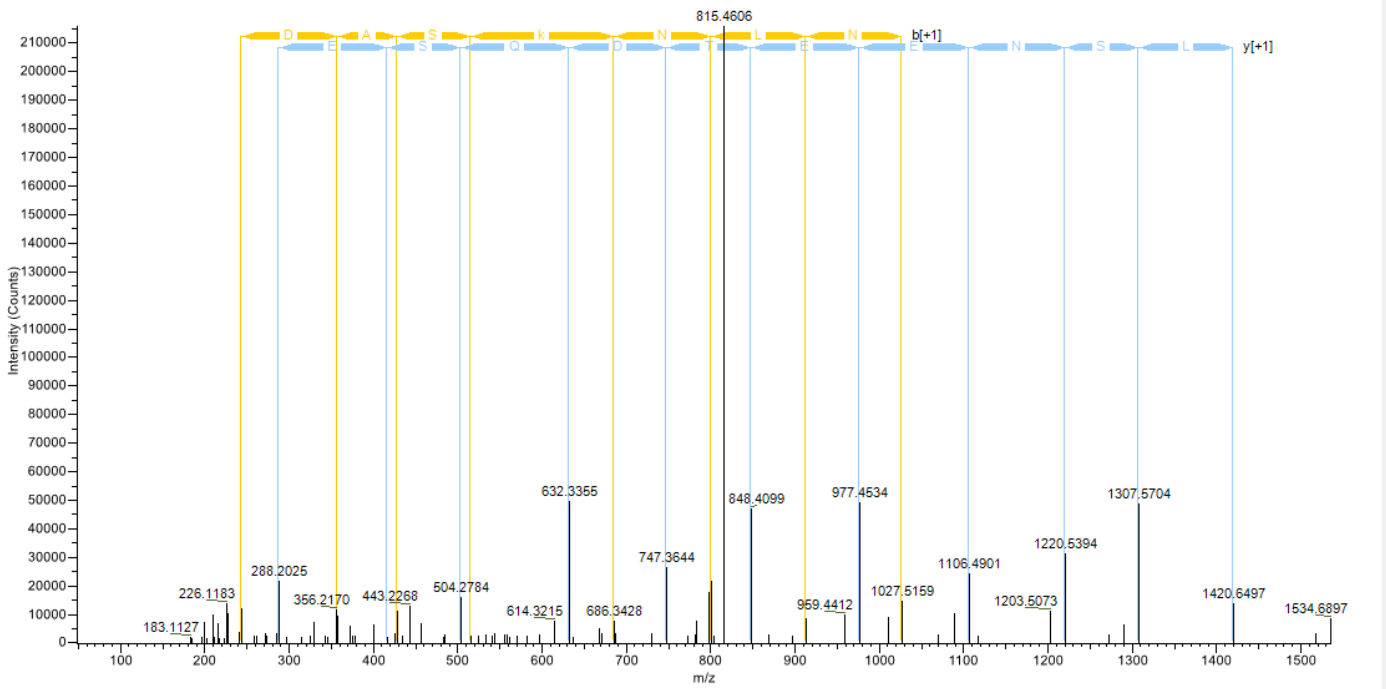

b
b*
b°
y
y°
y*
Immonium

Hide Table

	(NH3+) -	K>	<D	D>	<A	A>	<S	S>	<k	k>	<N	N>	<L	L>	<N	N>	<L	L>	<S	S>	<N	N>	<E	E>	<E	E>	<T	T>
b (+1)	115.05021	243.14518		358.17213		429.20925		516.24128		686.34681		800.38974		913.47381		1027.51674		1140.60081		1227.63284		1341.67577		1470.71837		1599.76097		1700.80
b*(+1)	98.02366	226.11863		341.14558		412.18270		499.21473		669.32026		783.36319		896.44726		1010.49019		1123.57426		1210.60629		1324.64922		1453.69182		1582.73442		1683.78
b°(+1)	97.03964	225.13461		340.16156		411.19868		498.23071		668.33625		782.37918		895.46325		1009.50618		1122.59025		1209.62228		1323.66521		1452.70781		1581.75041		1682.75
y (+1)	2333.12164	2205.02667		2089.99972		2018.96260		1931.93057		1761.82503		1647.78210		1534.69803		1420.65510		1307.57103		1220.53900		1106.49607		977.45347		848.41087		747.36
y*(+1)	2316.09509	2188.00012		2072.97317		2001.93605		1914.90402		1744.79848		1630.75555		1517.67148		1403.62855		1290.54448		1203.51245		1089.46952		960.42692		831.38432		730.33

Value Type: Theo. Mass [Da]

N K D A S k N L N L S N E E T D Q S E I R

Tolerance: Da Charge State: 1

PALB2 K480-ac

Peptide Consensus View

Sequence: TSQKLLSLTK
K4-Acetyl (42.01057 Da)
Charge: +2, Monoisotopic m/z: 580.84656 Da (-1.36 mmu/-2.34 ppm), MH+: 1160.68584 Da, RT: 27.67 min,

Extracted from: D:\Data_D_90362\Marjorie Fournier\C130424_037.raw #8561 RT: 27.67
FTMS, HCD, z=+2, Mono m/z=580.84656 Da, MH+=1160.68584 Da, Match Tol.=0.05 Da

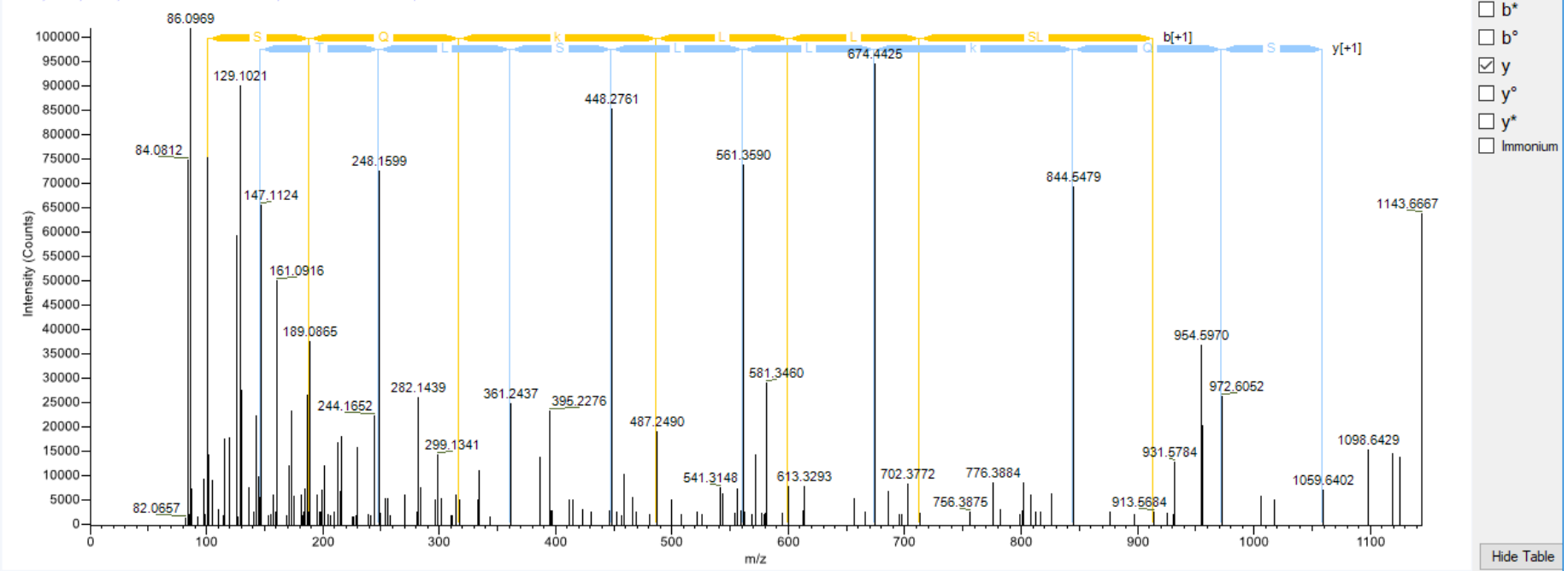

☑ b
☐ b*
☐ b°
☑ y
☐ y°
☐ y*
☐ Immonium

Hide Table

	(NH3+) -	S>	Q>	k>	<L	L>	<L	L>	<S	S>	<L	L>	<T	T>	<K	K - (COOH)
b (+1)	102.05496	189.08699	317.14557	487.25110		600.33517		713.41924		800.45127		913.53534		1014.58302		1142.67799
b*(+1)	85.02841	172.06044	300.11902	470.22455		583.30862		696.39269		783.42472		896.50879		997.55647		1125.65144
b°(+1)	84.04439	171.07642	299.13500	469.24054		582.32461		695.40868		782.44071		895.52478		996.57246		1124.66743
y (+1)	1059.64088	972.60885	844.55027	674.44473		561.36066		448.27659		361.24456		248.16049		147.11281		1160.68856
y*(+1)	1042.61433	955.58230	827.52372	657.41818		544.33411		431.25004		344.21801		231.13394		130.08626		1143.66201
y°(+1)	1041.63031	954.59828	826.53970	656.43417		543.35010		430.26603		343.23400		230.14993		129.10225		1142.67799

Value Type: Theo. Mass [Da]

T S Q k L L S L T K

z y
b c

Tolerance: Da Charge State: 1

PALB2 K515-ac

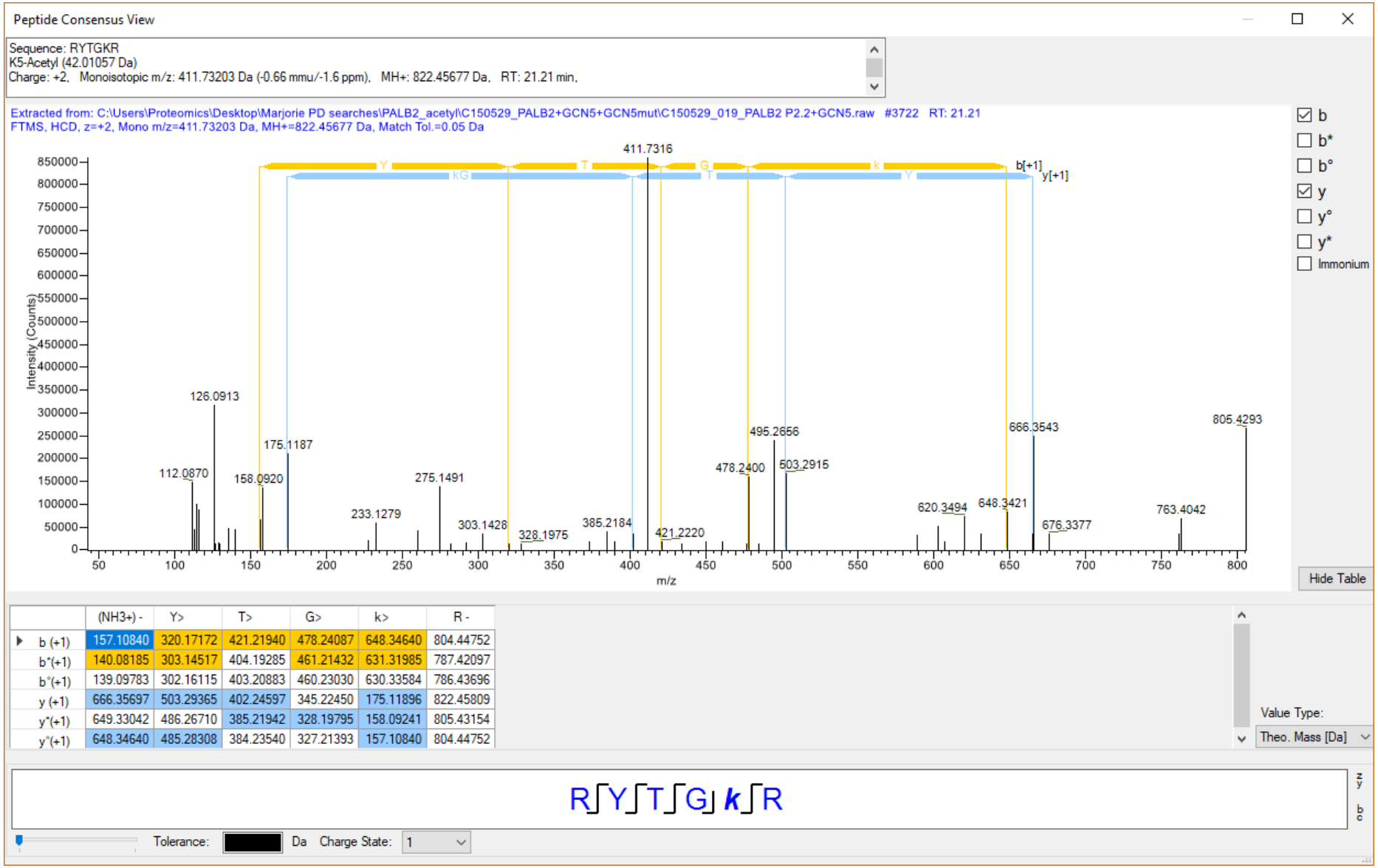

	(NH3+) -	Y>	T>	G>	k>	R -
b (+1)	157.10840	320.17172	421.21940	478.24087	648.34640	804.44752
b*(+1)	140.08185	303.14517	404.19285	461.21432	631.31985	787.42097
b°(+1)	139.09783	302.16115	403.20883	460.23030	630.33584	786.43696
y (+1)	666.35697	503.29365	402.24597	345.22450	175.11896	822.45809
y*(+1)	649.33042	486.26710	385.21942	328.19795	158.09241	805.43154
y°(+1)	648.34640	485.28308	384.23540	327.21393	157.10840	804.44752

PALB2 K517-ac

Peptide Consensus View

Sequence: KSACTPASDHCEPLLPTSSLSIVNR
K1-Acetyl (42.01057 Da), C4-Carbamidomethyl (57.02146 Da), C11-Carbamidomethyl (57.02146 Da)
Charge: +3, Monoisotopic m/z: 928.12097 Da (-0.53 mmu/-0.57 ppm), MH+: 2782.34836 Da, RT: 42.63 min,

Extracted from: C:\Users\Proteomics\Desktop\Marjorie PD searches\PALB2_acetyl\C150529_PALB2+GCN5+GCN5mut\C150529_019_PALB2 P2.2+GCN5.raw #10209 RT: 42.63
FTMS, HCD, z=+3, Mono m/z=928.12097 Da, MH+=2782.34836 Da, Match Tol.=0.05 Da

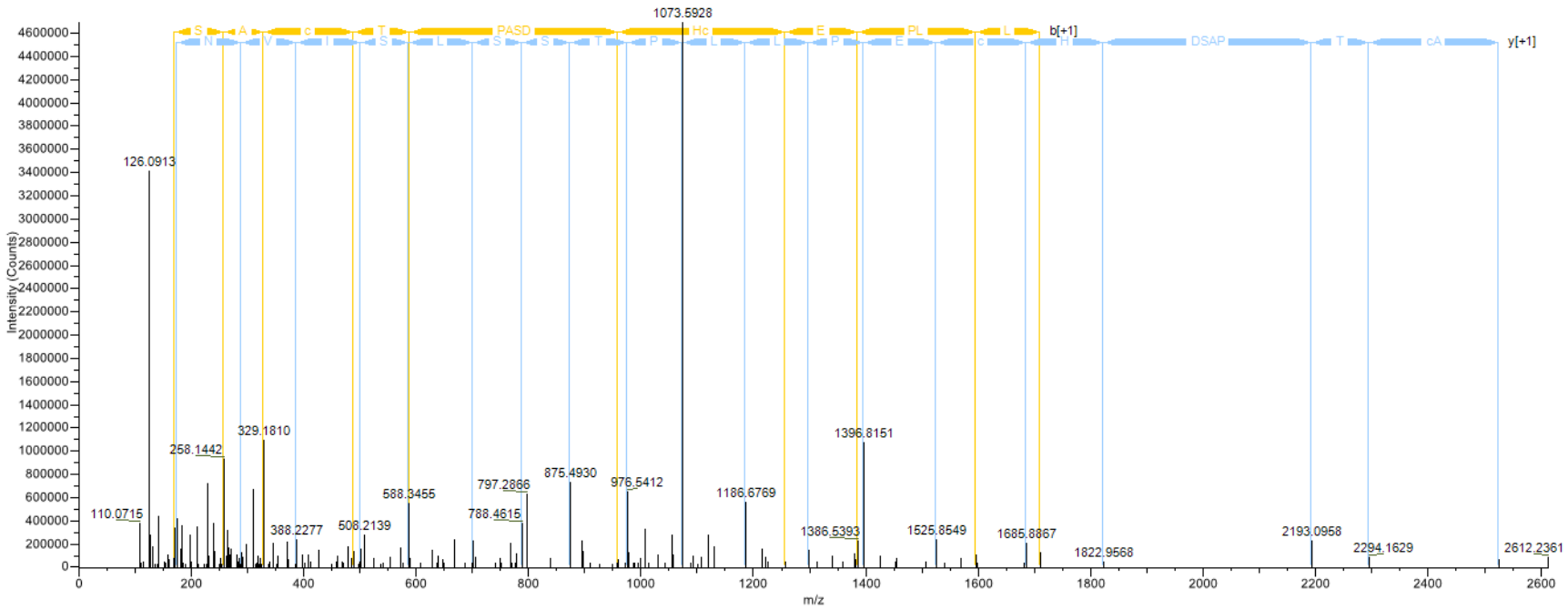

☑ b
☐ b*
☐ b°
☑ y
☐ y°
☐ y*
☐ Immonium

Hide Table

	(NH3+) - k>	S>	<A	A>	<c	c>	<T	T>	<P	P>	<A	A>	<S	S>	<D	D>	<H	H>	<c	c>	<E	E>	<P	P>	<L	L>	<L	L>	<P	P>	<T	T>	<S	S>	<S	S>
b (+1)	171.11281	258.14484	329.18196	489.21262	590.26030	687.31307	758.35019	845.38222	960.40917	1097.46808	1257.49873	1386.54133	1483.59410	1596.67817	1709.76224	1806.81501	1907.86269	1994.89472	2081
b*(+1)	154.08626	241.11829	312.15541	472.18607	573.23375	670.28652	741.32364	828.35567	943.38262	1080.44153	1240.47218	1369.51478	1466.56755	1579.65162	1692.73569	1789.78846	1890.83614	1977.86817	2064
b°(+1)	153.10225	240.13428	311.17140	471.20205	572.24973	669.30250	740.33962	827.37165	942.39860	1079.45751	1239.48816	1368.53076	1465.58353	1578.66760	1691.75167	1788.80444	1889.85212	1976.88415	2063
y (+1)	2612.24442	2525.21239	2454.17527	2294.14462	2193.09694	2096.04417	2025.00705	1937.97502	1822.94807	1685.88916	1525.85850	1396.81590	1299.76313	1186.67906	1073.59499	976.54222	875.49454	788.46251	701
y°(+1)	2595.21787	2508.18584	2437.14872	2277.11807	2176.07039	2079.01762	2007.98050	1920.94847	1805.92152	1668.86261	1508.83195	1379.78935	1282.73658	1169.65251	1056.56844	959.51567	858.46799	771.43596	684

Value Type: Theo. Mass [Da]

k S A ***c*** T P A S D H ***c*** E P L L P T S S L S I V N R

z y
b c

Tolerance: Da Charge State: 1

PALB2 K563-ac

Peptide Consensus View

Sequence: LFIQVKGK
K8-Acetyl (42.01057 Da)
Charge: +2, Monoisotopic m/z: 487.80368 Da (-1.65 mmu/-3.38 ppm), MH+: 974.60008 Da, RT: 44.16 min,

Extracted from: C:\Users\Proteomics\Desktop\Marjorie PD searches\PALB2_acetyl\C150703_PALB2+GCN5+GCN5mut\Qex02_SVH_150703_MarjorieFournier_4_PALB2-P2.2+GCN5.raw #15093 RT: 44.16
FTMS, HCD, z=+2, Mono m/z=487.80368 Da, MH+=974.60008 Da, Match Tol.=0.05 Da

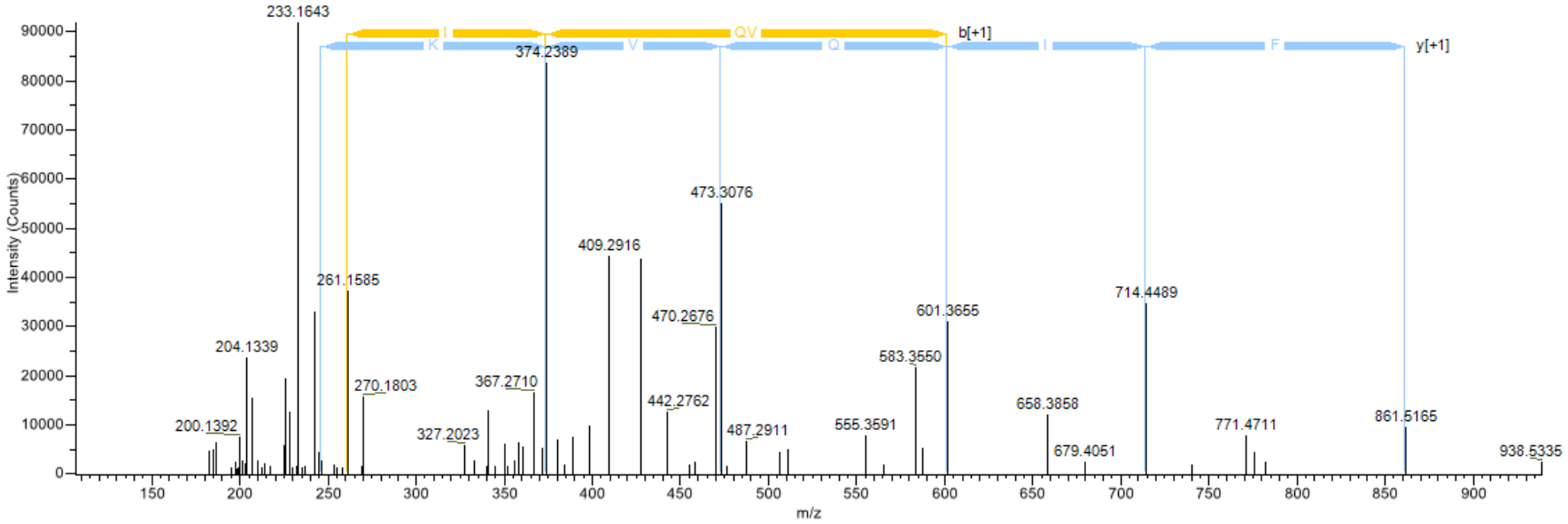

☑ b
☐ b*
☐ b°
☑ y
☐ y°
☐ y*
☐ Immonium

Hide Table

	(NH3+) -	F>	<I	I>	<Q	Q>	V>	K>	G>	k -
b (+1)	114.09135	261.15977	374.24384	502.30242	601.37084	729.46581	786.48728	956.59281		
b*(+1)	97.06480	244.13322	357.21729	485.27587	584.34429	712.43926	769.46073	939.56626		
b°(+1)	96.08078	243.14920	356.23327	484.29185	583.36027	711.45524	768.47671	938.58225		
y (+1)	861.51931	714.45089	601.36682	473.30824	374.23982	246.14485	189.12338	974.60338		
y*(+1)	844.49276	697.42434	584.34027	456.28169	357.21327	229.11830	172.09683	957.57683		
y°(+1)	843.50874	696.44032	583.35625	455.29767	356.22925	228.13428	171.11281	956.59281		

Value Type: Theo. Mass [Da]

L ⌈F⌋I ⌋Q⌈V⌋K⌈G k

z y
b c

Tolerance: Da Charge State: 1

PALB2 K681-ac

Peptide Consensus View

Sequence: RMDTEMEDLEEDLIVLPGKSHPK
K19-Acetyl (42.01057 Da)
Charge: +3, Monoisotopic m/z: 908.77802 Da (-0.85 mmu/-0.94 ppm), MH+: 2724.31949 Da, RT: 64.94 min.

Extracted from: C:\Users\Proteomics\Desktop\Marjorie PD searches\PALB2_acetyl\C150703_PALB2+GCN5+GCN5mut\Qex02_SVH_150703_MarjorieFournier_3_PALB2-FL+GCN5.raw #14904 RT: 64.94
FTMS, HCD, z=+3, Mono m/z=908.77802 Da, MH+=2724.31949 Da, Match Tol.=0.05 Da

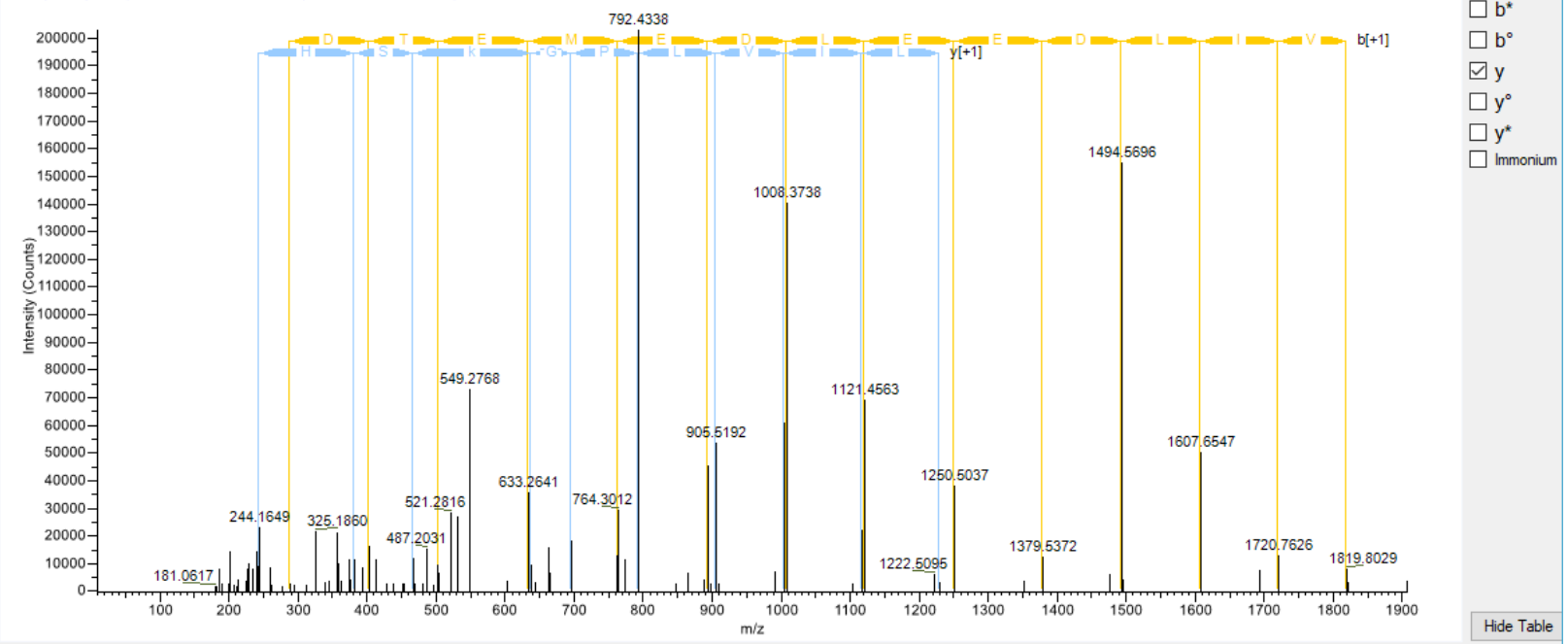

☑ b
☐ b*
☐ b°
☑ y
☐ y°
☐ y*
☐ Immonium

Hide Table

	(NH3+) -	M>	<D	D>	<T	T>	<E	E>	<M	M>	<E	E>	<D	D>	<L	L>	<E	E>	<E	E>	<D	D>	<L	L>	<I	I>	<V	V
b (+1)	157.10840	288.14890		403.17585		504.22353		633.26613		764.30663		893.34923		1008.37618		1121.46025		1250.50285		1379.54545		1494.57240		1607.65647		1720.74054		18
b*(+1)	140.08185	271.12235		386.14930		487.19698		616.23958		747.28008		876.32268		991.34963		1104.43370		1233.47630		1362.51890		1477.54585		1590.62992		1703.71399		18
b°(+1)	139.09783	270.13833		385.16528		486.21296		615.25556		746.29606		875.33866		990.36561		1103.44968		1232.49228		1361.53488		1476.56183		1589.64590		1702.72997		18
y (+1)	2568.22093	2437.18043		2322.15348		2221.10580		2092.06320		1961.02270		1831.98010		1716.95315		1603.86908		1474.82648		1345.78388		1230.75693		1117.67286		1004.58879		9
y*(+1)	2551.19438	2420.15388		2305.12693		2204.07925		2075.03665		1943.99615		1814.95355		1699.92660		1586.84253		1457.79993		1328.75733		1213.73038		1100.64631		987.56224		8

Value Type: Theo. Mass [Da]

R M D T E M E D L E E D L I V L P G k S H P K

z y
b c

Tolerance: Da Charge State: 1

PALB2 K883-ac

Peptide Consensus View

Sequence: AGCKEPCIITACEDVVSLWK
C3-Carbamidomethyl (57.02146 Da), K4-Acetyl (42.01057 Da), C7-Carbamidomethyl (57.02146 Da), C12-Carbamidomethyl (57.02146 Da)
Charge: +2, Monoisotopic m/z: 1189.56396 Da (+0.82 mmu/+0.69 ppm), MH+: 2378.12065 Da, RT: 69.08 min.

Extracted from: C:\Users\Proteomics\Desktop\Marjorie PD searches\PALB2_acetyl\C150703_PALB2+GCN5+GCN5mut\Qex02_SVH_150703_MarjorieFournier_3b_PALB2-FL+GCN5.raw #12500 RT: 69.08
FTMS, HCD, z=+2, Mono m/z=1189.56396 Da, MH+=2378.12065 Da, Match Tol.=0.05 Da

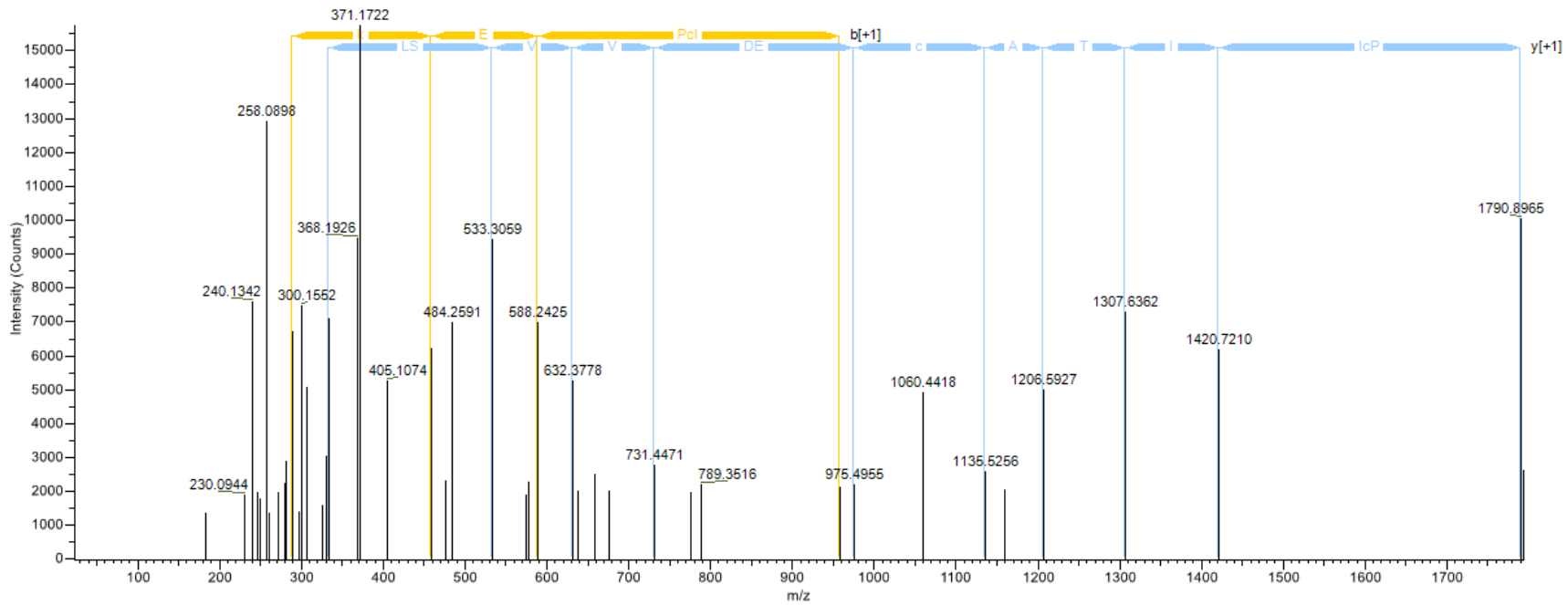

☑ b
☐ b*
☐ b°
☑ y
☐ y°
☐ y*
☐ Immonium

Hide Table

	(NH3+) -	G>	<c	c>	<k	k>	<E	E>	<P	P>	<c	c>	<I	I>	<I	I>	<T	T>	<A	A>	<c	c>	<E	E>	<D	D>	<V	V>	<V	V>	<S
b (+1)	72.04440	129.06587		289.09652		459.20206		588.24466		685.29743		845.32808		958.41215		1071.49622		1172.54390		1243.58102		1403.61167		1532.65427		1647.68122		1746.74964		1845.81806
b*(+1)	55.01785	112.03932		272.06997		442.17551		571.21811		668.27088		828.30153		941.38560		1054.46967		1155.51735		1226.55447		1386.58512		1515.62772		1630.65467		1729.72309		1828.79151
b°(+1)	54.03383	111.05530		271.08596		441.19149		570.23409		667.28686		827.31751		940.40158		1053.48565		1154.53333		1225.57045		1385.60111		1514.64371		1629.67066		1728.73908		1827.80750
y (+1)	2307.08190	2250.06043		2090.02977		1919.92424		1790.88164		1693.82887		1533.79822		1420.71415		1307.63008		1206.58240		1135.54528		975.51462		846.47202		731.44507		632.37665		533.30823
y*(+1)	2290.05535	2233.03388		2073.00323		1902.89769		1773.85509		1676.80232		1516.77167		1403.68760		1290.60353		1189.55585		1118.51873		958.48807		829.44547		714.41852		615.35010		516.28168

Value Type: Theo. Mass [Da]

A G c k E P c I I T A c E D V V S L W K

z y
b c

Tolerance: Da Charge State: 1